

**RECOGNIZING ICE-CONTACT TRACHYTE-PHONOLITE LAVAS AT THE
MOUNT EDZIZA VOLCANIC COMPLEX, BRITISH COLUMBIA, CANADA**

by

Kristen A. LaMoreaux

B.S., Kent State University, 2002

Submitted to the Graduate Faculty of
Arts and Sciences in partial fulfillment
of the requirements for the degree of
Master of Science

University of Pittsburgh

2008

UNIVERSITY OF PITTSBURGH

ARTS AND SCIENCES

This thesis was presented

by

Kristen A. LaMoreaux

It was defended on

June 17, 2008

and approved by

Dr. Michael Ramsey

Dr. Thomas Anderson

Thesis Director: Dr. Ian Skilling

Copyright © by Kristen A. LaMoreaux

2008

RECOGNIZING ICE-CONTACT TRACHYTE-PHONOLITE LAVAS AT THE MOUNT EDZIZA VOLCANIC COMPLEX, BRITISH COLUMBIA, CANADA

Kristen A. LaMoreaux, M.S.

University of Pittsburgh, 2008

Mount Edziza Volcanic Complex (MEVC) lies within the Northern Cordilleran Volcanic Province (NCVP), in northwest British Columbia, Canada. The eruption products have been emplaced in a variety of subaerial, sub-ice and subaqueous environments from about 8Ma to less than 2000 y.b.p. (Souther, 1992). Ice Peak Formation (IPF) trachyte lava flows of approximately 1Ma age (Souther, 1992) are exposed at Ornostay Bluff (OB) and Koosick Bluff (KB). These flows comprise basal flow breccias overlain by massive conchoidally-fractured lava with large, poorly-developed columns, and local flow banding. Edziza Formation (EF) approximately 1Ma (Souther, 1992) phonolite is exposed at Triangle Dome (TD). TD can broadly be divided into an upper and lower zone. The upper zone comprises poorly-developed columns in addition to prominent jointing. In the lower zone the columns are planar and 75cm-3m-wide in the interior of the complex grading into fan-like and curved subhorizontal columns <75cm-wide in the outer margins of the lower zone. The upper zone is interpreted as an “entablature” where slow cooling was overprinted by joints formed during abrupt cooling due to water ingress. Local areas with well-developed columnar jointing in the upper zone may reflect endogenous growth by late-stage intrusive emplacement, or areas where water ingress was less efficient. The lower zone is interpreted as a “lower colonnade” with slower cooling and less water ingress during cooling. The fan-like columns in the outer margins of the lower zone reflect cooling by direct contact with curved margins of the ice cavity. The estimated minimum

thickness of the ice-contact zone is ~60m reflected by the thickness of the lower zone.

Identifying ice-contact structures in trachytic-phonolitic lavas is difficult, especially in glacially eroded examples such as OB and KB, where marginal cooling-columns and structures caused by direct contact with ice have been eroded. Trachyte lavas display a wide range of viscosities, flow thicknesses, and aspect ratios therefore caution is required in interpreting “overthick” flows as having formed by confinement by former ice. Studies that focus on comparisons of estimated flow velocities and rates of ice melting are useful, though there are numerous unaccounted for variables in these models.

TABLE OF CONTENTS

PREFACE.....	XIII
1.0 GOAL OF RESEARCH	1
2.0 MOTIVATION.....	2
3.0 INTRODUCTION.....	6
4.0 LOCATION	7
5.0 PREVIOUS WORK AT MOUNT EDZIZA VOLCANIC COMPLEX	11
6.0 REGIONAL GEOLOGIC SETTING OF MOUNT EDZIZA VOLCANIC COMPLEX	12
7.0 GEOLOGIC HISTORY OF MOUNT EDZIZA VOLCANIC COMPLEX.....	15
7.1 RASPBERRY FORMATION.....	18
7.2 LITTLE ISKUT FORMATION.....	19
7.3 ARMADILLO FORMATION.....	19
7.4 NIDO FORMATION.....	20
7.5 SPECTRUM FORMATION.....	20
7.6 PYRAMID FORMATION.....	21
7.7 ICE PEAK FORMATION.....	22
7.8 PILLOW RIDGE FORMATION	23
7.9 EDZIZA FORMATION.....	23

7.10	KLASTLINE FORMATION.....	24
7.11	ARCTIC LAKE FORMATION.....	24
7.12	KAKIDDI FORMATION.....	24
7.13	BIG RAVEN FORMATION	25
8.0	PREVIOUS WORK ON TRACHYTE-PHONOLITE LAVAS AT MOUNT EDZIZA VOLCANIC COMPLEX.....	26
8.1	ARMADILLO FORMATION TRACHYTE	28
8.2	SPECTRUM FORMATION TRACHYTE.....	28
8.3	PYRAMID FORMATION TRACHYTE	31
8.4	ICE PEAK FORMATION TRACHYTE	31
8.5	MOUNT EDZIZA FORMATION TRACHYTE.....	33
8.6	KAKIDDI FORMATION TRACHYTE	35
9.0	OVERVIEW OF EMPLACEMENT AND STRUCTURE OF INTERMEDIATE AND FELSIC LAVAS.....	36
9.1	SUBAERIAL INTERMEDIATE AND FELSIC LAVAS.....	36
9.2	STRUCTURES RELATED TO FLOW EMPLACEMENT	39
9.3	STRUCTURES FORMED BY COOLING-CONTRACTION.....	39
9.4	SUBAQUEOUS INTERMEDIATE AND FELSIC LAVAS	44
9.5	SUB-ICE AND/OR ICE-CONTACT INTERMEDIATE AND FELSIC LAVAS	45
10.0	DISCUSSION OF EMPLACEMENT MECHANISMS AND STRUCTURES OF TRACHYTE LAVA FLOWS	57
10.1	SUBAERIAL TRACHYTE LAVA FLOWS.....	57

10.2	SUBAQUEOUS TRACHYTE LAVAS.....	58
10.3	SUBGLACIAL AND ICE-CONTACT TRACHYTE LAVAS.....	59
11.0	DISCUSSION OF VISCOSITY, ASPECT RATIOS, AND DIMENSIONS OF TRACHYTE LAVA FLOWS	61
12.0	DESCRIPTION OF STUDIED TRACHYTE LAVAS AT MOUNT EDZIZA VOLCANIC COMPLEX	70
12.1	TRIANGLE DOME.....	72
12.2	ORNOSTAY BLUFF.....	83
12.3	KOOSICK BLUFF	99
13.0	INTERPRETATION OF STUDIED TRACHYTE LAVAS AT MOUNT EDZIZA VOLCANIC COMPLEX.....	103
13.1	INTERPRETATION OF TRIANGLE DOME.....	104
13.2	INTERPRETATION OF ORNOSTAY AND KOOSICK BLUFFS.....	109
14.0	DISCUSSION OF STUDIED TRACHYTE FLOW VELOCITY AND ICE MELTING RATES.....	112
15.0	DISCUSSION: RECOGNIZING ICE-CONTACT TRACHYTE LAVAS.....	116
16.0	FUTURE WORK	122
17.0	CONCLUSIONS	123
	APPENDIX A	126
	APPENDIX B	137
	APPENDIX C	148
	REFERENCE	157

LIST OF TABLES

Table 1: MEVC stratigraphy.....	16
Table 2: Description of fractures	41
Table 3: Table of comparison of MEVC trachyte flows.....	63
Table 4: Intermediate lava viscosities from the literature.....	65
Table 5: Trachyte lava flow aspect ratios	67
Table 6: MEVC dome dimensions.....	68
Table 7: Geochemical data.....	71
Table 8: Jeffreys Equation	113

LIST OF FIGURES

Figure 1: Distribution of Neogene and Quaternary volcanic rocks in the Canadian Cordillera.....	3
Figure 2: Map showing the approximate extent of the Cordilleran Ice Sheet (CIS)	4
Figure 3: Location of Mount Edziza Volcanic Complex (MEVC) and two nearby volcanic complexes	8
Figure 4: Map showing the outline of the Mount Edziza Volcanic Complex (MEVC).....	9
Figure 5: The field area is located on the western flanks of MEVC.....	10
Figure 6: Principal physiographic elements as indicated by Souther (1992).....	15
Figure 7: Simplified geological map showing the three field areas studied (TD, OB, KB).....	27
Figure 8: Sketch showing the morphology of distal and proximal facies of Spectrum Formation	30
Figure 9: A schematic sketch of formation of shrinkage cracks in cooling lava flows.	43
Figure 10: Photos of columnar jointing from the eastern flank of Bláhnúkur, Torfajökull.....	46
Figure 11: Sketches showing structural cross-sections and column distributions.....	48
Figure 12: Idealized sketches showing cross sectional views of an ice-contact andesite-dacite lava.....	50
Figure 13: Cross section sketches of proposed ice-marginal formation of ridge-forming	52
Figure 14: Photographs of secondary column structures from Spörli and Rowland's (2006).....	55

Figure 15: Chart showing calculated effects of crystal content on the viscosity of Ornostay Bluff	69
Figure 16: TAS diagram	70
Figure 17: Aerial photo of Triangle Dome and surrounding areas.....	73
Figure 18: Photo of Triangle Dome from the north.....	74
Figure 19: Overlay of Triangle Dome	75
Figure 20: Photo mosaic of Triangle Dome with close-up images of structures.....	77
Figure 21: Radial fanning columnar jointing at Triangle Dome.....	78
Figure 22: Photo of ‘C’ and ‘S’ curves at Triangle Dome.....	79
Figure 23: Photo of radial columns at Triangle Dome	80
Figure 24: Vertical to sub-horizontal fanning columns	81
Figure 25: The ends and ‘lizard skin’ appearance on the lower portions of Triangle Dome.	82
Figure 26: Radial columnar jointing at Triangle Dome.....	82
Figure 27: Aerial photo of Koosick Bluff (KB) and Ornostay Bluff (OB) and surrounding area.	84
Figure 28: Ornostay Bluff column orientation diagram and aerial photo.....	86
Figure 29: Ornostay Bluff photo mosaic overlay.	88
Figure 30: Photo of Ornostay Bluff from the north.....	89
Figure 31: Ornostay Bluff mosaic and close-up images.....	90
Figure 32: Photo of the southwest corner of OB and the first waterfall.....	91
Figure 33: Ornostay Bluff.....	92
Figure 34: Ornostay Bluff columnar and platy jointing on the north side of the bluff.....	93
Figure 35: Ornostay Bluff Unit 3.....	94

Figure 36: Photos of the top of Ornostay Bluff.	95
Figure 37: Ornostay Bluff Unit 3 further east along the bluff's southern face.....	96
Figure 38: Ornostay Bluff cooling-contraction columns all within Unit 3.....	97
Figure 39: Ornostay Bluff stratigraphy column.....	98
Figure 40: Ornostay Bluff field photos.....	99
Figure 41: Koosick Bluff, view from the north	101
Figure 42: Koosick Bluff	102
Figure 43: Sketches of fracture morphologies in ice-contact lava flows.....	104
Figure 44: Curved columnar structures formed in basalt lava flows.....	106
Figure 45: Typical intraflow structures present in Grande Ronde Basalt flows.....	108
Figure 46: Possible emplacement scenario for Triangle Dome.	109
Figure 47: Sketch showing progression of fracture from a void along the flow base inward towards the flow interior.	110
Figure 48: Simplified lava flow emplacement scenarios for Ornostay and Koosick Bluffs.	111
Figure 49: Estimated velocity of the Koosick Bluff lava flow compared with typical ice melting rates.	114
Figure 50: The model for formation of 'column-on-column' structures	119

PREFACE

First, to my committee members: Ian Skilling, Mike Ramsey, and Thomas Anderson:

Ian Skilling, for being so incredibly patient, for so many opportunities, and teaching me so much and then some

Mike Ramsey for being an inspiring lecturer and field instructor (and fellow outdoor gear junkie)

Thomas Anderson for invoking excitement about geology and leading one of the best courses I have ever had the pleasure of taking

Also to:

Charlie Jones, for the love of rocks and 'old school' geology and passing that onto young geologists

Veronica Peet for making thin sections amusing and for always being supportive, no matter what the circumstances

Lizzie Simoneau for being my closest colleague, making me feel like we were in this together, helping me through the discouraging times with friendship and thoughtfulness (and camo)

My better half, Daniel Worley, for being patient and understanding, forcing me through the toughest moments because you believed in me; without you this achievement would not have been possible

My parents, Anne and John, for providing endless love, a good laugh, and relaxing moment when it was most needed

My grandpa, Dave, for providing continuous support and encouragement

1.0 GOAL OF RESEARCH

The main purpose of this research has been to document evidence that will allow the distinction to be made between trachyte/phonolite lavas that have contacted ice-water from those which have not. Lava flows which have contacted ice include those emplaced entirely beneath ice, as well as those emplaced subaerially against ice along their margins. Note that some authors (e.g. Head and Wilson, 2007) use intrusive terms such as “sill” and “dike” for initial emplacement beneath ice. During the early phases of intrusion into ice strain rates can be very high and the ice may behave like a rock. Under these conditions it is therefore more appropriate to use such terms. However, for the sake of simplicity, terms associated with effusive emplacement are used here, namely, “lava” and “lava flow”.

The most important research question that we are trying to answer in this project is **“How do trachyte-phonolite lavas that have contacted ice differ from those emplaced in a ice-free environment?”**

2.0 MOTIVATION

There has been a large growth of interest in the processes and products of volcano-ice interaction both on Earth and Mars in the last decade (e.g. Squyres et al., 1987; Mouginis-Mark, 1989; Garvin et al., 2000; Wilson and Head, 2007; Smellie and Chapman, 2002; Head and Wilson, 2007; McGarvie et al., 2007; Morris and Mouginis-Mark, 2006; Schopka et al., 2005; Milkovich et al., 2006). This expansion of research interest is related to several factors, including the observation that (1) such results can provide a record of the presence of former ice and its thickness; (2) large volumes of meltwater generated during such eruptions or between eruptions can provide an important habitat for extremophiles (on Earth and maybe Mars); (3) such eruptions can provide a potential mechanism for destabilization of ice sheets (Smellie, 2002; Blankenship, 1993; Corr and Vaughan, 2008) and (4) such eruptions can generate serious flood hazards in places like south Iceland (Stevenson et al., 2006; Tómasson, 1996; Scharrer et al., 2007; Alho et al., 2004).

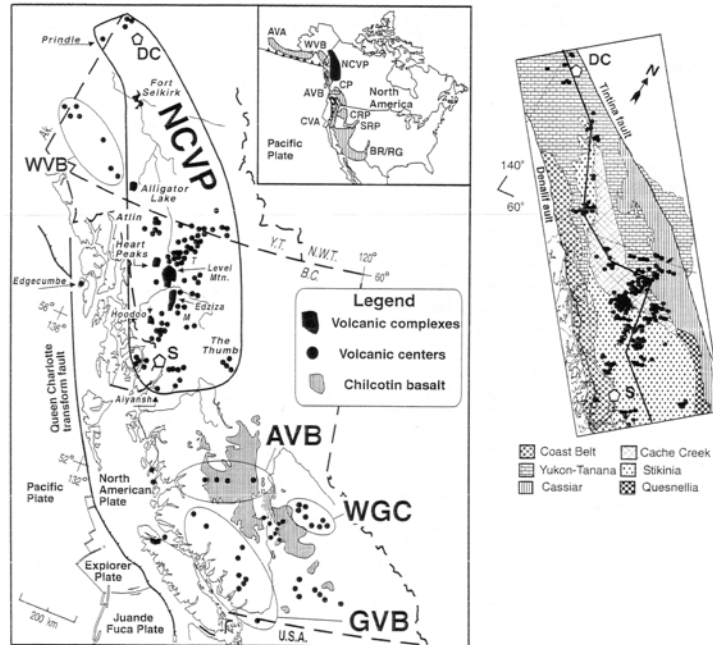


Figure 1: Distribution of Neogene and Quaternary volcanic rocks in the Canadian Cordillera

GVB – Garibaldi volcanic belt, WGC – Wells Gray-Clearwater volcanic field, AVB – Anaheim volcanic belt, WVR – Wrangell volcanic belt, and NCVP – the northern Cordilleran volcanic province. The NCVP extends from DC – Dawson Creek, Yukon Territory in the north, south to S – Stewart, British Columbia. Inset Fig shows the relationship of the NCVP and other volcanic areas in North America including: AVA – Aleutian volcanic arc, CVA – the Cascade volcanic arc, CP – Chilcotin plateau basalts, CRP – the Columbia River plateau basalt field, SRP – the Snake River Plain, and BR/GR – the Basin and Range-Rio Grande rift system. Additionally (right), the distribution of volcanic centers in the NCVP with respect to the major tectonostratigraphic terrane boundaries and the Denali and Tintina fault systems (after Edwards and Russell, 2000).

Ice-contact lavas are arguably more important than clastic rocks with regard to their potential use as a record of former ice conditions, because they are generally more easily dated. Ice-contact lavas of intermediate (such as trachytes) or felsic composition are of particular importance as they are more easily dated by ^{39}Ar - ^{40}Ar than mafic lavas. Lavas are generally

better preserved than clastic sequences in the rock record, and are more likely to preserve evidence of confinement against ice than clastic deposits.

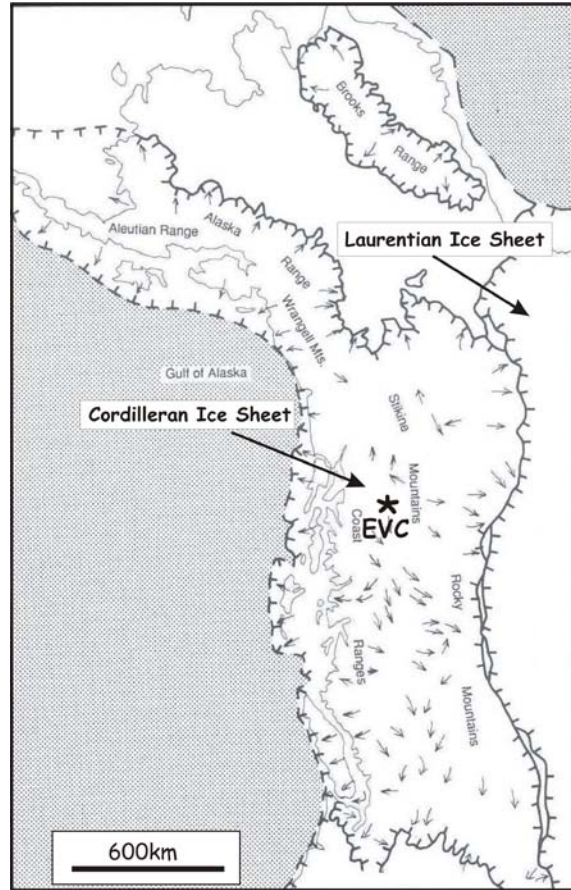


Figure 2: Map showing the approximate extent of the Cordilleran Ice Sheet (CIS) at Late Glacial Maximum. Location of Mount Edziza Volcanic Complex (EVC) and ice flow directions are illustrated (after Dawson, 1992)

Trachytic and phonolite lavas that have been interpreted as having been emplaced beneath or in contact with ice have only been recorded from two areas on Earth, namely the Northern Cordilleran Volcanic Province (NCVP) of Canada (Edwards and Russell, 2000; Fig 1) and west Antarctica (LeMasurier, 2002). The trachyte lavas of the NCVP are particularly

important in a North American context as they offer us an insight into the thickness and extent of the Cordilleran Ice Sheet (CIS), which once covered this entire volcanic province (Fig 2).

There are very few studies on the emplacement of trachytic lavas in any subaqueous environment, so this study will add to this body of literature (e.g. Sohn, 1995; LeMasurier, 2002). In addition, most trachytic magmas are compositionally and hence rheologically similar to andesites, which are very much more common as lava flows on many stratovolcanoes around the world, therefore the results of this study could also be applied to these more common volcanic products.

3.0 INTRODUCTION

In order to address the principal research question of this project as to “**How do trachyte-phonolite lavas that have contacted ice differ from those emplaced in an ice-free environment?**” the study was divided into four parts. The sections of this thesis which correspond to these parts are given in parentheses.

(1) *Detailed field study of three extensive exposures of trachyte and phonolite lavas, at the Mount Edziza Volcanic Complex (MEVC), northern British Columbia (Fig. 4). The lavas, exposed in three bluffs were previously interpreted as having been emplaced during glacial times (Souther, 1992; Section 12)*

(2) *Compilation of descriptions and interpretation of emplacement mechanisms and resultant structures of subaerial and submarine felsic to intermediate (with emphasis on trachyte) lavas in the literature for comparison with the above field study of likely ice-contact trachytes at the MEVC (Section 9)*

(3) *Compilation of all known viscosity and flow dimensional data on trachyte lavas from the literature and comparison of this data with new data calculated from MEVC trachyte analyses and their estimated flow thicknesses and aspect ratios. (Section 11)*

(4) *Study of rate of trachyte lava flow advance at MEVC compared with the estimated rate of ice melting to see if direct ice contact or just meltwater generation would have occurred. (Section 14)*

4.0 LOCATION

The Mount Edziza Volcanic Complex (MEVC, 57°43'0"N, 130°38'0"W; UTM 402906E, 6398705N) is an aerially extensive, long lived (> 5 m.y.), voluminous complex that lies in the Regional District of Kitimat-Stikine, British Columbia, Canada (Figs 1 and 3).

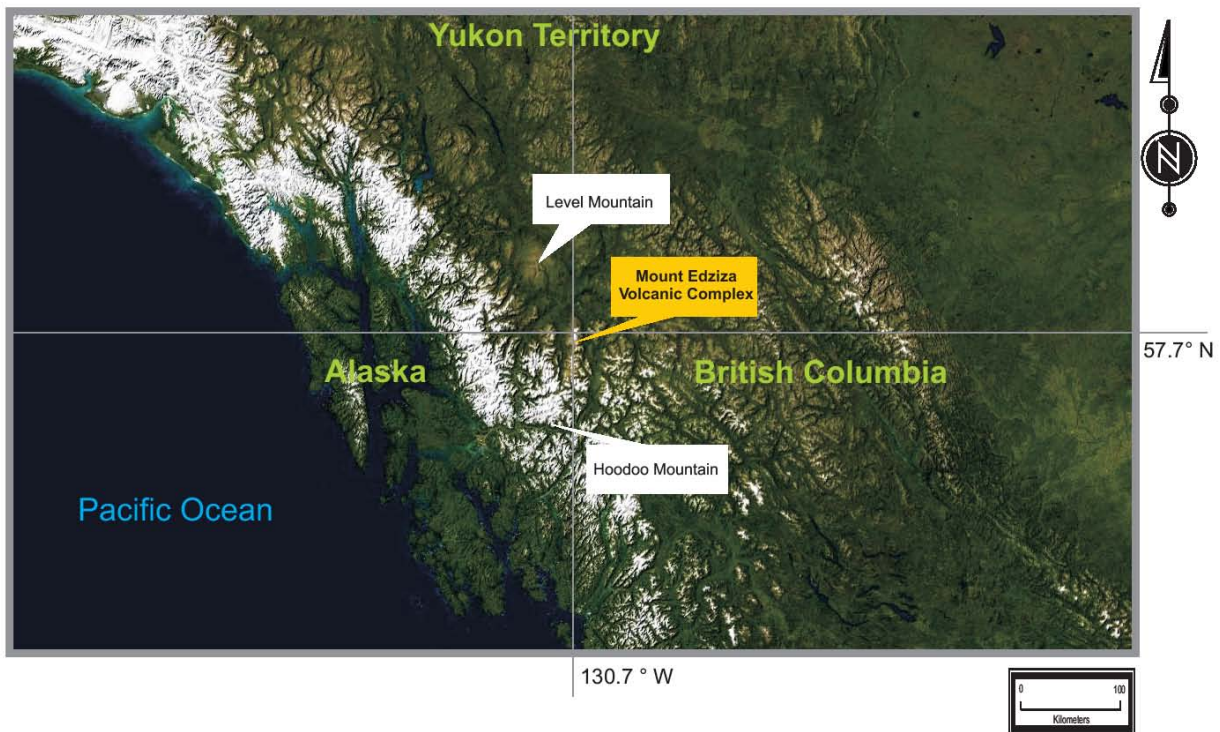


Figure 3: Location of Mount Edziza Volcanic Complex (MEVC) and two nearby volcanic complexes where ice-contact evidence has been observed, namely Level Mountain and Hoodoo Mountain. Image data from NASA I-Cubed ESAT World Landsat 7 Mosaic with 15 m resolution, image composed with NASA World Wind 1.4.

The MEVC is comprised of a large (~ 1000 km²), steep sided plateau, approximately 75 km long and 20 km wide, situated between the Klastline River Valley to the north, the Mess Creek Valley and larger Stikine River Valley to the west and the Iskut River Valley to the east (Fig 4). The plateau rises to elevations of 1500 m to 1800 m with peaks to 2590 m. The present day summit at Mount Edziza’s peak is glacier filled and has been interpreted as a caldera (Souther, 1992). Several other glaciers still cover the central portions of the complex including Tencho Glacier (Fig 6).

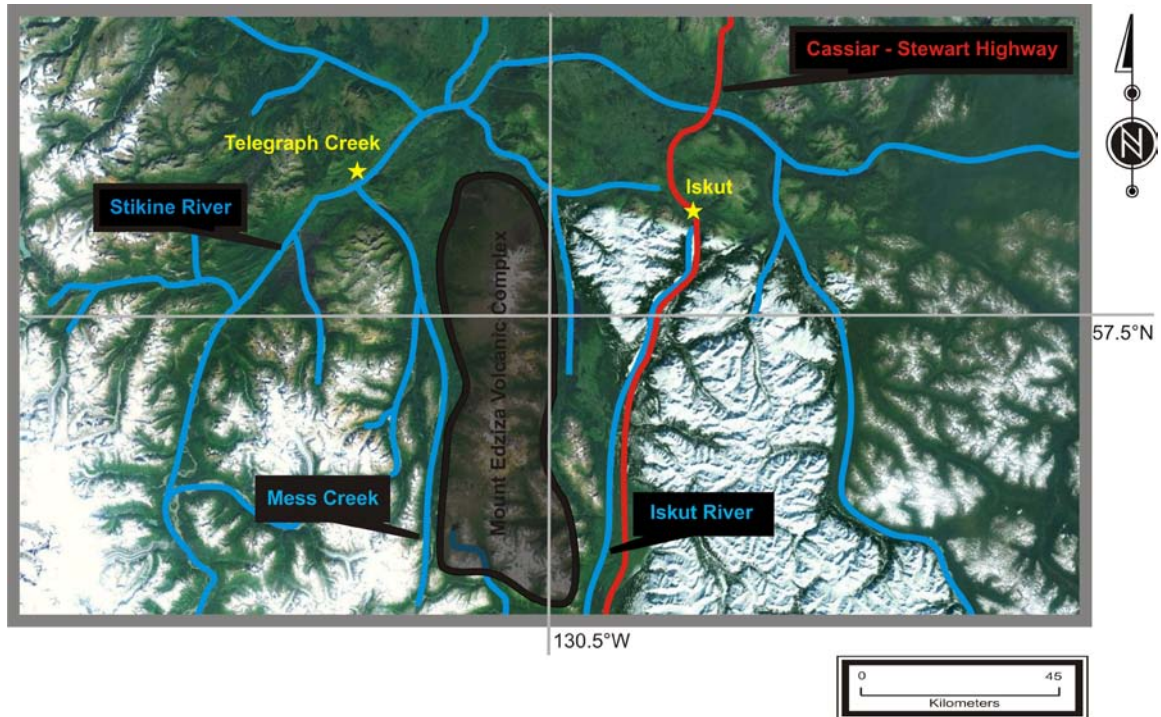


Figure 4: Map showing the outline of the Mount Edziza Volcanic Complex (MEVC) main vehicle access route (Cassiar-Stewart Highway), principal rivers (Stikine River, Mess Creek, and Iskut Rivers) and main settlements (Iskut and Telegraph Creek). Image data from NASA I-Cubed ESAT World Landsat 7 Mosaic with 15 m resolution, image composed with NASA World Wind 1.4.

There are no roads into the area, the closest roadway being the Cassiar-Stewart Highway to the east. Access to the area can be achieved most efficiently by helicopter from the nearby towns of Iskut or Dease Lake (Fig 4).

The three bluffs of trachyte-phonolite lava studied at the MEVC for this project are Ornostay Bluff (OB), Koosick Bluff (KB), and Triangle Dome (TD, Fig 5)

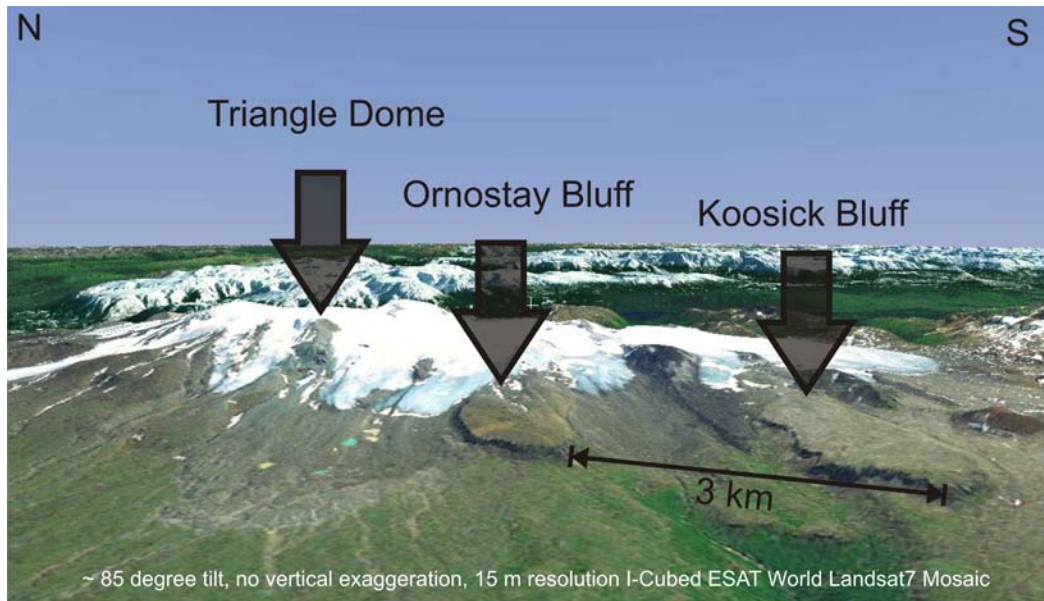


Figure 5: The field area is located on the western flanks of MEVC.

Triangle Dome, the feature furthest to the north, as well as Koosick Bluff and Ornostay Bluff are shown. Image data from NASA I-Cubed ESAT World Landsat 7 Mosaic with 15 m resolution, image composed with NASA World Wind 1.4.

5.0 PREVIOUS WORK AT MOUNT EDZIZA VOLCANIC COMPLEX

Previous geologic work at the MEVC began in the 1940's when Kerr described erosional remnants of basaltic lava flows resting on river gravels in the Stikine Valley near Telegraph Creek (Kerr, 1948). Work subsequent to Kerr's would not begin until Souther, working in conjunction with the Geological Survey of Canada (GSC), embarked on a mapping project, where he delineated the boundaries of the Mount Edziza Volcanic Complex (MEVC). This work resulted in a 1:250,000 geological map of the Telegraph Creek area (Souther, 1972). Souther also undertook extensive field-based research for the GSC at the MEVC in 1965-1967, and also briefly revisited the area in 1968 and 1976. Much of Souther's work has been published in multiple summary and topical papers (Souther, 1968; Souther, 1972a; Souther, 1972b; Souther, 1975; Souther, 1977; Souther, 1981a; Souther, 1981b; Souther and Hickson, 1984; Souther and Symons, 1974; Souther et al., 1984). But the most up-to-date account of the geology of the MEVC is the GSC Memoir of Souther (1992), from which the background geology in the rest of this section, and all of the base geology maps used in the research project were taken.

6.0 REGIONAL GEOLOGIC SETTING OF MOUNT EDZIZA VOLCANIC COMPLEX

The MEVC is underlain by Late Paleozoic and Mesozoic sedimentary, plutonic, and volcanic rocks of Stikinia, the largest in a group of several terrains collectively known as the Insular Superterrane. These terranes likely collided with the continental margin during late Mesozoic transpressional and calc-alkaline volcanism of Stikinia during the Late Cretaceous – Early Tertiary (Souther, 1992). However, by Late Miocene time extension and/or transtension is suggested by the mafic alkaline volcanics at MEVC (Edwards and Russell, 2000).

According to Souther (1992) the history of the MEVC spans several episodes of bimodal volcanism, erosion, and periods of regional and alpine glaciation advance and retreat. The MEVC lies within the Northern Cordillerian Volcanic Province (NCVP; Edwards and Russell, 2000), a broad, arc shaped volcanic belt of Miocene and younger volcanoes. This belt runs roughly parallel to the North American – Pacific plate margin through western Yukon Territory and British Columbia, Canada (Fig 1). The NCVP is one of the largest Neogene volcanic provinces in western North America. The province contains numerous volcanic centers, predominately of alkaline olivine basalt composition, which lie between the Tintina and Denali faults. The rocks within the NCVP range from 20 Ma to ca 200 yr BP (Edwards and Russell 2000).

The MEVC comprises $\sim 775 \text{ km}^3$ of basalt, trachyte and rhyolite erupted in a variety of subaerial, sub-ice and subaqueous environments from about 8Ma to $<2000 \text{ y.b.p.}$ It forms a major component of the Stikine peralkaline subprovince of the central part of the NCVP in northwestern British Columbia, Canada. The MEVC has been formed by five cyclical periods of magmatic activity, each beginning with a mafic phase and ending with felsic magmas. Predominantly basaltic lava flows dominate the base of the complex, capped by thicker, more evolved peralkaline trachytic to rhyolitic lavas and domes as well as pyroclastic products (Souther, 1992). The origin of the more evolved magmas of MEVC can be attributed either fractionation of a mafic magma, fractionation accompanied by crustal contamination and assimilation, or crustal contamination alone (Edwards et al., 2002). The bimodal composition and cyclical nature of volcanism at MEVC are attributed to the presence of a slab window and related tectonics driven by changes in relative plate motion, from compressional to transtensional, between the Pacific and North American plates approximately 15-10 Ma (Edwards and Russell, 2000; Madsen et al., 2006).

Four main composite volcanoes that define a north-south axis form the main eruptive centers of the MEVC. The Spectrum Range is the furthest south of these centers and is comprised mainly of a large rhyolite dome complex of approximately 3 – 7 Ma in age (Souther, 1992; Souther, 1984). Just to the north of it lies the heavily eroded Armadillo Peak (12-6Ma) that may have once comprised a caldera, and which may have had several satellite domes (Souther, 1992). North of Armadillo Peak are the overlapping centers of Ice Peak (4.7-1.2Ma) and Mount Edziza. Mount Edziza is the youngest of the four MEVC centers at 1.2 – 0.4 Ma in age and has an ice capped summit (Souther, 1992).

The three exposures studied for the field-based part of this project (Section 12) would be considered part of the Ice Peak and Mount Edziza eruptive centers, and would also be part of their respective formations of the same name (see below) according to Souther (1992).

7.0 GEOLOGIC HISTORY OF MOUNT EDZIZA VOLCANIC COMPLEX

This section summarizes descriptions by Souther (1992) of the formations of the MEVC (Figs 6 and 7, Table 1) with **particular focus on his interpretation of the interaction of lava or magma with ice and/or water.** All of the dates given in this section are K-Ar dates of Souther (1984). Table 1 is a stratigraphic column for the MEVC illustrating the names of the formations, as defined by Souther (1992), the most recent dates (Souther, 1984) and a brief description of the products of each formation.

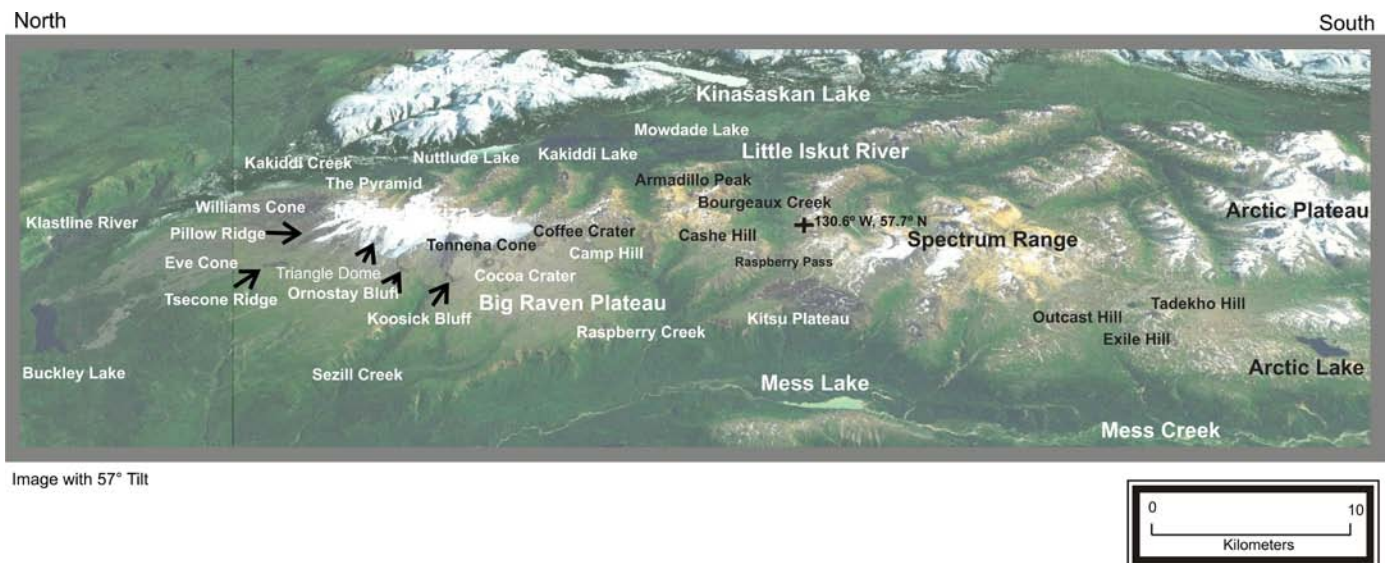


Figure 6: Principal physiographic elements as indicated by Souther (1992) of the Mount Edziza Volcanic Complex. Image data from NASA I-Cubed ESAT World Landsat 7 Mosaic with 15 m resolution, image composed with NASA World Wind 1.4.

Table 1: MEVC stratigraphy

Mount Edziza Volcanic Complex Stratigraphic Column				
Unit	Age	Souther's (1992, 1984) Age Date	Description	
SURFICIAL DEPOSITS	Holocene		Fluvial, glacial, talus, and landslide deposits	
BIG RAVEN FORMATION	Pleistocene	10-1±6 ka	Hawaiite, alkali olivine basalt, and comenditic trachyte cones, lava flows, air fall tephra, tuff-breccia, pumice, bombs and agglutinate, pillow breccia, pillow lava	
KLASTLINE FORMATION		0.62±0.04 Ma	Alkali olivine basalt pyroclastic breccia, agglutinate, tuff breccia, lava flows, minor pillow lava with some lenses of fluvial gravel and glacial deposits	
KAKIDDI FORMATION		0.31±0.07 - 0.28±0.2 Ma	Trachyte agglutinated pumice, lava flows, breccia	
ARCTIC LAKE FORMATION		0.71±0.05 Ma	Alkali olivine basalt bombs, agglutinate, minor tuff breccia, pillow breccia, lava flows, minor pillow lava, lenses fluvial gravel and glacial deposits	
EDZIZA FORMATION		0.9±0.3 Ma	Trachyte and comenditic trachyte pyroclastic breccia, lahar, ash flow deposits, lava flows, endogenous domes, vent breccia, lava lakes	
PILLOW RIDGE FORMATION		0.9±0.3 Ma	Alkali olivine basalt and hawaiite tuff breccia, pillow breccia, lava flows	
ICE PEAK FORMATION		3.7±1.0 - 1.2±0.1 Ma	Alkali olivine basalt, trachybasalt, tristanite, mugearite, benmoreite, and trachyte lava flows, domes, pyroclastic breccia, locally intercalated with fluvial and glacial deposits	
PYRAMID FORMATION		1.2±0.4 - 0.94±0.12 Ma	Comendite, comenditic trachyte, and pantellerite lacustrine tuff, pyroclastic breccia, lahar deposits, till and glacial-fluvial gravel, lava flows and domes	
SPECTRUM FORMATION		Pliocene	5.9±1.1 - 2.9±0.1 Ma	Alkali olivine basalt, domes, intercalated fluvial gravel and paleosols, subvolcanic intrusions
NIDO FORMATION			7.8±0.3 - 4.5±0.3 Ma	Alkali olivine basalt tuff breccia, pillow lava, intrusives, lava flows, flow breccia, agglutinate, ice-contact facies and intercalated gravel
ARMADILLO FORMATION	Miocene	10.2±1.4 Ma - 6.1±0.1 Ma	Comendite and trachyte pumice, ash flows, tuff, lava flows and domes, vent breccia, and subvolcanic intrusions	
LITTLE ISKUT FORMATION		7.2±0.3 Ma	Trachybasalt lava flows, flow breccia, crackle breccia, and subvolcanic structures	
RASPBERR FORMATION		11.4±1.5 - 5.5±0.1 Ma	Alkali olivine basalt lava flows, flow breccia, agglutinate, minor pillow lava, tuff breccia, and intercalated gravel deposits	
SLOKO GROUP	Eocene		Rhyolite, dacite, and andesite pyroclastic breccia, epiclastic breccia, debris flow and landslide deposits, minor lava flows, and intrusive pluton	
SUSTUT GROUP	Cretaceous and Paleocene		Chert-pebble conglomerate, quartzose sandstone, arkose, siltstone, carbonaceous shale, and minor coal	
UNDIVIDED BASEMENT ROCKS			Sedimentary, volcanic, and metamorphic	

Activity began at the MEVC about $11.4 \text{ Ma} \pm 1.5$ ago (Souther, 1992) with the eruption of basalts comprising the Raspberry Formation. Subaqueous eruptions of trachybasalt comprising the Little Iskut Formation followed at approximately 7.2 ± 0.3 Ma ago. Explosive volcanism then ensued with the eruption of pyroclastics and associated felsic and basaltic lavas of the Armadillo Formation approximately 10.2 ± 0.1 Ma ago. Later, approximately 7.2 ± 0.3 Ma, 6 basaltic volcanoes mapped as Nido Formation by Souther (1992) became active. Some of these centers encountered alpine glacial ice, namely Beta Peak and Gamma Peak. Nido volcanism was followed by eruptions of mainly rhyolite and trachyte lavas beginning approximately 5.9 ± 1.1 Ma ago that comprise the Spectrum Formation. Another particularly explosive period followed with the eruption of rhyolite and trachyte products of the Pyramid Formation between 1.2 ± 0.4 Ma and 0.94 ± 0.12 Ma. Eruptions of Pyramid Formation rhyolite at Sphinx Dome as well as Pharaoh Dome also likely encountered ice. Also during this time, accumulation of lacustrine tuff in a glacially dammed lake (Tut Lake) provides further evidence of the prolonged periods of glaciovolcanism (or potential glaciovolcanism) at the MEVC. According to Souther (1992), the Cordillieran Ice Sheet (Fig 2) advanced across the Pyramid Formation rocks at the close of this period. During the following Ice Peak Formation time, beginning approximately 3.7 ± 1.0 Ma ago, eruption of both basaltic and trachytic lavas took place. Pillows and tuff-breccias of Ice Peak Formation formed where advancing lava flows contacted glacial ice. The eruptions that form present day Camp Hill, (also Ice Peak Formation basalt), began beneath ice with the formation of tuff-breccia, pillow lava, pillow breccia, and quenched pahoehoe lava flow toes. Another sub-ice basaltic eruption formed Tsekone Ridge and Pillow Ridge of the Pillow Ridge Formation at 0.9 ± 0.3 Ma. The Edziza Formation followed at approximately 0.9 ± 0.3 Ma and involved mostly trachytic and phonolitic lava flows. The

basaltic lava flows of the Klastline Formation created the large plateaus in the northeastern portions of the MEVC, at 0.62 ± 0.04 Ma as well as the Klastline Cone which begun beneath alpine glacial ice. Two small volcanoes are the principal components of the subsequent Arctic Lake Formation (0.71 ± 0.05 Ma) period of basaltic effusive and explosive activity that erupted subaerially (Outcast Hill, Tadekho Hill), during glacial maximum (Wetalth Ridge), and during glacial retreat (Thaw Hill, Knobs 1 and 2, and flows from Source Hill), according to Souther (1992). The Kakiddi Formation (0.31 ± 0.7 Ma) comprises mostly trachyte lavas. Alkali olivine basalt, hawaiiite, and small quantities of comenditic trachyte of the Big Raven Formation (1 ± 6 ka) are the result of the most recent activity at MEVC which post dates the most recent episode of regional glaciations, although some interactions with residual valley ice may have occurred (Souther, 1992).

7.1 RASPBERRY FORMATION

Raspberry Formation (11.4 ± 1.5 Ma – 5.5 ± 0.1 Ma): This eruption of basaltic lava flows that form the first units of this formation mark the beginning of activity at MEVC at approximately 11 Ma (Souther, 1992). The vent or vents that were the source of the basalts are believed to be located near Raspberry Pass (Fig. 6). These flows total more than 83 km^3 with a proximal total preserved thickness of up to 300 m. On the western edge of the MEVC, Raspberry volcano formed an estimated 2100 m high edifice (Souther, 1992). An intense period of erosion followed this activity (Souther, 1992).

7.2 LITTLE ISKUT FORMATION

Little Iskut Formation (7.2 ± 0.3 Ma): Around this time a large lake became ponded in the upper Little Iskut Valley (Fig 6) due to damming by the basaltic flows of the Raspberry Formation. Eruptive activity began within the lake. Layers of ash settled on the bottom of the lake and formed the base of a shield volcano (Little Iskut Volcano), which eventually emerged above lake level. Breccia and flows also soon displaced much of the lake water and lava was emplaced over the Raspberry Formation surface (Souther, 1992).

7.3 ARMADILLO FORMATION

Armadillo Formation (10.2 ± 1.4 Ma – 6.1 ± 0.1 Ma): Armadillo Formation activity began with an explosive eruption of rhyolite and trachyte pumice from a vent near the northern edge of a dome. Proximal deposits were more than 150 m in thickness where as distal deposits were up to 15 m thick (Souther, 1992). Welded ash flow deposits extended as much as 10 km from their source in the early stages but viscous lava later dominated the activity. The lava first formed steep-sided overlapping domes around the vent. Lava flows eventually spread further from the vent eventually covering most of the southeastern landscape of MEVC with trachyte and rhyolite.

7.4 NIDO FORMATION

Nido Formation (7.8 ± 0.3 Ma – 4.5 ± 0.3 Ma): At least six major volcanoes were active at the MEVC during this stage of activity. The newly formed valleys from Armadillo time were soon filled with more fluidal basaltic lava flows of the Nido which in turn altered drainage patterns and created lava dams. Three composite volcanoes (Alpha, Beta and Gamma Peaks) formed north of Armadillo Peak in the central area of the MEVC. During their formation, permanent snow became a fixture in the MEVC landscape. Alpine glaciers formed at higher elevations and flowed into river valleys. Periods of advance and retreat over several thousands of years were accompanied by the eruption of more Nido basaltic lava flows. At times during glacial advance, Beta peak was enveloped by ice from an ice cap that covered Gamma peak and surrounding areas. The basalts that erupted during this time quenched against ice and formed piles of pillows and tuff-breccias in melt water ponds. **These lavas of the Nido Formation are the earliest recorded evidence of volcano-ice interaction at the MEVC.** Souther (1992) suggested that towards the end of Nido time the MEVC was covered by an extensive ice-cap, indicated by the presence of a widespread glaciated pavement at the top of this formation

7.5 SPECTRUM FORMATION

Spectrum Formation (5.9 ± 1.1 Ma – 2.9 ± 0.1 Ma): Souther (1992) suggested that a glacially scoured MEVC emerged from beneath the ice and streams began to deposit fluvial sediments approximately 2 Ma ago. A new vent complex (Spectrum Formation) developed in the south of the area and was probably centered around what is now Yeda peak. Early Spectrum

Formation lavas are rhyolitic and up to 150 m thick, 13 km long, and emplaced in a single event of activity. A broad dome of lava was eventually created that is 20 km across and at least 750 m thick at its center (Souther, 1992). A total of over 100 km³ of rhyolite and trachyte were erupted during the Spectrum stage of activity (Souther, 1992).

7.6 PYRAMID FORMATION

Pyramid Formation (1.2 ± 0.4 Ma – 0.94 ± 0.12 Ma): A period of volcanic quiescence that lasted approximately 1 Ma followed the eruptions of Spectrum stage lavas (Souther, 1992). During this time, streams and glacial ice carved the landscape. Periods of glacial advance and retreat covered much of the MEVC plateau with glaciofluvial deposits. This period of quiet ended with the explosive eruption of rhyolitic pumice and rock fragments along the northeaster edge of MEVC. Explosive eruptions were accompanied by pyroclastic surges and basaltic lava flows. This early activity in the Pyramid stage was mostly buried beneath felsic domes and flows that dominated the most of the later Pyramid activity. A plug of lava, up to 40% crystallized, was too viscous to create flows as it erupted from the Pyramid Dome, about 1km wide and 400m high. Souther (1992) suggested that a later dome (Sphinx Dome) may have grown within an ice-confined lake. The Sphinx dome eventually grew to over 5 km across and 800 m high. Another vent began to erupt at this time, also beneath the ice. At this vent, Pharaoh Dome began to form as melt water quenched the outer margins of the effusive lava producing large piles of tuff-breccia. The dome eventually grew above the thickness of the surrounding ice. This nunatak projecting above the ice was later to become completely

enveloped in ice as a period of massive regional glaciation (Cordillieran Ice Sheet, CIS) ensued and MEVC become dormant once again (Souther, 1992).

7.7 ICE PEAK FORMATION

Ice Peak Formation (3.7 ± 1.0 Ma – 1.2 ± 0.1 Ma): At the beginning of Ice Peak time, and the onset of the eruption of Ice Volcano, the regional (CIS) ice sheet had begun to recede, according to Souther (1992). Large areas of the plateau were ice-free and now covered by glacial fluvial, morainal and till deposits. Other areas of MEVC were however still covered by ice (Souther, 1992). The initial eruptions of Ice Peak time were in this still-glaciated area. During this stage glacial melt water mixed with newly erupted materials creating debris flows. As the central edifice of Ice Volcano continued to grow, the flows that encountered ice created melt water lakes. As additional lava flowed into these lakes, pillow lava and tuff-breccias formed. Most of the lavas, both trachytic and basaltic in composition, that comprise the main eruptive center of this formation (Ice Volcano) were however erupted subaerially. Eventually Ice Volcano grew to 2400 m high with three thick, steep sided lobes of blocky trachytic lava extending from satellite domes along its western flank (Souther, 1992). Camp Hill and Cache Hill lie south of Ice volcano (Fig 6) and likely first erupted when ice was still present on the MEVC plateau. As lava entered the ice above a vent, melt water ponds were formed. Successive lavas that entered the melt water were quenched and fractured. This fragmental material was disturbed by phreatic eruptions. A tuff cone was eventually created that in time rose above the level of the water within the melt water lake. Subsequent eruptions built a pyroclastic cone atop the original tuff ring. Cache Hill erupted when almost all the glacial ice

had receded. The first flows from Cache Hill flowed across a valley, damming a river and ponding a small lake. Later flows that traveled into the lake formed pillow lava and tuff-breccia (Souther, 1992). During the long period of Ice Peak activity, alpine glaciers advanced and retreated cutting cirques into Ice Volcano. Towards the end of Ice Peak activity, approximately 0.5 to 1 Ma this alpine ice joined to meet regional ice forming part of a regional Pleistocene ice sheet. It is expected that only the tallest peaks may have been visible over the ice sheet that was at least 2285 m thick (Souther, 1992).

7.8 PILLOW RIDGE FORMATION

Pillow Ridge Formation (0.9 ± 0.3 Ma): The regional ice sheet was near its maximum thickness and extent when the basaltic Pillow Ridge erupted (Fig 6) beneath the ice.

7.9 EDZIZA FORMATION

Edziza Formation (0.9 ± 0.3 Ma): By the beginning of Edziza stage of activity, the regional ice sheet that had covered the MEVC had receded from the upper slopes and surrounding plateau, according to Souther (1992). Viscous trachyte magmas created a bulge of rubble that would become Mount Edziza peak (Fig 6) approximately 900,000 years ago (Souther, 1992). The growth of Mount Edziza was characterized by periods of effusion of trachyte lavas, formation of steep-sided domes, and vent-clearing explosions.

7.10 KLASTLINE FORMATION

Klastline Formation (0.62 ± 0.04 Ma): From vents along the northeastern flank of Mount Edziza (Fig 6), basaltic lava erupted as the first products of the Klastline Formation. Three to six centers were active during this time each producing lava flows that traveled up to 25 km from their vents.

7.11 ARCTIC LAKE FORMATION

Arctic Lake Formation (0.71 ± 0.05 Ma): Approximately the same time that Klastline lavas were erupting to the north, Arctic Lake stage activity began with the eruption of two small basaltic volcanoes to the south. Outcast Hill (Fig 6) was a composite cone that ultimately rose more than 300 m from the plateau below (Souther, 1992). Another vent to the south of Outcast Hill formed Tadekho Hill (Fig 6). Souther (1992) suggested that the regional ice sheet likely covered Tadekho and Outcast Hill with at least 300 m of ice.

7.12 KAKIDDI FORMATION

Kakiddi Formation (0.31 ± 0.07 Ma – 0.28 ± 0.2 Ma): About 0.5 Ma ago, a 1 km wide and 60-90 m thick lava flow eventually covered 20 km^3 was emplaced and marked the beginning of Kakiddi stage activity (Souther, 1992) This eruption marks the last major eruption of intermediate composition lavas from a central vent at MEVC.

7.13 BIG RAVEN FORMATION

Big Raven Formation (10 – 1 ± 6 ka): The plateau of MEVC began to emerge from the Pleistocene glaciations, covered with glacial debris and marked with glacial striations during this time. The central ice cap retreated and meltwater streams deposited silt and gravel along the plateau. Then, approximately 2600 years ago, the glaciers again began to advance during Neoglaciation (Souther, 1992). Glacial advance and recession during Neoglacial time produced the moraine visible today that rises 18 m above the plateau of the MEVC (Souther, 1992). During this time eruptions of basalt from numerous satellite cones throughout MEVC ensued as well as a single climactic eruption of trachytic pumice.

8.0 PREVIOUS WORK ON TRACHYTE-PHONOLITE LAVAS AT MOUNT EDZIZA VOLCANIC COMPLEX

This section focuses on previously published descriptions and interpretations of the trachyte-phonolite lavas at the MEVC by Souther (1992) and, in particular, on any structures he described that provide evidence of their emplacement or cooling histories. This section also describes any evidence from previous work for ice-contact or nearby ice at the time of their emplacement.

This section in particular includes description of Souther's (1992) evidence for ice-contact of the lavas at the three field sites chosen for this study, i.e. Ornostay Bluff and Koosick Bluff (both Ice Peak Formation) and Triangle Dome (Edziza Formation).

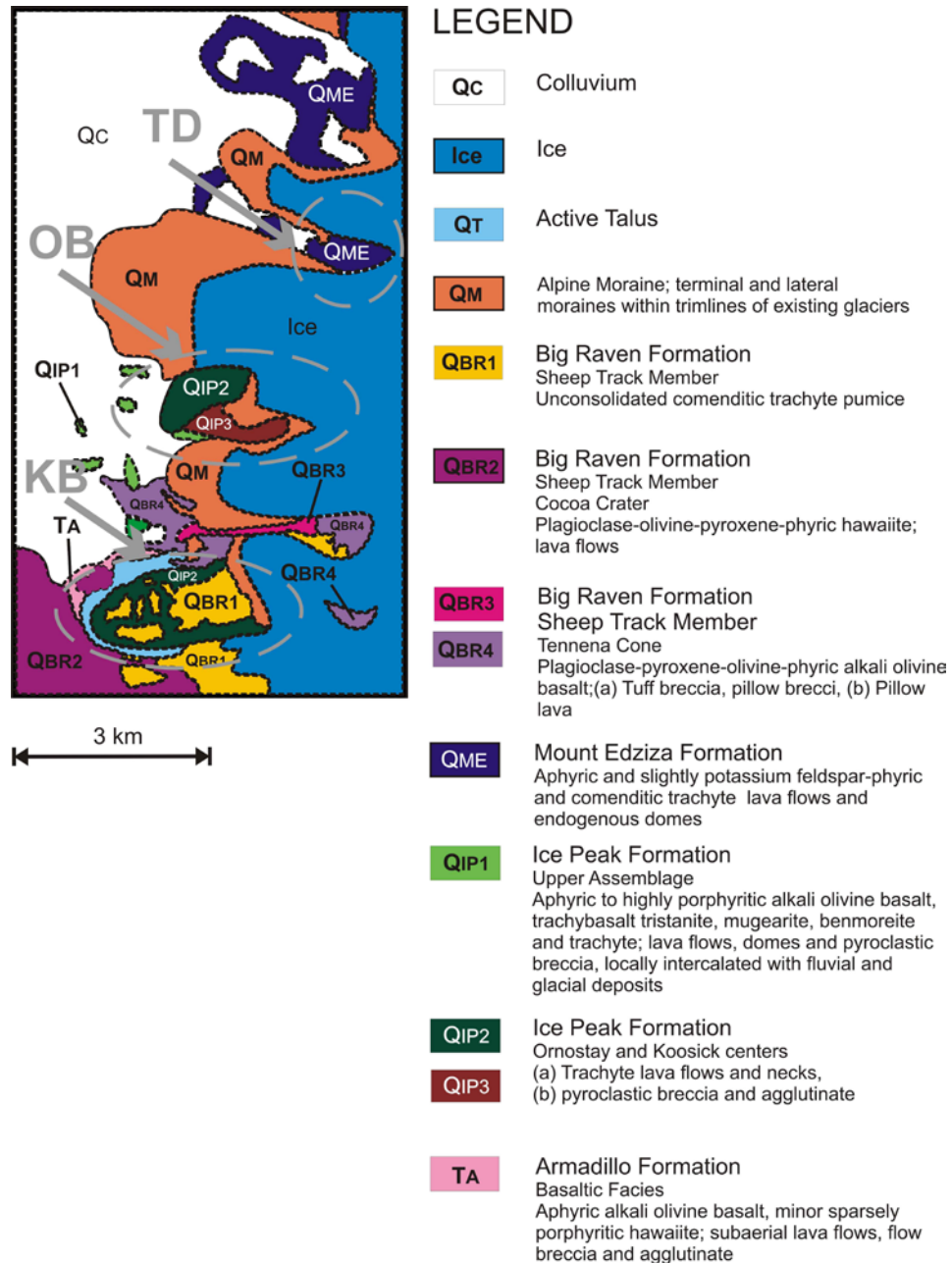


Figure 7: Simplified geological map showing the three field areas studied (TD, OB, KB) (after Souther,1992).

8.1 ARMADILLO FORMATION TRACHYTE

Within the Armadillo Formation, trachyte lavas occur at several locations at the MEVC (Souther, 1992). A 9-18 m thick trachyte flow lies upon an east-dipping surface of the underlying Cartoon Ridge comendite lava flows. Trachyte can also be found within the Armadillo caldera. Inside the structure, rocks below 1975 m elevation are highly fractured trachytes and breccias that have undergone hydrothermal alteration. The trachytes here are massive, green, fine grained, and porphyritic. Overlying these rocks is 180 m thick dark olive green trachyte lava flows each 3-9 m thick. There is little to no pyroclastic material between the units, rarely any textural or color change, or alteration of flow boundaries. Grooves and striations on trachyte lava surfaces identified at certain locations within the formation are attributed by Souther (1992) to cooling lava continuing to move until the flow was almost completely solid. Armadillo trachytes have been interpreted by Souther (1992) to have been erupted in predominately subaerial settings.

8.2 SPECTRUM FORMATION TRACHYTE

Souther (1992) identified four characteristic zones within the trachyte lava flows of the Spectrum formation (Fig 8). A basal quenched zone is composed mainly of glass (or devtrified glass) overlain by a lower flow zone with layering/banding, followed by a central massive core capped by an upper breccia zone. The relative thickness and proportion of these four zones varies with distance from the vent, with composition, and with flow thickness. The basal zone is relatively thin proximally and is replaced by a relatively thick layer of basal flow breccia distally.

Flow layering in general is less distinct than the layering seen within the interbedded rhyolite flows. Most of the trachytes within the Spectrum Range are medium to dark olive-green aphanitic rocks with small 1-2 mm randomly oriented feldspar phenocrysts. Distally, these flows develop thick basal and upper breccia zones which commonly exceed in thickness the massive core. At the top and bottom of these flows, the massive core is cut by a boxwork of healed fractures formed by autobrecciation of the nearly solid lava during late stage movement.

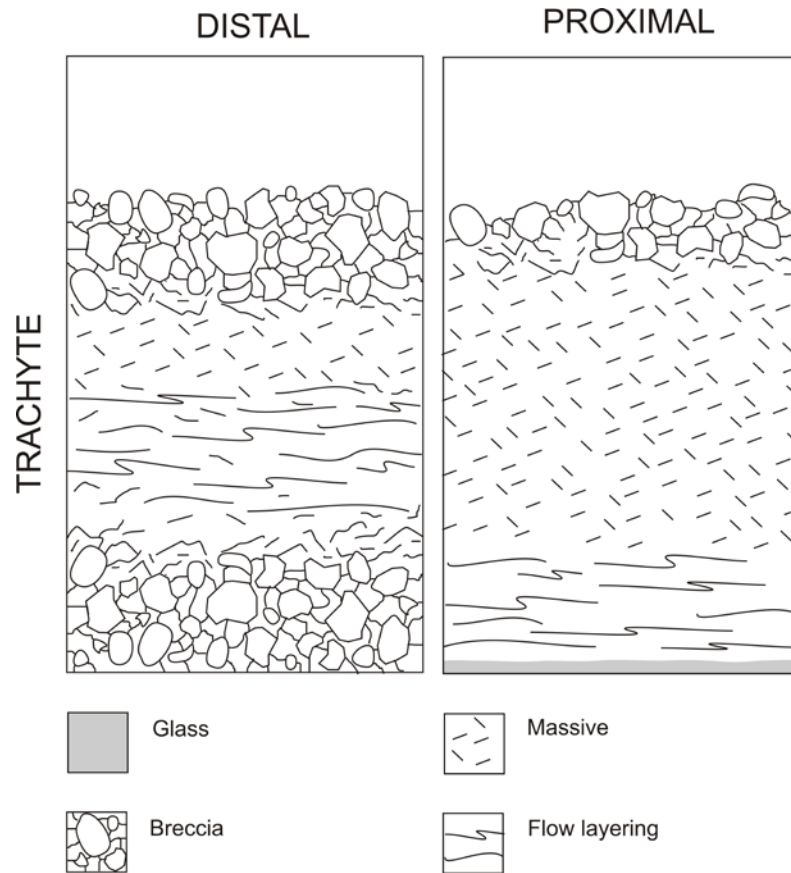


Figure 8: Sketch showing the morphology of distal and proximal facies of Spectrum Formation trachyte lava flows. (after Souther, 1992). Note the increase in proportion of basal breccia with distance and corresponding decrease in basal flow layering. Such a change presumably reflects an increase in viscosity on cooling with distance from the vent. The exact mechanism of emplacement is not clear from this sketch or Souther’s description/interpretation, but flow banding on this scale is typical of highly viscous lava flows that are mostly emplaced “en masse” (“plug-like”) with some internal ductile deformation in proximal/hotter regions, and brittle zones developing in areas of higher shear and lower temperature (especially at the base and distally)

The massive core zone comprises the majority of the flow in thicker flows. Proximally flows tend to have thicker basal vitreous layers and thinner upper breccia zones than distal flows. Distal flows have thicker basal breccias. Both of these textural changes with distances presumably reflect an increase of viscosity on cooling. Such textures also appear to suggest that

the Spectrum trachytes were most likely emplaced by a plug flow mechanism proximally evolving into aa-flow like traction with distance. Souther (1992) suggested that the Spectrum formation was erupted in a subaerial environment.

8.3 PYRAMID FORMATION TRACHYTE

The Pyramid is a trachyte dome within the Pyramid formation (Fig 6). The dome is about 366 m high and slightly more than 1 km across. Concentric and inward dipping joint sets are well developed within the dome. The trachyte here is coarsely and abundantly porphyritic with up to 50% stout, euhedral alkali feldspar phenocrysts from 0.5-2 cm across in a white aphanitic matrix with opaque oxides. Souther (1992) suggested that Pyramid dome formed (i.e. dammed) Tut Lake, a glacial lake with which later eruptions interacted, although Pyramid Dome itself likely erupted subaerially approximately 0.94 ± 0.5 Ma (Souther, 1992).

8.4 ICE PEAK FORMATION TRACHYTE

The trachytic lava flows of the Ice Volcano edifice are greenish grey flows of up to 90 m thick displaying long smooth columns and flaggy flow cleavage. They are either non-porphyritic or contain a small percentage of clear, tabular feldspar crystals less than 1 cm long. They are pale green to greenish grey with long smooth columns and flaggy flow cleavage. Most of these flows are underlain by light colored pyroclastic breccia or ash. The main flow unit grades from a dense dark flaggy trachyte at the base to a lighter green, less dense porous trachyte towards the

top of the main unit. The neck is a trachytic body approximately 300 m in diameter and 215 m high on Sorcery Ridge. The neck is a satellite center of Ice Peak age and consists of two main structural zones. The first is an outer cylinder of concentric shells from 2.5-2.5 m thick of fine grained foliated trachyte. This zone also exhibits centripetal arrangements of horizontal columns, normal to the cylinder walls that are well developed. The second zone is the inner core of vertical, closely stacked planar or gently curved tabular bodies of similar, although coarser grained trachyte. The arrangements of columns in this zone are similar to that of the first zone, although they are larger and less regular and have developed normal to the walls of the intrusion. Each of these outer shell and inner tabulate cores has developed its own distinct tier of columns separated from the next tier by a 15 cm to 0.5 m zone of structureless, greenish-grey porous trachyte. Altered and sintered basaltic pyroclastic deposits of Sorcery Ridge enclose the massive trachyte core of the neck. The tabular, dike-like bodies of the interior core are dark grey, lustrous, coarse-grained trachyte lacking any obvious fabric (Souther, 1992).

Ornostay Bluff (OB) and **Koosick Bluff (KB)** comprise thick trachytic lava flows and/or sequence of lava flows within the Ice Peak Formation and are two of the three selected field sites for this study (Figs 5 and 6). What follows in this section is the description of these two bluffs according to Souther (1992). New descriptions of these bluffs are given in section 12 and interpreted in section 13. Both features rise above the surrounding plateau by 60-90 m. Koosick Bluff is nearly 2 km long and over 1 km wide. These flows slope from east to west at an approximate gradient of 5%. The trachyte within Koosick is generally dense and dark green in appearance. Some structures such as flaggy jointing, flow layering, and large diameter columns that persist throughout the majority of the flow are also present at Koosick. According to Souther's account (1992), the upper most portions of Koosick are a 9-12 m zone of structureless

porous trachyte that only locally exhibits flow banding. Koosick appears to be comprised of only one flow unit. The source for Koosick Bluff is concealed by talus near the summit ice cap. The source for OB is also concealed by talus near the summit ice cap although part of a tephra cone also exists in this area. The tephra cone exposed in nunataks and beneath the southern edge of the flow consists of fine, lapilli sized pumice, glassy trachyte, and rock fragments in a matrix of brown altered ash and iron oxide cement. The tephra is well bedded with a westwardly dip of approximately 8°. Souther (1992) attributes the steep frontal cliffs of both Koosick and Ornostay bluffs to potential ponding against ice. Further evidence, a K-Ar age date of 1.5 +/- 0.4 Ma, may also put the time of eruption as coinciding with a glacial advance in the area (Souther 1992).

8.5 MOUNT EDZIZA FORMATION TRACHYTE

The central composite cone of Mount Edziza, a member of Mount Edziza Formation is presently largely covered by an ice cap (Fig 6). The 3 km diameter summit crater can be distinguished by a circular trace of nunataks that protrude through the ice. The spires of trachytic lava are greenish grey in appearance having randomly oriented laths of feldspar 3-5 mm across. Structures within the spires include well-formed, vertically extensive, small diameter columns (Souther, 1992). Along other exposed portions of the cone Edziza Formation lava flows and breccias are observable. The base of the cone is comprised of a chaotic pile of breccias and crudely columnar jointed trachyte lenses up to 120 m long and 15 m in thickness. Moving upwards, massive lava flows begin to predominate over the breccias with individual cooling units reaching 150 m in thickness. These lava flows exhibit well-developed flow layering that

commonly creates zones of weakness and flaggy textures as the result of weathering. Small diameter columns are common throughout the flows and develop normal to the flow cleavage.

Three other “domes” of Edziza Formation age exist of the flanks of the main Edziza cone, namely Nanook Dome, Triangle Dome, and Glacier Dome. Note that the term “dome” is used in the geomorphological sense and was not used by Souther (1992) nor this author to necessarily indicate emplacement in the volcanological sense of a lava dome. Nanook Dome is the largest (0.75 km in diameter) of the three and exhibits steep sides that rise 150-200 m. Flow cleavage and fanning columns within the inner portions along with an outer rind of vesicular agglutinate trachyte characterize this domes appearance. The base of the dome is exposed in one location revealing a 15 m section of spherulitic glass and pumice. Tiers of short, well-formed columns that fan outward are observable along the northeastern corner of the dome. The 150 m of nearly vertical sides of Nanook Dome are actually formed by three trachyte cooling units with weaker less resistant layers between them (Souther, 1992). Glacier Dome, a 210 m high construct, is comprised of light silvery-green porphyritic trachyte with crudely aligned alkali feldspar up to 1 cm across and 1 mm to 5 cm hackly elongate voids. Flow layering observed around the dome’s margins dips from 45° to 60° outward (Souther, 1992). Both Glacier Dome and Triangle Dome have concentric flow layering parallel to the present surface as well as long thin columns normal to the surface (Souther, 1992). Souther (1992) describes Triangle Dome high on the west side of the Mount Edziza central cone (Figs 5 and 6), composed of light silvery-green porphyritic trachyte containing small, crudely aligned laths of clear alkali feldspar up to 1 cm across. The lava of Triangle dome also contains ragged, polygonal voids, varying from less than 1 mm to 3-5 cm in size, with rough hackly interior surfaces.

Souther (1992) suggested that most eruptive products during Edziza Formation time erupted subaerially, although there is the possibility that the regional glaciation that culminated just prior to Edziza time, could have lingered into this time period approximately 0.9 Ma (Souther, 1992).

8.6 KAKIDDI FORMATION TRACHYTE

A single (?) trachyte lava flow from the Kakiddi Formation is continuously exposed for 7 km, is almost 1 km in width, and ranges from 60-120 m in thickness. The sources of this flow are unknown and shrouded by current ice along the summit. The flow(s) has consistently subhorizontal flow layering. In areas where the flow has been eroded to reveal the inner portion, large 1-2 m thick columns extend vertically through the flow. The lava was interpreted to have erupted subaerially (Souther, 1992).

9.0 OVERVIEW OF EMPLACEMENT AND STRUCTURE OF INTERMEDIATE AND FELSIC LAVAS

This section is a brief overview of the emplacement mechanisms and resultant structures in lava flows of intermediate and felsic composition. Structures related to cooling (including columnar jointing) are also briefly reviewed in this section.

Note that discussion on the emplacement mechanisms and structures in trachytic lavas is given in the next section (section 10).

9.1 SUBAERIAL INTERMEDIATE AND FELSIC LAVAS

Lava flows are the surface manifestation of an outpouring of coherent lava from a volcanic vent. Subaerially erupted lavas can produce flows with varying characteristics, thicknesses, and aspect ratios depending on several factors including the topographic surface upon which the flows erupt, the eruption temperature, the chemical composition, crystal content, volatile content, and viscosity of the lava. All of these variables may also change as the flow moves away from its source.

Lavas erupted onto the surface commonly display features that are attributed to flowage. Examples of these features include; planar domains of differing crystal abundance that create flow banding, crystal alignment often interpreted as shear zones (Smith, 2002), local internal

deformation of crystals such as brittle boudinage, elongate vesicles, and amygdales, and imbrications of elongate crystals (Smith, 2002; Ventura et al., 1995). Ductile tearing and subsequent brittle fracture record flow movement during the brittle-ductile transition. These features are formed when the driving forces of the flow (gravity, magma pressure, eruption velocity) overcome resistive forces (viscosity, basal friction). When driving forces dominate, flow-related textures may be more developed. Alternatively, when resistive forces prevail, the flow and therefore associated features terminate (Smith, 2002).

Crystal alignment is a relatively common structural texture in volcanic rocks. The crystals involved may be those within the groundmass or phenocrysts, or both. Specifically, the trachytic textures involve the sub-parallel to parallel alignment of microcrystalline feldspar laths. Repeated domains of textural features, such as crystal alignment, define textural domains within the igneous rock. Two main types are identified, crystal abundance and crystal orientation (Smith, 2002). Crystal alignment domains are commonly planar and contain alternating zones of crystals aligned at low-angle with respect to the domain boundary with crystals aligned at higher-angles. Banding common to felsic to intermediate composition lava flows comprise crystal abundance domains. Both types of domains may vary from millimeter to meter in thickness (Smith, 2002). Furthermore, these planar domains may be further deformed. Banding and crystal alignment textures may be folded creating a complex swirling pattern. Boudins, evident as segments separated by gaps or thin ribbons, are another observable result of planar feature deformation. In the case of boudins, brittle (resulting in the formation of gaps) or ductile (resulting in the formation of ribbons) deformation is attributed to planar-parallel tension (Smith, 2002).

Microphenocrysts may show structural domains surrounding larger phenocrysts. Microphenocrysts may appear folded or otherwise disturbed by the presence of the phenocryst. Another common attribute of volcanic rocks are vesicles. Surface tension and bubble pressure dictate that vesicles are typically spherical during gas expansion. Any alteration in this shape, including ellipsoidal or elongate vesicles, is associated with magma or lava flow or movement of the vapor phase through the magma. Deflation of vesicles due to escape of vapour or cooling and volume reduction of the vapour can result in partially to completely collapsed vesicles (Smith, 2002). Elipsoidal or elongate vesicles may form linear or planar domains. Larger scale changes in structural domains can be further related to zones within a flow of differing deformation patterns (Ventura et al., 1995). Deformation commonly increases from the center of the flow outward towards the margins that are more viscous from being cooler relative to the lava at the center of the flow. This viscosity and rheological difference leads to the development of discrete preferred orientation and imbrication of elongate crystals. Additionally the random orientation of crystals in the inner zone supports a plug flow mechanism of a pseudoplastic lava. The zones of crystal alignments and imbrication structures may be the result of a more plastic plug flow moving between two non-deforming walls (Ventura et al., 1995).

Textures in volcanic rocks preserve the syn-kinematic, or related directly to flow of the lava. All of these structures mentioned may act as gauges of strain, vorticity, stress, pressure, strain rate, temperature and rheology of the lava. The rheological behavior trend from brittle to ductile is most commonly associated with temperature changes and heat loss over time as lava cooled. Crystal contents, especially at high concentrations influence rheology and result in strong crystal interactions producing unpredictable lava behavior. Fabrics of crystals interlocked into a mesh can be pulled apart by tension allowing residual melt to be drawn up into the

resulting voids (Smith, 2002). It is further suggested that high crystal concentrations dictate the change from shear thinning to shear thickening lava flows (Smith, 1996).

9.2 STRUCTURES RELATED TO FLOW EMPLACEMENT

Flow-related structures from magma transport and extrusion are syn-kinematic textures. Post-kinematic structures include those that are taking place as the lava cools and crystallizes. These can include crystallization, column and joint formation, devitrification and hydrothermal mineralization (Smith, 2002). Strain rates within lava flows changes over time, starting at high rates and decreasing over time as the flow loses heat. The viscosity also increases over time through cooling, crystallization and volatile loss and thus changing deformation from ductile and plastic to brittle. Strain may not always be uniformly distributed over the flow either, rather focusing in localized areas as shear zones. These areas become weaker than the surrounding magma and strain continues to focus in this area resulting in localized structures. Similarly, cooling is not uniform over the extent of the flow either. Chilled outer rinds of lava flows develop and result in folding of the surface of the flow, independent of the interior (Smith, 2002).

9.3 STRUCTURES FORMED BY COOLING-CONTRACTION

Lava cooling is dominated by three major mechanisms: conduction, convection, and radiation. Cooled lava flows can exhibit various structures within that provide evidence of

movement (flow banding, tension gashes, stretched vesicles, aligned phenocrysts, etc), cooling structures (columnar jointing and fracturing, etc), and associated characteristic weathering patterns (flaggy jointing). Many subaerially and subaqueously cooled lavas have columnar joints that form with fracture orientation perpendicular to the cooling surface and joints that propagate normal to the direction of maximum tensile stress. (Aydin and DeGraff, 1988). Lescinsky and Fink (2000) suggest further that magma composition also plays a role in column fracture and spacing, reporting that silicic lavas have more narrow columns whereas mafic lavas are much greater in diameter.

Table 2: Description of fractures

Description of fractures found in lavas that have interacted with ice (after Lescinsky and Fink, 2000)

Fracture Type	Description	Inferred Origin
<i>Glassy Flow Margins</i>		
Shards	Small fragments of glassy lava, commonly altered to palagonite; found disaggregated as hyaloclastites in association with lava pillows or pillow fragments	Rapid cooling and fracturing (granulation) of lava in contact with water, in some cases followed by spallation.
Hackly fractures	Chaotic, arcuate fractures with a range of orientations and crosscutting relationships; may have palagonite along fractures	Rapid cooling and fracture sometimes "explosively" steam migration disrupting isotherms
Pseudopillow fractures and secondary fractures	Arcuate fractures with associated small, perpendicular, secondary fractures; palagonite along fracture	Cooling by water/steam penetration into rock with relatively well-established isotherms that become locally disrupted resulting in secondary fractures.
Sheet-like fractures	Parallel, planar fractures extend beyond the sides of an individual column, in some places reaching lengths of more than 5 m; may be palagonite along fracture	Cooling with well-established isotherms with extension of wide fractures with well-developed orthogonal cross cutting fractures
Polygonal fractures, columnar joints	Adjacent fractures intersect to define regular polygons. Normally parallel, but may fan or bend	Cooling with well-established isotherms with isotropic stress field; little or no fluid flow
<i>Crystalline Flow Interior</i>		
Platy fractures, sheeting joints	Fractures for overlapping plates that are often closely spaced and break around phenocrysts. Fractures tend to be parallel to the flow base, except near the boundary with the carapace, where they are oriented parallel to the flow margin.	Since these interior fractures parallel flow direction and occurred after the lava had substantially crystallized, they are probably related to late stage shear of the lava flow and or microlite orientation
Broad polygonal fractures, megacolumns	Broad polygonal joint sets cutting through flow interior. Fractures break around phenocrysts.	Late stage cooling and contraction, somewhat irregular due to preexisting platy fractures; in some cases, one face will have formed earlier, prior to development of platy fractures

Column size generally changes within the mass of the flow as well as seen by column widths increasing towards the interior of the flow due to fracture termination as the fractures propagated (Fig 9). The fractures create ridges along the surfaces of the columns preserving evidence for staggered periods of crack propagation. Columns at the base of flows are typically larger as well, fining upward (Lescinsky and Fink, 2000). Cooling by radiation and atmospheric convection at the surface of the lava flow is slower than convective cooling by steam or water penetrating the flow (Lescinsky and Fink, 2000). These different mechanisms of cooling cause the difference in textures and identification of zones within the cooling unit (Table 2). Columns are more developed with increased fracture spacing as flow cooling rates decrease. The cooling rate of any lava is primarily dependent upon the lava's thermal diffusivity, those having higher thermal diffusivities such as rhyolite cooling more quickly than their lower diffusivity basaltic counterparts. Column fracture spacing is also controlled by the physical properties of the magma that vary with composition such as Young's modulus, Poisson's ratio, and thermal expansivity causing smaller columns in felsic lavas and larger columns in mafic lavas (Lescinsky and Fink, 2000).

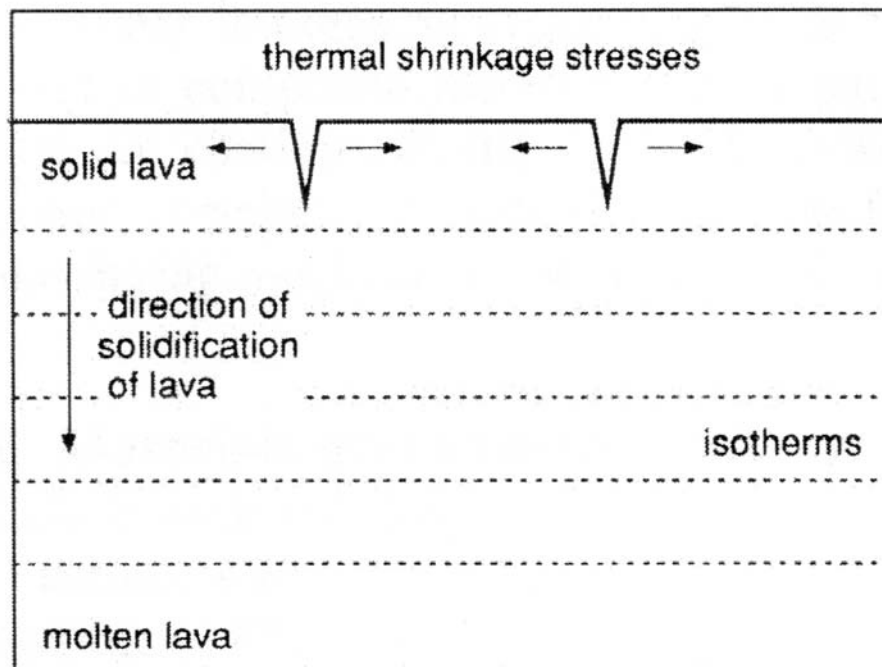


Figure 9: A schematic sketch of formation of shrinkage cracks in cooling lava flows.

**Note the cracks begin at the surface and propagate inward towards the molten interior of the flow.
(after Hull and Caddock, 1999)**

The Columbia River Basalt Group exhibits well-developed colonnades of well-formed polygonal columns and entablature structures of smaller column diameters and irregular fracture patterns that formed during the cooling of individual basaltic lava flows (Long and Wood, 1986). Generally, the colonnade is found in the lowermost 10-30% of the flow and sometimes the uppermost 10-20% and the entablature occupies the central 60-70%. What is remarkable about the two structural regions is the textural features are reverse of what would be expected for normal conductive cooling of flow margins compared with the interior of the flow. Rocks of the colonnade have coarser oxide crystals and less glass than those of the entablature which exhibit

smaller oxide crystals and much more glass (Long and Wood, 1986). The increased rate of cooling is attributed to influx and downward migration of water through cracks causing convective cooling of the underlying lava. Through modeling it has shown that the water infiltrations from above can explain the presence of the thick, quenched, flow interior and resulting entablature if the infiltration front moves downward through the flow just behind the lava solidification front.

9.4 SUBAQUEOUS INTERMEDIATE AND FELSIC LAVAS

Pillows are commonly associated with subaqueous basaltic lava eruptions, but they have also been identified in many andesites in Japan and other areas. DeRita, et al. (2001) noted that the main difference between subaqueously and subaerially erupted rhyolitic lava domes is that in subaqueous eruptions, pervasive brecciation is much more common. Therefore, subaqueously emplaced domes are typically dominated by brecciated hyaloclastite instead of coherent lava (see also Scutter et al., 1998). In subaqueous environments, the final shape of the dome as well as the rheologic behavior of the lava as it is extruded is largely controlled by the thickness of this hyaloclastite layer. The hyaloclastite layer is analogous to the crust that forms on subaerial lava flows, therefore the thickness of this layer dictates how well the interior of the flow is insulated from cooling as well as creating avenues of weakness for further lava intrusion to follow (DeRita et al., 2001). Lava is initially erupted into the bottom of a body of water where it produces hyaloclastite of varying degrees. The degree of brecciation of this initial effusive flow generally decreases inward, from fine through coarse grained hyaloclastite to a coherent section of lava flow. The extent of brecciation and hyaloclastite grain size is a direct representation of the

efficiency of magma- water interaction. As further pulses of lava intrude into the loose pile of brecciated hyalocastite they produce concentric and radial fractures as well as normal faulting. These fractures allow further infiltration of water into the pile and further fragmentation. Lava intruding after these processes typically follows the newly created fractures and faulting to fill areas of saturated hyalocastite.

The cooling rate and environment determine the gross morphology of final dome structures. Rapid cooling rates favor thicker breccias layers at the surface of the dome, causing domes to grow taller faster than their slower cooling rater counterparts in subaerial environments. The substrate surface texture, if rough, may impede the flow of cooling water through the base of the dome also resulting in taller rather than wider domes (DeRita et al., 2001). Both of these mechanisms favor vertical growth, but there are several factors that work against tall domes. The dome still will not exceed the gravity stability threshold without slides of hyaloclastite flowing down the sides of the structure forming a wider base. Obviously, the thicker layers of loose breccias that occur in subaqueous domes provide more material for collapse and slides making it easier to widen the base of a subaqueous dome when compared with a subaerial dome (DeRita et al., 2001).

9.5 SUB-ICE AND/OR ICE-CONTACT INTERMEDIATE AND FELSIC LAVAS

There is an increasing amount of literature concerned with subglacial or ice-contact lavas of felsic or intermediate composition. Most of this literature either relates to studies of rhyolitic magma/lava emplaced explosively or effusively beneath ice in Iceland (e.g. Tuffen et al., 2001; Fig 10) or to subaerially emplaced andesitic and dacitic lavas that contacted ice along their

margins in the western USA (e.g. at Mount Rainier, Lescinsky and Sisson, 1988; Lescinsky and Fink, 2000; Figs 11 and 12). Some examples from both of these groups of bodies of literature are discussed in this section. There are also two studies of ice-contact andesite lavas from Mount Ruapehu, New Zealand (Sporli and Rowland, 2006) and at Mt Ember in British Columbia (Kelman et al., 2002). Both of these examples are also discussed below.

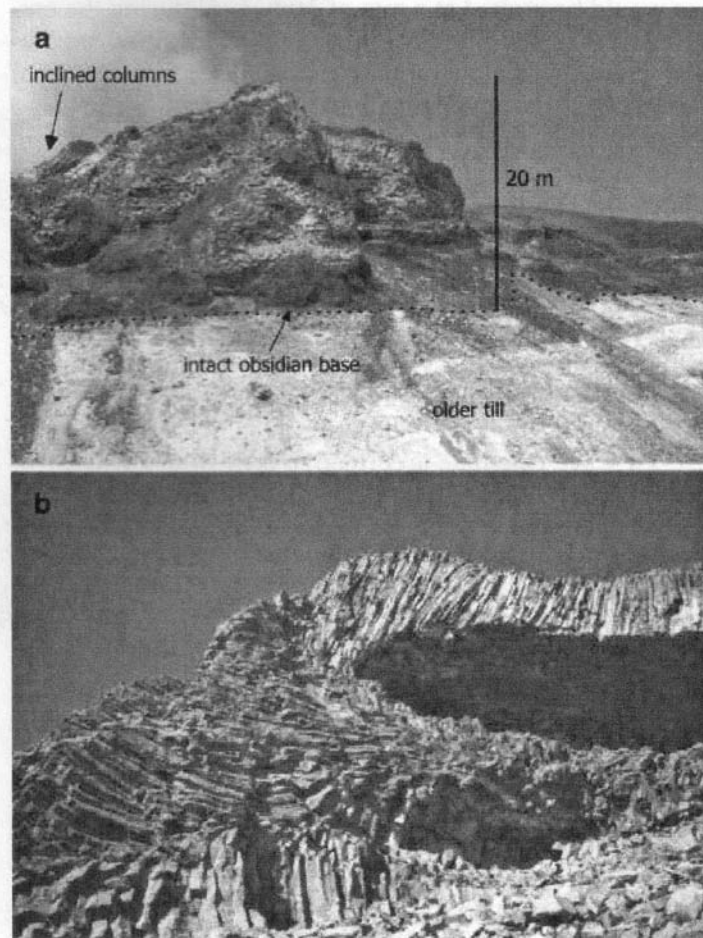


Figure 10: Photos of columnar jointing from the eastern flank of Bláhnúkur, Torfajökull

A 20 m thick rhyolite lava flow with well developed columnar jointing from the eastern flank of Bláhnúkur, Torfajökull, Iceland. A 4 m thick section of obsidian base is visible in image a. Image b shows cooling-joint patterns that suggest this lava chilled against a sub-horizontal ice-cavity roof with steeply inclined ice walls. From Tuffen et al, 2001.

A rhyolitic lava flow emplaced beneath ice at Bláhnúkur, Torfajökull, Iceland, 200 m long and 20 m thick is triangular in cross section with large columnar joints propagating in three main directions (Tuffen, et al 2001; Fig 10). There is a basal zone of columns normal to flow base, then two other orientations each running diagonally from the center of the flow towards each side and the flow margins. These columns are 10-30 cm wide with flow banding parallel to the flow base. Columns near the chilled margins of the flow are typically slightly smaller in diameter, between 10-15 m. A basal breccia is largely absent from the flow although areas of peperite are observable (Tuffen et al., 2001). Tuffen et al. (2002) suggests that the rhyolite bodies formed in small cavities in the ice. Along the upper carapaces of these flows, columnar jointing forms normal to a former steep vertical surface. Interpretation suggests this orientation shows that flow lobes were emplaced at the base of a glacier, into cavities where lava cooled against the side-walls of sub-ice cavities.

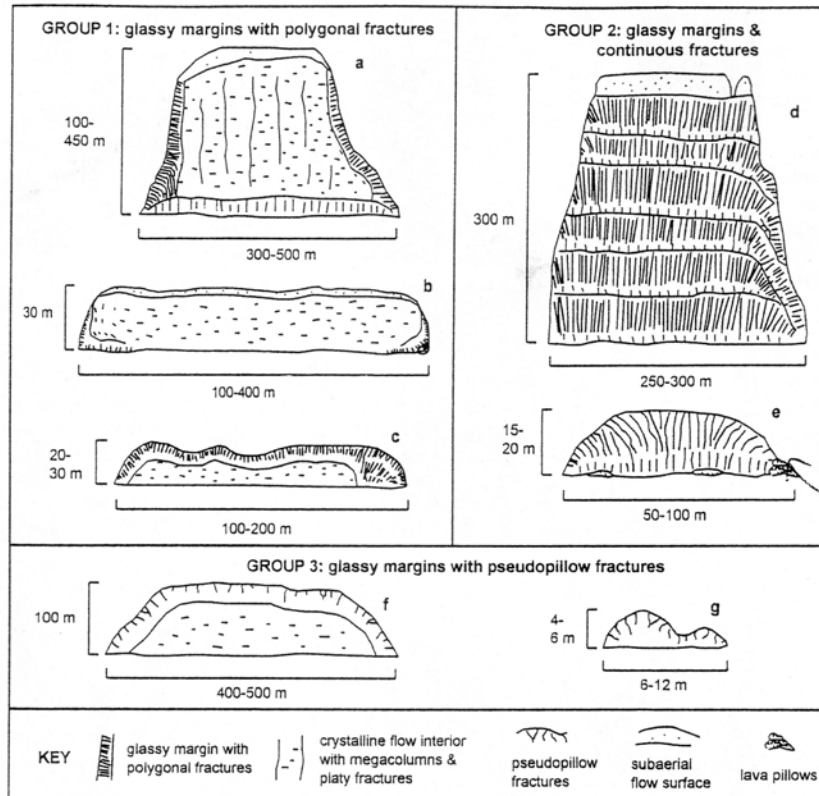


Figure 11: Sketches showing structural cross-sections and column distributions in different lava flow landforms associated with lava-ice interaction at stratovolcanoes. Group 1 landforms: (a) ridge forming lava flow; (b) smaller lava flow; (c) polygonally jointed subglacial dome. Group 2 landforms: (d) flat-topped mountain; (f) esker-like lava flow. Group 3 landforms: (f) subglacial dome with pseudopillow fractures; (g) pillow lobe flow. Sketch a and b of Group 1 relate to both Koosick Bluff and Ornostay Bluff at MEVC. Sketch c of Group 1 most represents Triangle Dome of this study. OB and KB are more difficult to interpret and may represent the interior or eroded remnant of a Group 1 type flow.. (after Lescinsky and Fink, 2000).

Subaerial, ice-contact steep – walled, ridge forming, rhyolite to andesite lava flows up to 450 m thick and extending 25 km from their source are accompanied by less extensive smaller flows of only 20-30 m in thickness are both found at Mount Rainier and are suspected to have

been emplaced in an ice-contact (alpine glacier) environment (Lescinsky and Sisson, 1998). In this location it appears that the glassy flow surface that is suspected to be common with ice contact flows is more prevalent as the thickness of the flow decreases. The upper portions of the aforementioned flows are up to 30 m sections of crystalline vesicular lava usually altered and oxidized. Just below this zone is the upper “entablature” zone composed of smaller columns accompanied by other jointing creating platy and polygonal fracturing. The basal zone of the flows have broad (30-40 cm) vertically oriented columns forming the lower colonnade zone. Less glass is apparent at the flow base and basal breccias may be minimal to completely absent (Fig 11).

Fractures in the glassy flow margins occur during the lava advance and during lava-ice interaction not post-emplacment. These fractures started at the very margin of the flow and propagated inward incrementally by thermal contraction as evident by the ridges produced on the fracture face. An irregularity in fracture spacing from irregular and closely spaced (shard-forming and hackly; Table 2) at the flow margin to regular and more widely spaced (sheet-like and polygonal; Table 2) toward the flow interior. This variable fracture spacing corresponds to decreasing cooling rates across the flow. Large variances in cooling mechanisms cause these marked changes in cooling rates. Cooling by radiation and atmospheric convection along the flow’s surface is slower and less efficient than convective cooling via water and/or steam penetrating the flow through fractures. These different mechanisms produce the zones of well-developed polygonal fracturing (“colonnade” zone) as well as the poorly-developed irregular fracturing (“entablature” zone) as seen in columnar basalts (Long and Wood, 1986). The lowest cooling rates, and therefore most organized jointing is associated with subaerial settings where higher cooling rates and more chaotic fracturing is the result of subaqueous emplacement

(Lescinsky and Fink, 2000). Large fracture spacing is the result of smaller thermal gradients whereas large thermal gradients result in closer fracture spacing. Furthermore, lava composition may dictate fracture spacing. Silicic magmas, relative to mafic magmas, have higher thermal diffusivities and enable more rapid cooling. Silicic magmas also comparatively have lower values of Young's modulus and Poisson's ratio and higher thermal expansivity, which enable closer fracture spacing (Lescinsky and Fink, 2000). Although there are correlations between fracture spacing, cooling rate, and composition, they are still poorly constrained.

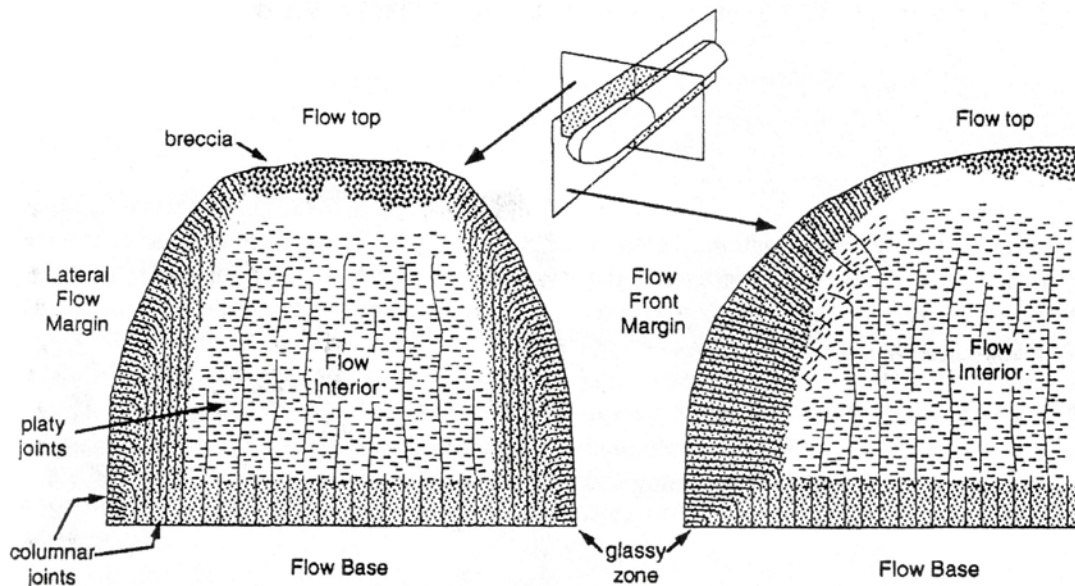


Figure 12: Idealized sketches showing cross sectional views of an ice-contact andesite-dacite lava flow and resulting structures. Note the sub-horizontal to horizontal columnar joints along the margins as well as the larger scale vertical columnar joints along the base. Vertical exaggeration ~ 5x. (after Lescinsky and Sisson, 1998).

Rhyolitic lava flow bases at Mount Rainier have 30-40 cm in diameter polygonal columnar joints oriented normal to the basal flow contact (Fig 11). Some flow banding is observable and generally parallels the underlying flow base. These columns extend 2-4 m into

the flow where they terminate at another zone of columnar joints or within the flow interior. The contact between the glassy zone and the main flow unit in the interior is a sharp transition. The flow interior is massive and well crystallized with platy joints spaced 1-5 cm apart. Unlike the polygonal columnar joints, the platy joints break around rather than through phenocrysts. The platy joints are predominately parallel to the flow base, but are more irregularly oriented near flow margins. Poorly formed cooling columns, 50-80 cm in diameter, are common in the flow interiors but are not easily distinguished except from a distance. The outermost columns are subhorizontal and perpendicular to the present day near-vertical cliff exposures that face adjacent valleys (Lescinsky and Sisson, 1998).

At Mount Rainier, steep flow sides approximately 50 m high with subhorizontal columns suggest extensive near-vertical cooling surfaces which are unlikely to have been the result of emplacement within river valleys. A possible scenario for flow movement suggests that molten flow interior moves within a solid thermally protective 'shell' (Fig 12). Additionally, situational evaluation of these flows also suggests ice-contact environment. During a period of glacial advance, lava erupted from Mount Rainier flowed down the sloped of the volcano bounded on either side by ice-filled valleys on either side (Fig 13). These thick ridge-forming perched lava flows preserve the presence of former ice and measurement and study of these types of flows leads to minimum ice thickness measurements (Lescinsky and Sisson, 1998).

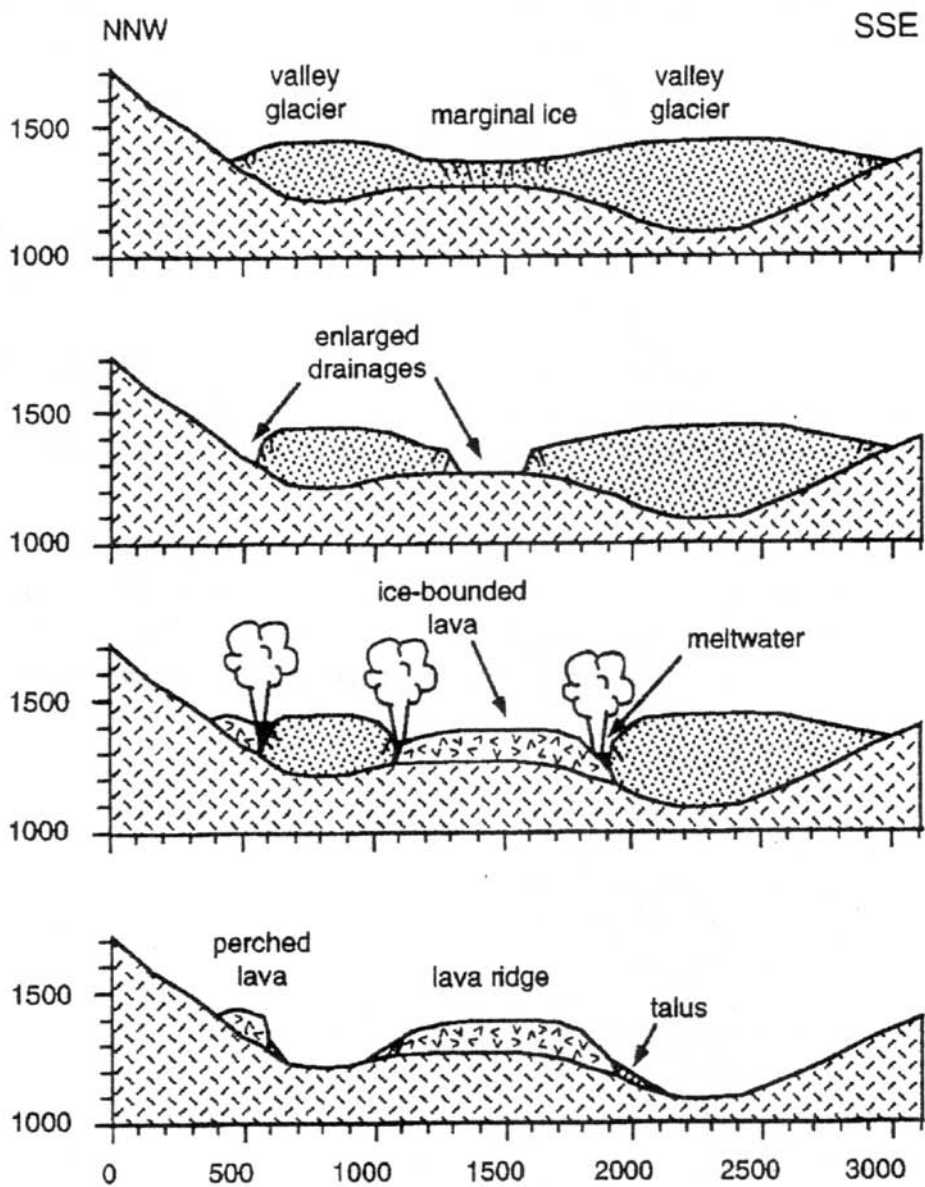


Figure 13: Cross section sketches of proposed ice-marginal formation of ridge-forming and perched lava flows at Mount Rainier, Washington. Elevations and horizontal distances in meters (after Lescinsky and Sisson, 1998).

At Ruapehu andesite volcano, New Zealand, small (10-20 cm thick) secondary columns observed approximately perpendicular to larger (0.5-3 m thick) primary cooling joints are interpreted as originating during a secondary cooling period at temperatures between the low creep and elastic regimes involving a rapid influx of large volumes of water (Sporli and Rowland 2006; Fig 14). Neither the primary or the secondary cooling joints exhibit glassy rinds that would indicate quench or rapid cooling of molten lava. The primary cooling joints are well-formed and likely formed in absence of water by conductive cooling only. The secondary columns, however, represent a secondary, stronger cooling event and may also be from a period of larger and more rapid temperature drop. This cooling event propagated from inward from the already formed primary column fracture surfaces. During this period of cooling, the andesite had solidified below the glass transition temperature; the tensile strength of the andesite would have increased along with a slight decrease in the coefficient of expansion (Sporli and Rowland, 2006). Only water could cause such a drastic period of rapid cooling in these conditions. Initial contact of the cold water and hot outer surface of the primary columns created an initial, shallow network of polygonal cracks. After further cooling and intrusion of water increasing crack-tip stresses would the fractures progress into the interior of the primary columns. Some of these secondary fractures flare, feather, and terminate prior to reaching the center of the primary column indicating an inward decrease in thermal stress. A decrease of thermal stresses in this case would suggest a change in cooling mechanism back to conductive cooling without water. This is interpreted as indicating either the supply of water became limited or was boiled away before it could interact and propagate fully through the secondary columns. These early terminations of secondary columns before reaching the interior of the primary columns are less common in the lower portions of the flow. Although there is no direct evidence, this may

suggest an abundant supply of water. There is little evidence at Ruapehu for the glassy rinds observed at Mount Rainier (Lescinsky and Sisson, 1998). The temperature drops that produced the fractures within the flow at Ruapehu occurred later in the cooling history, or below the glass transition temperature of andesite, than those of Mount Rainier. Orientations of the secondary columns are similar to the pseudopillow fractures of Lescinsky and Fink (2000) (Sporli and Rowland, 2006). It is postulated that the outer solidified skin of the flow provided a physical barrier to prevent further water influx during primary fracture formation. Water then began to seep into these fractures as the outer rind of the flow cooled allowing the presence of water during secondary fracturing event (Sporli and Rowland, 2006).

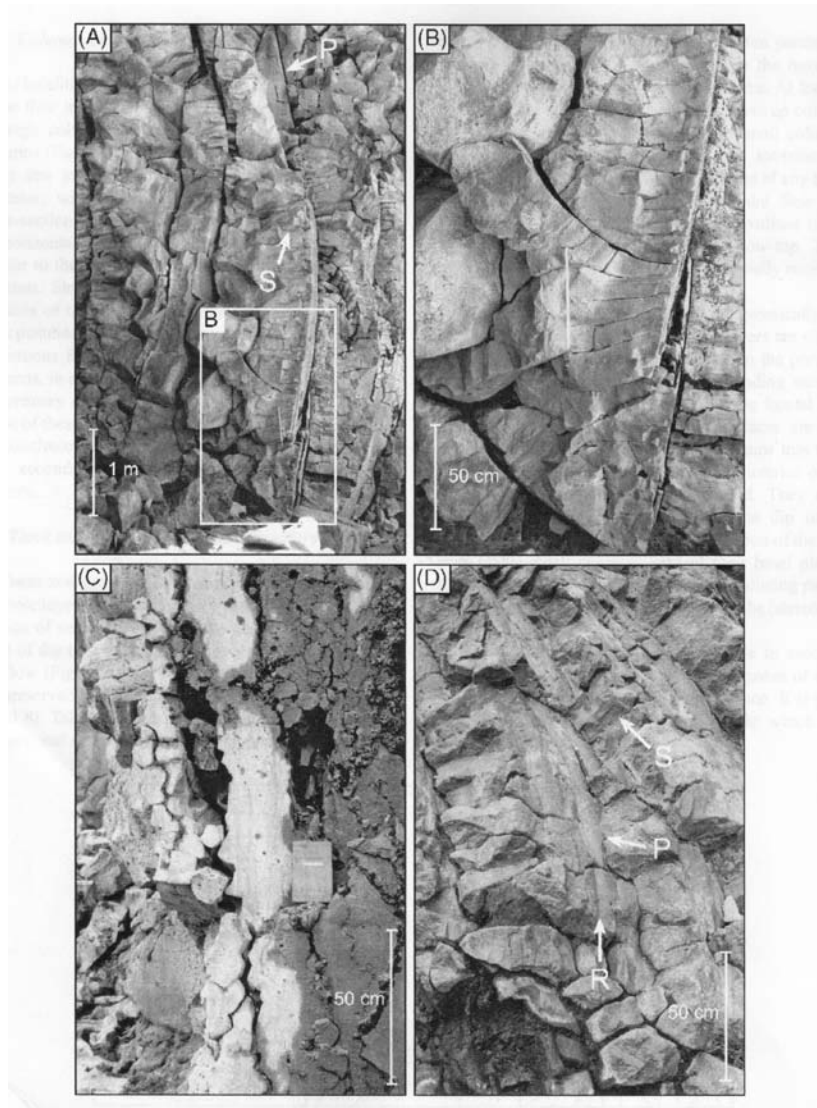


Figure 14: Photographs of secondary column structures from Spörli and Rowland's (2006)

'column on column' structures in Mount Ruapehu andesite: (A) Curved primary columns (P) with subhorizontal, smaller secondary columns (S). (B) Enlarged view of image A. The flaring of secondary columns towards the center of the primary columns is visible here. (C) Down-flow face of a primary column showing the polygonal ends of secondary columns. (D) Primary and secondary columns in frontal rind of the lava lobe. The columns here are slab-like in shape with prominent down-dip ribbing indicating horizontal fracture propagation (after Spörli and Rowland, 2006).

Steep-sided andesitic lava flows at Ember Ridge, Mount Cayley volcanic field in southwestern British Columbia display fine-scale (15-30 cm) complexly oriented columnar jointing indicating an overall domal-shaped cooling surface. Column size typically increases toward the lowest portions of the outcrop. Where column size decreases, column orientations become more chaotic. Planar jointing perpendicular to columns (10 cm) and flaggy jointing (<1 cm) occur at numerous locations. The presence of plentiful, poorly-formed, fine-scale cooling joints as well as bulbous rounded cooling surfaces and abundant glass observed at the least eroded outcrop all suggest Ember Ridge lava has cooled rapidly in a confined environment (Kelman et al., 2002). It is suggested that moderate to large quantities of hyaloclastite may also have been present surrounding these lavas shortly after eruption but has since been removed by weathering and erosion and was therefore not observed at most locations.

10.0 DISCUSSION OF EMPLACEMENT MECHANISMS AND STRUCTURES OF TRACHYTE LAVA FLOWS

The emplacement of trachyte or phonolitic lava flows has not been the focus of much research. Most of the examples of such lava flows in the literature are brief descriptions within broader accounts. This section focuses specifically on descriptions of trachyte lava flows in the literature, particularly descriptions of flow dimensions, especially thicknesses and aspect ratios, structures and emplacement mechanisms.

The purpose of this discussion is to understand if the studied bluffs, specifically Ornostay Bluff and Koosick Bluff at MEVC, have been overthickened by being ponded against ice, or if their thickness does not require any confinement. This relates to the principal research question of the project “How do trachyte-phonolite lavas that have contacted ice differ from those emplaced in a non-glacial environment?”

10.1 SUBAERIAL TRACHYTE LAVA FLOWS

Research using interferometrically processed SIR-C radar data was used to provide basic maps, morphological data, and estimate the thickness of trachyte lava flows at Karisimbi Volcano, Rwanda (MacKay et al., 1998). The trachyte flows imaged at Karisimbi are found to be as long as 12 km and average 40 – 60 m in thickness although the actual number of flows

observed is undeterminable without additional imagery or field observations. Comparison of digital elevation models (DEMs) created from this data allowed maps of flow thicknesses and in turn flow volumes to be created, resulting in volume values of up to 1 km³ for individual flows (MacKay et al., 1998).

Highly fluid, columnar jointed trachyte lavas of the South Turkana volcanoes in the Kenya Rift cover areas up to 100 km² and have flow thicknesses of 30 m or less. These flows are holocrystalline throughout with thin basal breccias and often a thin chilled margin. Along with these thin, low viscosity flows, thick and stubby flows and domes of trachyte cover limited extents and are nearly entirely degassed. These thicker forms are also columnar and platy jointed (Webb and Weaver, 1976).

Viscous trachyte lavas at Emuruangogolak Volcano in the Kenya Rift are 10-30 m thick and composed of dark green lavas with alkali feldspar phenocrysts (Weaver, 1976).

Through examination of the limited research reporting trachyte lava flow dimensions, it is concluded that subaerially emplaced trachyte lava flows “typically” have flow thicknesses of few tens of meters and extend to 12 km or more.

10.2 SUBAQUEOUS TRACHYTE LAVAS

The trachytic subaqueous lava flows of Tok Island, Korea (Sohn, 1995) are coherent and are interpreted as domelike or lobate flows accompanied by autoclastic breccias that have been erupted and brecciated in a subaqueous environment. The breccias exhibit close-fitting clast boundaries. The clasts within the breccias are angular and blocky in shape with intergranular

textures which suggest these fragmented from solidified lavas, not from melt fragmentation. Radial-columnar, concentric, and square joints persist throughout the main coherent lava flows.

LeMasurier (2002) identified trachytic pillow lavas in west Antarctica at Mount Takahē. The pillows observed are generally tubular in shape, 2-4 m long, and 1-1.5 m in diameter. The pillow structure is commonly found surrounded by hyaloclastic debris. The pillows outer texture varies from glassy margins of 3-6 cm in thickness to partial glassy rims to no rind at all. The trachyte and benmoreite lava flows are 2-10 m thick indicating their relatively low viscosity which very likely played a role in pillow formation.

Of the subaqueous trachyte lavas in the literature, the flows tend to be dome-like or lobate in morphology. Most are associated with autoclastic breccia and some additionally with hyaloclastite. Joints within these flows may be radial columnar, concentric, or square shaped.

10.3 SUBGLACIAL AND ICE-CONTACT TRACHYTE LAVAS

The step like topography and bounding cliffs identified at several localities including Hoodoo Mountain volcano, northern Canadian Cordillera suggest that phonolitic (note these are not trachytic, but they are very similar compositionally) flows were pooled against ice (Edwards et al., 2002). At Hoodoo Mountain, the distinct vertical cliffs of lava that feature finely jointed flow fronts that form steep cliffs of 50 to 200 m in height at this locality may have resulted from lava flows being dammed and ponded against thick masses of ice (Edwards and Russell, 2002). The columns at this location are generally 30 m or less in diameter and often oriented perpendicular to the vertical cliff face, although areas of complex fanning joint patterns are also present. The pattern of columnar jointing patterns is also of particular interest and perhaps quite

diagnostic of emplacement environment. The lava bodies at Hoodoo are pervasively jointed with cooling joints that reflect highly irregular cooling surfaces are commonly encased in monomict breccias. In addition, samples from the surfaces of massive bounding cliffs are cryptocrystalline. These features suggest relatively quick cooling or quenching (Edwards and Russell, 2002).

Trachydacite (note again not trachytic or phonolitic, but similar in composition) lava flows at Oraefajokull stratovolcano in Iceland have thicknesses varying from 25 m to over 75 m. The base of the flow lies on breccias formed from the glassy margins of the flow whereas the interior of the flow grades from columnar jointed to massive. The basal breccia, another section of breccia within the flow, and the surfaces of columnar joints all have pervasive pink-red staining. This alteration has been attributed to the presence of steam caused by water infiltration at the flow's surface during cooling. There is, however, a distinct lack of flow front material within the basal breccia also indicates this flow may not have developed a typical lava flow front, suggesting the flow may have contacted ice directly (Stevenson et al., 2006).

From evidence of subglacial and ice-contact documented in the literature, there are several factors that are recognized in other localities suggesting lava-ice interaction. Step-like topography of volcanic forms as well as bounding vertical cliffs suggests ice-contact influenced volcanic morphology. On these cliff faces, columns perpendicular to the cliff face further indicate a vertical cooling surface. In other areas, complex entablature-like fanning and hydrothermal alteration reflect water interaction.

11.0 DISCUSSION OF VISCOSITY, ASPECT RATIOS, AND DIMENSIONS OF TRACHYTE LAVA FLOWS

The purpose of this section is to describe and discuss the variation in the calculated viscosity, estimated dimensions (Table 3), and aspect ratios of trachyte lava flows from the literature. This is in order to ascertain if we can use calculated viscosity and dimensional data for the lava flows in the study area (Tables 3 and 4) at the MEVC (specifically OB and KB) to suggest that the flows may have been overthickened by ponding against ice

This is the believed to be the first detailed compilation of calculated viscosity data based on a large dataset of trachyte compositional data.

Lava viscosity has been identified as one of the primary controlling factors of how lava flows and domes form, move and their resultant morphologies and structures. Highly viscous lavas, such as rhyolites and potentially some trachytes, tend to flow slowly and may form semi-solid and solid portions that may additionally reduce movement. These viscous lavas are more likely to form steep sided domes and thick flows that may not flow far from their source. Less viscous lavas, such as basalts, tend to flow more easily in comparison to their more viscous counterparts. These are more likely to form broader, thinner flows that travel further from their source.

The primary factors that control viscosity of melts are temperature, pressure, chemical composition, volatile content, and crystal and bubble content. The most influential factors are

temperature, chemical composition and volatile content, since small changes in these factors have great effects on the viscosity of the melt (by several orders of magnitude) (Whittington et al., 2001).

Very little has been published directly addressing the viscosity of trachytes. This is an important factor to consider since the viscosities control the aspect ratio of unconfined flows, flow morphology, structures, velocity, and potential interaction with their substrate. **Being able to easily compare viscosities across several locations and samples of trachyte is important to help recognize any anomalous thicknesses that may indicate ponding against ice, which is of most interest here versus unconfined flow emplacement.**

Table 3: Table of comparison of MEVC trachyte flows

(in bold) and other intermediate to felsic composition lava flow thickness from the literature.

Table 3: Flow Thicknesses

Construct	Type	Thickness	Notes
Ornostay Bluff (MEVC)	Flow	75 m	Trachyte, Individual flow
Ornostay Bluff (MEVC)	Flows	90 m	Trachyte, Sequence of flows
Koosick Bluff (MEVC)	Flows	90 m	Trachyte, Individual flow
Kakiddi (MEVC)	Flow(s)?	60-120 m	Trachyte, Unknown number of flows, Souther 1996
Armadillo (MEVC)	Flows	3-9 m	Trachyte, Individual flows, Souther 1996
Armadillo (MEVC)	Flows	180 m	Trachyte, Sequence of flows, Souther 1996
Mount Rainier, Washington	Flows	15-450 m	Andesite-dacite, Individual flows, Lescinsky and Sisson, 1998
Karisimbi Volcano, Rowanda	Flows	25-140 m	Trachyte, Individual flows, MacKay et al, 1998
Santiaguito Volcano, Guatemala	Flows	31-65	Dacite, Individual flows, Harris et al, 2004
Hoodoo Mountain, British Columbia	Flows	10 - 200 m	Phonolite - Trachyte, Individual and sequences, Edwards et al, 2002
Blahnukur, Torfajokull, Iceland	Flow	20 m	Rhyolite, Tuffen et al, 2001

Viscosities of the trachyte lava flows at Karisimbi Volcano, Rwanda have been estimated based upon the spacing of large folds as seen on DEMs derived from radar data. The results are from 10^{12} Pa s for surface viscosity to 10^{10} to 10^{11} Pa s for interior viscosity, for a strain interval of 1 day (25 hr) (MacKay et al., 1998). In another laboratory study, viscosities of hydrated synthetic iron-free phonolite and trachyte melts are reported between $10^{8.4}$ and $10^{13.1}$ Pa s for water contents between 0 and 5 wt% (Whittington et al., 2001). These results indicate that the effect of water on the viscosity of the melt is different on magmas that are already partially depolymerized as opposed to fully polymerized magmas (Whittington et al., 2001). Further

research suggests that increasing Na₂O content within trachytes allows greater solubility in the melt and therefore can also play a role in final viscosity (Di Matteo et al., 2004).

The results of the study of trachyte lava viscosities calculated from analyses in the literature and MEVC analyses are presented here:

Table 4: Intermediate lava viscosities from the literature

Table of calculated (using Giordano et al 2007, ‘Viscosity of magmatic liquids’ model) intermediate composition lava viscosities from the literature. MEVC lavas in bold. * indicates the calculations were from the published literature and not calculated by this author.

Table 4: Intermediate Lava Viscosities

Location	Composition	Temperature C	Viscosity log[n (Pas)]
MEVC - Koosick Bluff	Trachyte	850	7.64
MEVC - Ornostay Bluff	Trachyte	850	5.96
MEVC - Triangle Dome	Phonolite	850	7.6
Santiaguito Flow, Guatemala (Harris et al, 2004) *	Dacite	unknown	9-10
Karisimbi, Rwanda (Harris et al, 2004) *	Trachyte	unknown	10-11
Oraefajokull stratovolcano, Iceland (Stevenson et al, 2006)	Trachy-dacite	850	5.43
The Pitcarin hotspot in the South Pacific (Hekinian et al, 2002)	Trachyte	850	4.33
The Cerro Mancenares volcanic center, Baja California (Bigioggero et al,1995)	Alkali Rhyolite (Dacite)	850	4.55
Emi Koussi volcano, Tibesti, Chad (Gouraud and Vincent, 2003)	Phonolite	850	4.49
Northern Trans-Pecos magmatic province (Barker, 1977)	Trachyte	850	5.09
Alborz Mountains, northern Iran (Davidson et al, 2004)	Trachyandesite	850	4.33
Rallier-du-Baty Peninsula, Kerguelen Archipelago (Indian Ocean) (Gagnevin et al, 2003)	Trachyte	850	4.98
Vico Volcano, Central Italy (Perini et al, 2004)	Trachyte	850	5.20
Longonot Volcano, Kenya (Rogers et al, 2004)	Trachyte	850	4.40
Cape Verde Islands and Fernando de Noronha (Gunn and Watkins, 1976)	Trachyte/Phonolite	850	4.86
Hoodoo Mountain volcano, northern Canadian Cordillera (Edwards et al., 2002)	Trachyte	850	4.96
Thirtynine Mile volcanic field, central Colorado (Wobus et al, 1990)	Trachyte	850	5.78

Aspect ratio is a common tool used in describing three-dimensional shapes and is used in various disciplines and is not specific to volcanology. The aspect ratio of a shape is simply derived by comparison of its longer dimension to its shorter dimension. Although this is a

simple comparison it is also particularly problematic with natural landforms that are susceptible to erosion and inherently variable in shape and thickness. The thickness of a flow may vary greatly over the areal extent of that flow. Additionally, measurement of such variances is difficult and inaccurate in most cases. Nonetheless, it is another use of information that adds another element for comparison to the limited number of trachyte and phonolite flows that have been studied (Table 5).

Table 5: Trachyte lava flow aspect ratios

Aspect ratio (relationship of flow thickness to aerial extent) for speculative MEVC trachyte lavas (**bold**) and the trachyte lava flows of Karisimbi Volcano. Note that the MEVC trachyte lava flow dimensions are considered very speculative, especially regarding the length of the lava flow which is almost positively been eroded, to some unknown extent. There is also possible erosion from the top of the flow and therefore thickness is also speculative. Therefore, the resulting aspect ratio derived from these two measurements is very speculative.

Table 5: Trachyte Lava Flow Aspect Ratios

Location	Flow ID	Aspect Ratio
MEVC	KB	0.03
MEVC	OB (one flow)	0.069
MEVC	OB (entire unit)	0.08
Karisimbi Volcano, Rwanda	#3	0.11
Karisimbi Volcano, Rwanda	#6	0.16
Karisimbi Volcano, Rwanda	#10	0.095
Karisimbi Volcano, Rwanda	#11	0.06

Aspect ratio is the ratio of flow thickness to flow area extent. Generally speaking basalts have low aspect ratios (< 0.02), i.e. they are relatively thin and cover large areas. Rhyolites have higher aspect ratios, relatively thick flow of little extent. It is clear from Table 5 that trachytes are unique in that they can range between these two extremes and vary widely. **The range of**

known trachyte aspect ratios varies greatly and is hence not a particularly useful tool in identifying anomalous trachytic flow thicknesses that might have developed by confinement by ice.

Table 6: MEVC dome dimensions

Table of comparison of Triangle Dome (phonolite) and other MEVC “domal structure” dimensions.

Table 6: Dome Dimensions

Construct	Type	Height	Diameter	Notes
Triangle Dome (MEVC)	Dome	120 m	500 m	Trachyte
Pyramid Dome (MEVC)	Dome	366 m	1000 m	Trachyte (Souther, 1996)
Nanook Dome (MEVC)	Dome	150-200 m	750 m	Trachyte, Group of 3 units (Souther, 1996)
Glacier Dome (MEVC)	Dome	210 m	?	Trachyte (Souther, 1996)

Understanding the controls on magma viscosity help to identify interesting and anomalous flow structures related to viscosity (tension gashes) as well as flow morphology (thickness (Tables 3 and 6), aspect ratio (Table 5)) and may be further applied in velocity calculations. One factor affecting lava viscosity is the crystal content of the lava. The crystal contents as determined via thin section analysis for MEVC trachytes are between approximately 1% (TD) and 30% (KB, OB). Lava viscosity is calculated using the “Viscosity of Magmatic Liquids: A Model” (Giordano et al., 2008) using an estimated eruption temperature (850 C) and geochemical analysis data. The temperature selected in this case is only an estimate of an average intermediate lava eruption temperature. In addition to this assumption, the model inherently makes several assumptions as well, including a completely liquid melt. With all of

these assumptions, quantitative data for actual eruption viscosity is unachievable, but looking at the affect that changes in eruption condition variables have as well as trends in this data provides background knowledge for further interpretation. By direct comparison of magma viscosity of OB lava and crystal contents from 0% to 50% it becomes apparent there is a great impact of crystal content on flow viscosity (Fig 15).

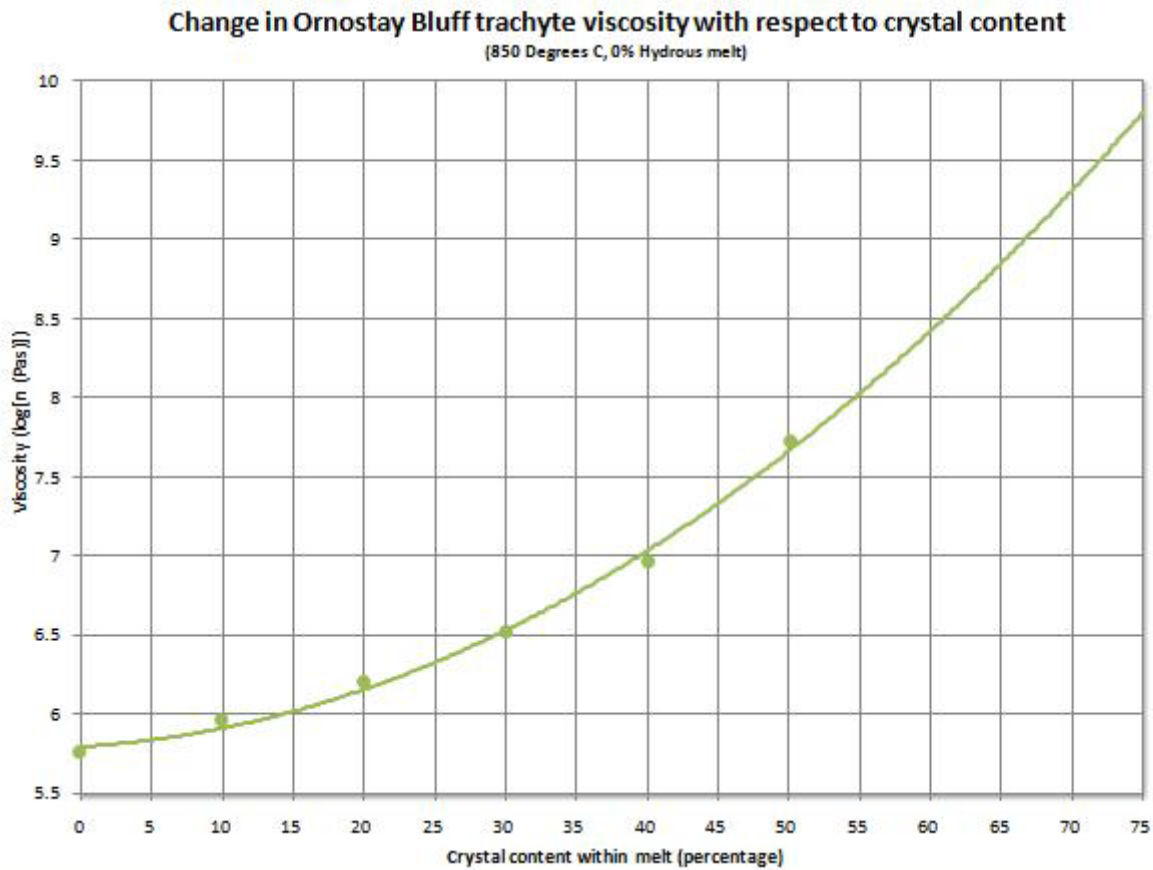


Figure 15: Chart showing calculated effects of crystal content on the viscosity of Ornostay Bluff trachyte.

12.0 DESCRIPTION OF STUDIED TRACHYTE LAVAS AT MOUNT EDZIZA VOLCANIC COMPLEX

The three bluffs of lavas studied at MEVC include Ornostay Bluff, Koosick Bluff, and Triangle Dome (Fig 5). Ornostay Bluff and Koosick Bluff are both composed of Ice Peak formation trachytic lava flows (Table 1) approximately 1.5 ± 0.4 Ma (Souther, 1992). Triangle Dome is another construct of phonolitic (Fig 16, Table 7) composition approximately 0.9 ± 0.3 Ma (Souther 1992). These areas were selected for study based on the preliminary field work, geochemical analysis, and age dating done by Souther (1992).

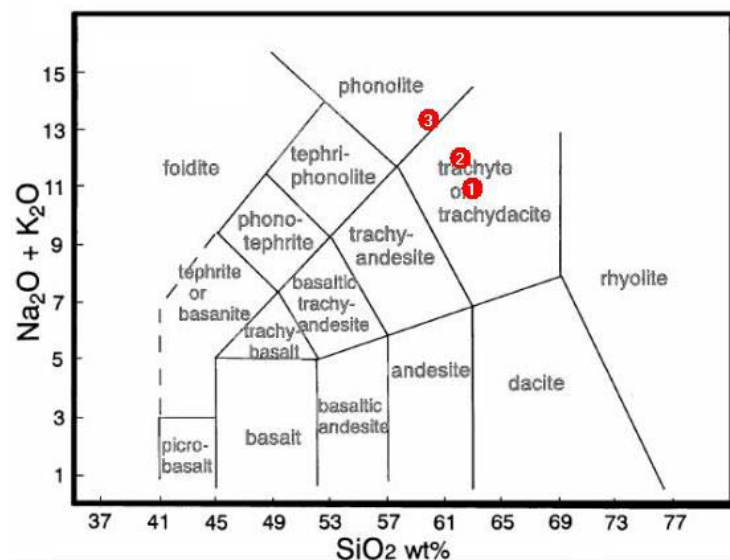


Figure 16: TAS diagram

Total Alkalis-Silica Classification of OB, KB, and TD compositions. Both OB (1) and KB (2) fall within the trachyte or trachydacite field where TD (3) is phonolite.

Table 7: Geochemical data

XRF Element Chemical Analysis of Intermediate MEVC Lavas

	E6CE5	E6KL22	E6KL23
	Ornostay Bluff	Koosick Bluff	Triangle Dome
	Trachyte	Trachyte	Phonolite
SiO ₂	62.94	62.07	59.88
TiO ₂	0.462	0.506	0.293
Al ₂ O ₃	13.4	16.38	18.21
Fe ₂ O ₃	8.71	6.72	5.41
MnO	0.157	0.134	0.127
MgO	0.13	0.27	0.26
CaO	1.07	1.68	1.19
Na ₂ O	6.44	6.35	7.66
K ₂ O	4.54	5.69	5.70
P ₂ O ₅	0.046	0.078	0.064
BaO	<d/l	114	33
Ce	195	107	144
Co	<d/l	<d/l	<d/l
Cr ₂ O ₃	18	22	18
Cu	4	13	24
Ni	5	7	7
Sc	<d/l	<d/l	<d/l
V	<d/l	<d/l	<d/l
Zn	298	118	114
LOI	1.85	0.35	1.40
Total	99.8	100.27	100.23

Note: The results are expressed as weight percent, the trace elements (BaO to Zn) as ppm (ug/g).

Total iron present has been recalculated as Fe₂O₃. In cases where most of the iron was originally in the ferrous state (usually the case with unaltered rocks) a higher total is the result.

Analyses done on fused beads prepared from ignited samples.

Detection limits are based on three times the background sigma values.

12.1 TRIANGLE DOME

Triangle Dome (Fig 17) is a spiny (Fig 18) ridge-like edifice that protrudes above the lower plateau of the MEVC, collared by alpine ice, and is located along Mount Edziza caldera's western rim. The "dome" is approximately 120 m high, 600 m wide, and 1000 m long oriented along an east-west axis. The northern, eastern, and most of the southern faces of the dome are surrounded by the alpine ice cap that currently occupies the Mount Edziza caldera. The western side of Triangle Dome is steep terrain of Edziza formation lavas and younger alpine glacial moraine. This feature is comprised of approximately 0.03 km³ of coherent lava with concentric flow layering and spectacular columnar jointing structures (Fig 19). The basal zone of the dome has long (up to 40 m), 50 cm wide, well developed, regular polygonal columns (Fig 20) and very steep sides. These columns are oriented so that they splay outwards slightly at the base (from 90° vertical to approximately 75°). Moving upwards, in some locations, a relatively thin 1 m layer of 'S' and 'C' curved columns (Fig 22) is visible capping the much larger and more well formed columns of the basal zone. From here upward the next structural zone comprises the bulk of the exposed face. These are fanning sets of columns (Fig 21), smaller in diameter than those of the basal zone and not as well-formed (Figs 23 and 24). At some locations the long axis of the columns are visible while in other areas the ends of columns are visible creating a 'lizard skin' or scaly appearance (Figs 25 and 26). This section is also geomorphically more irregular with weathered spires and spines. The uppermost sections of the dome are fissile highly weathered areas of crudely columnar jointed lava with pervasive platy jointing.

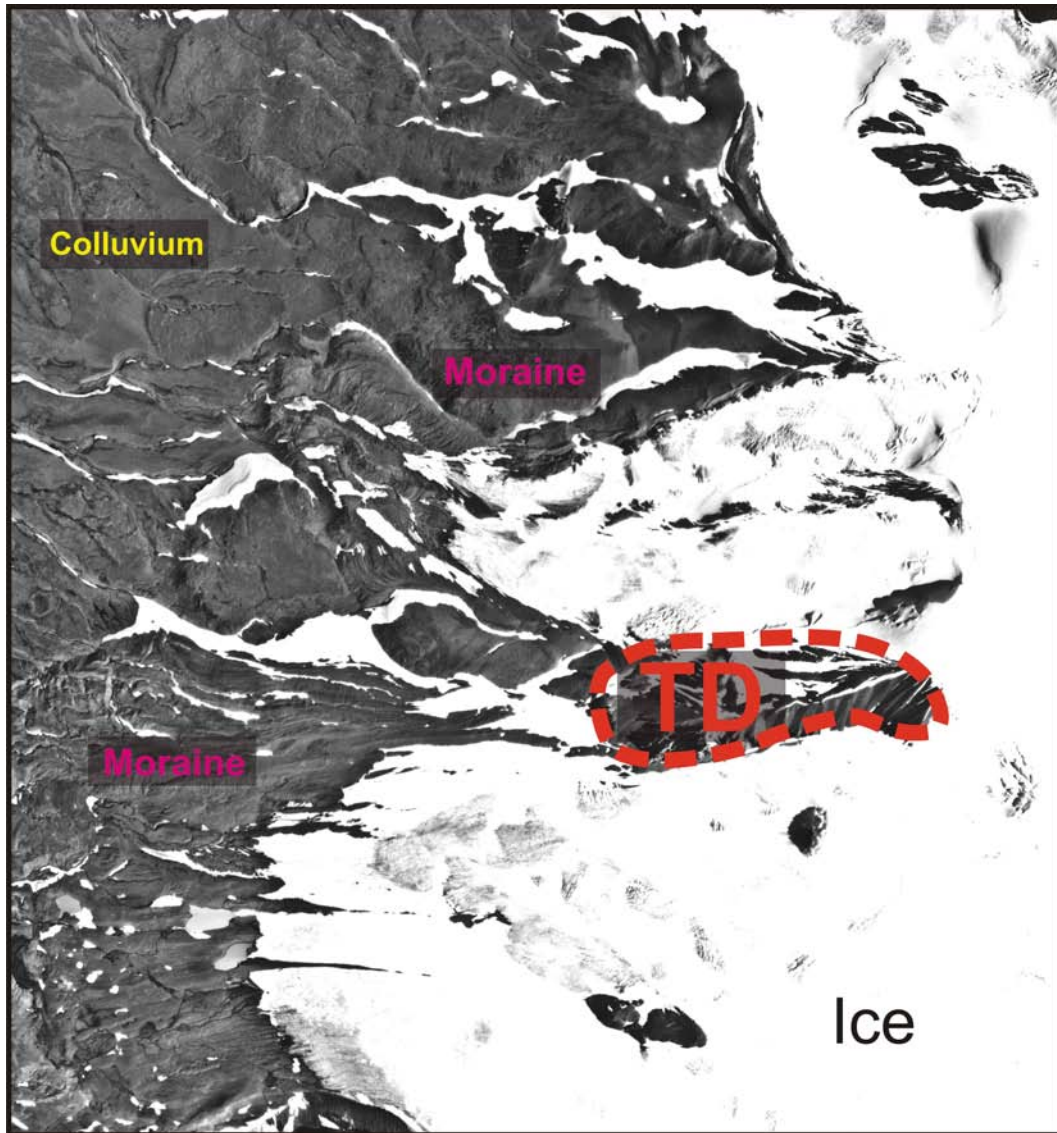


Figure 17: Aerial photo of Triangle Dome and surrounding areas.

Ice, colluvium, and moraine dominate the landscape. The evidence for recent and continued glacial interaction of TD can be seen in the collar of ice and surrounding moraine.

TD preserves a complex pattern of curvilinear, planar columnar and hackly/blocky jointing (Fig 20), but can broadly be divided into an upper and lower zone at about a maximum

of 60m above its exposed base (Fig 19). The top most portion of TD is dominated by hackly to poorly developed columnar joints and pervasive platy jointing. Local sill and dike-like areas of well-developed columnar joints and more coherent lavas are discernable by the differential weathering that has occurred along their contacts with the rest of the structure.

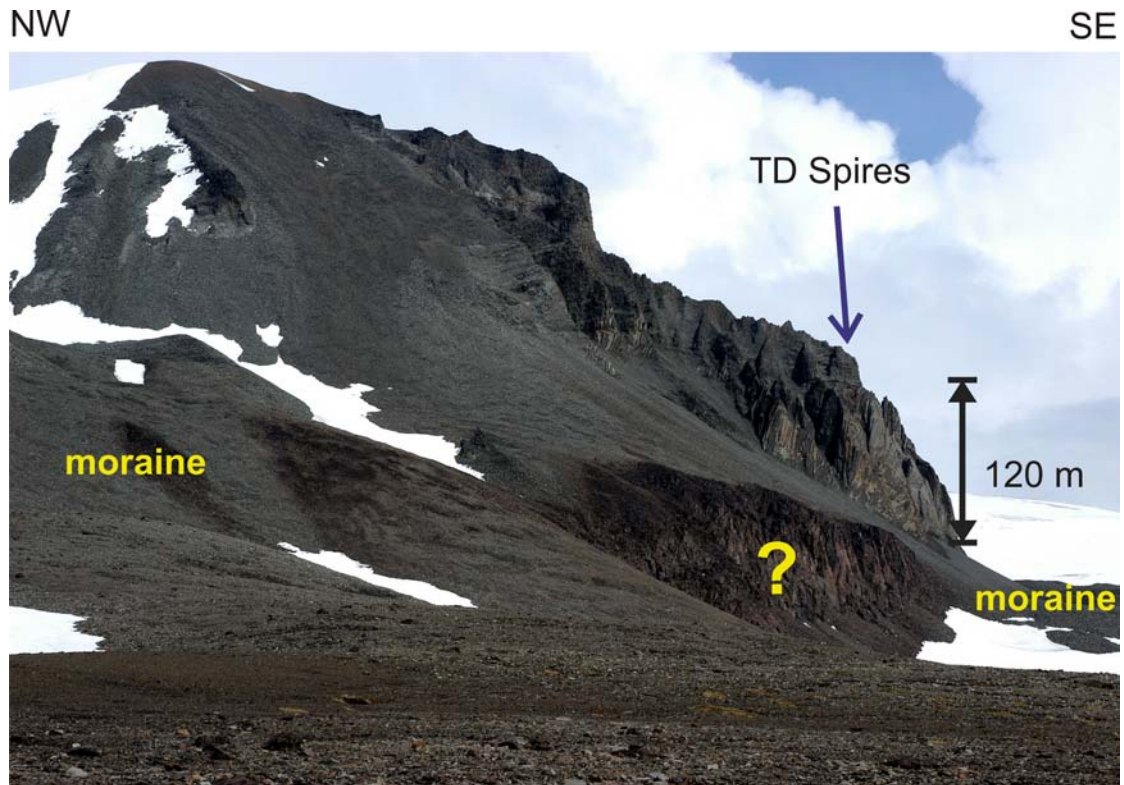


Figure 18: Photo of Triangle Dome from the north.

From this location the nearest cliff outcrop are lavas beneath the main portion of the “dome” that was studied. The spires of TD are visible here as well as an underlying outcrop (yellow ?) cliff that was not studied but may be related to TD.

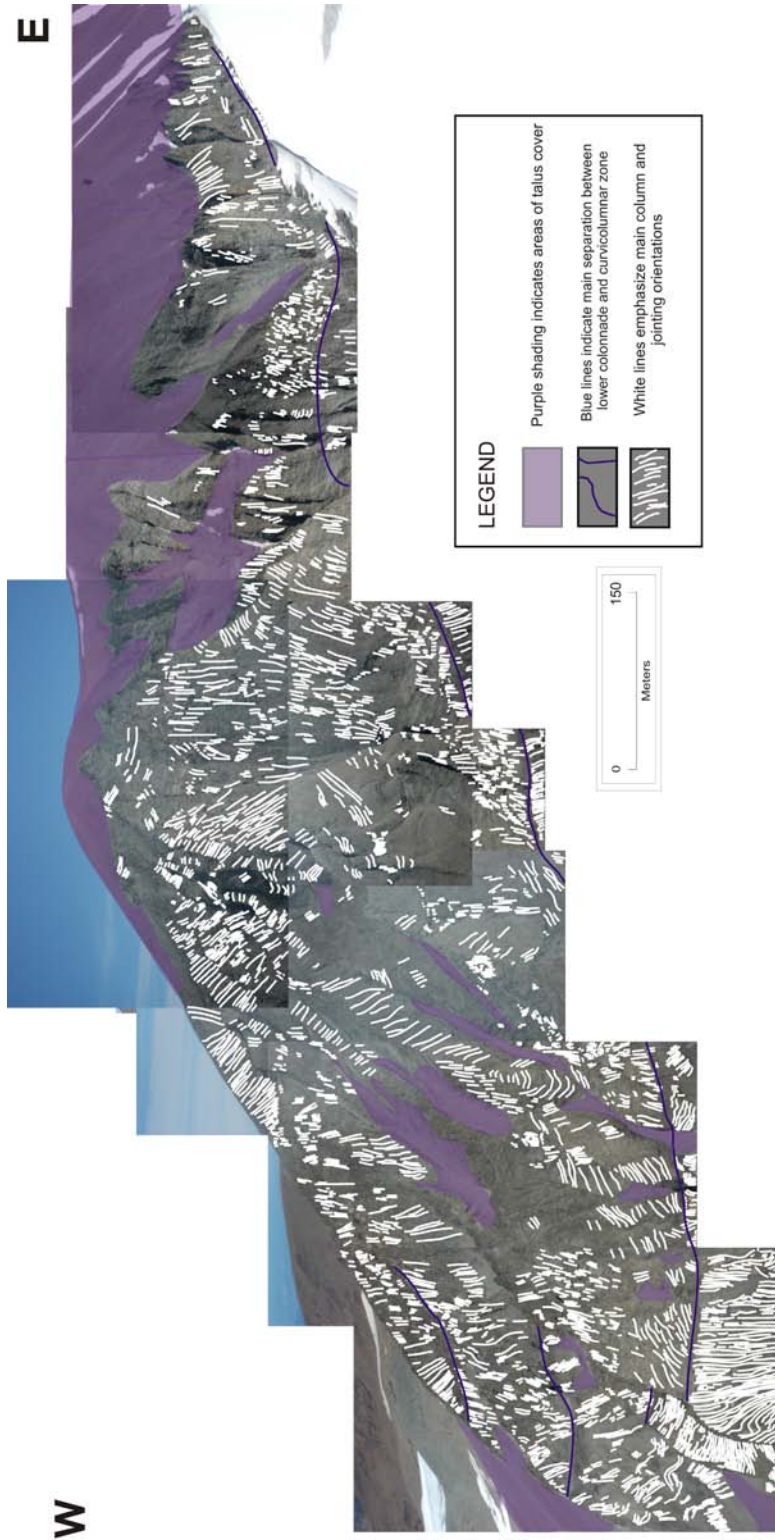


Figure 19: Overlay of Triangle Dome TD photo mosaic with accents of column orientation (white), division between lower colonnade and upper entablature (blue) and denotation of talus cover (purple shading). View of TD from the west.

Triangle Dome is comprised of light grey-green microporphritic phonolite of the Edziza Formation dominated by alkali feldspars. Microphenocrysts are mostly euhedral alkali feldspar laths, up to 1 cm in size, with well developed twinning although some pyroxenes are also present. The groundmass is predominantly interlocking clusters or contorted flow layered alkali feldspar crystals of lath or tabular shape and sparse interstitial aenigmatite. Souther (1992) dated the Edziza Formation from a sample of pantelleritic trachyte collected from lavas on the western slopes of Mount Edziza ($57^{\circ} 44.5' N$, $130^{\circ} 34.5' W$) at 0.9 ± 0.3 Ma using whole rock K-Ar methods.

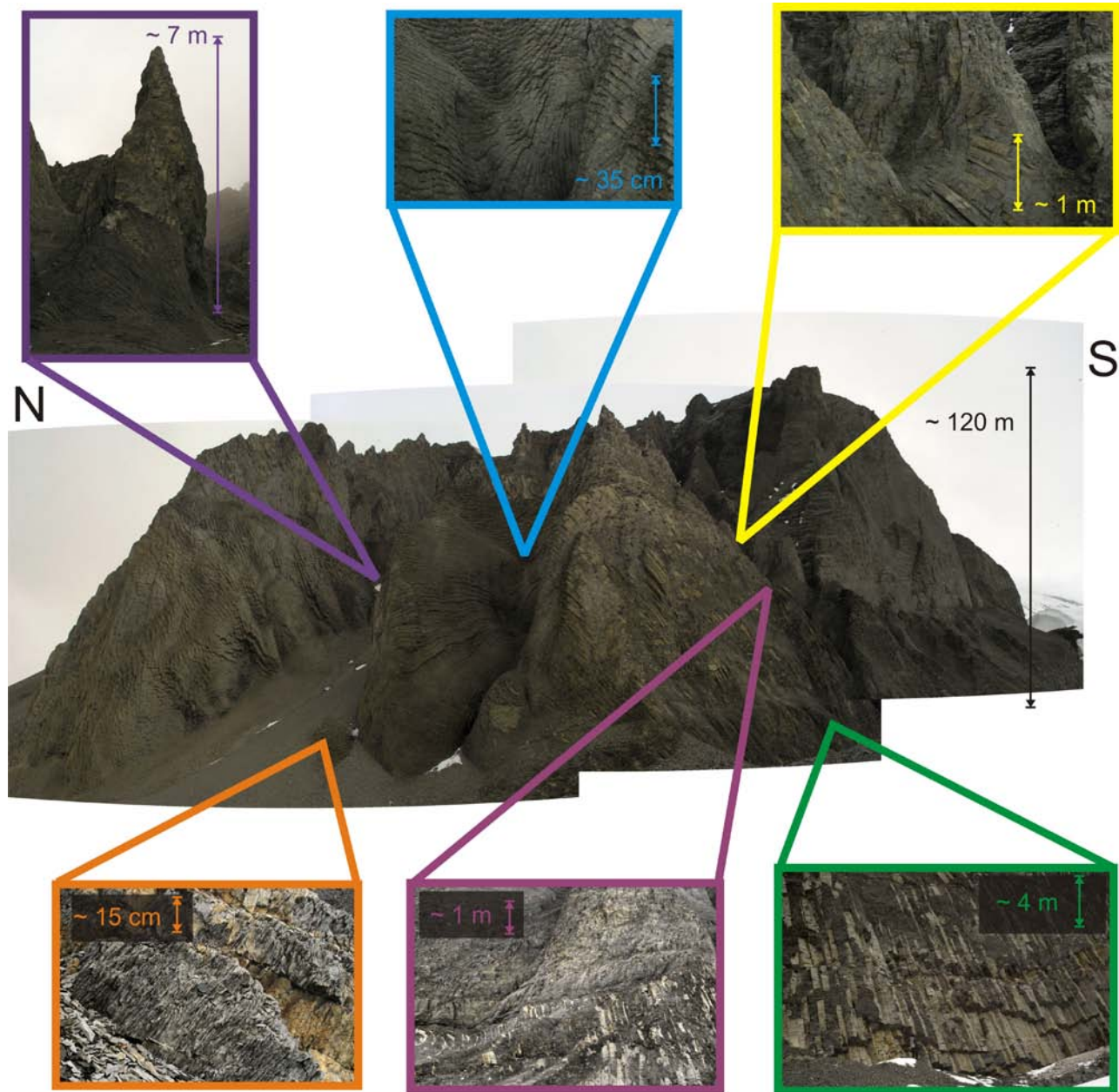


Figure 20: Photo mosaic of Triangle Dome with close-up images of structures.

(clockwise from the top) Purple: Spire within the upper entablature portion of TD. Blue: ‘Lizard skin’ appearance of columns when viewed from the ends. Yellow: ‘Lizard skin’ and radial columnar jointing. Green: Larger, well developed, hexagonal columnar jointing at the base of TD. Pink: Section of ‘S’ and ‘C’ shaped curved columns just above the lower colonnade. Orange: Fine scale platy jointing in the upper entablature portion of TD.



Figure 21: Radial fanning columnar jointing at Triangle Dome.

Lens cap for scale (arrow).

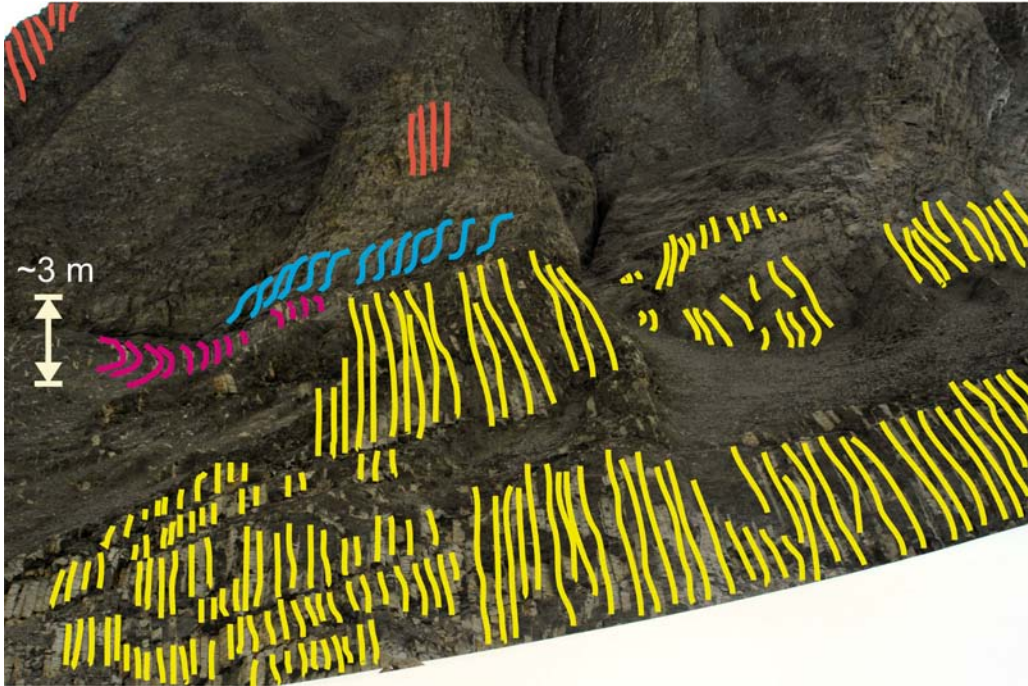


Figure 22: Photo of ‘C’ and ‘S’ curves at Triangle Dome

This photo shows the transition area between the lower colonnade and upper entablature and the area of ‘C’ and ‘S’ columns that were observed in some areas between these two zones, this area may be interpreted as a sill-like intrusive feature. Yellow lines highlight the long axis of the well-formed lower polygonal columns. Pink ‘C’ and blue ‘S’ curves highlight those columns. Red lines highlight the long axis only a few areas of organized columns.

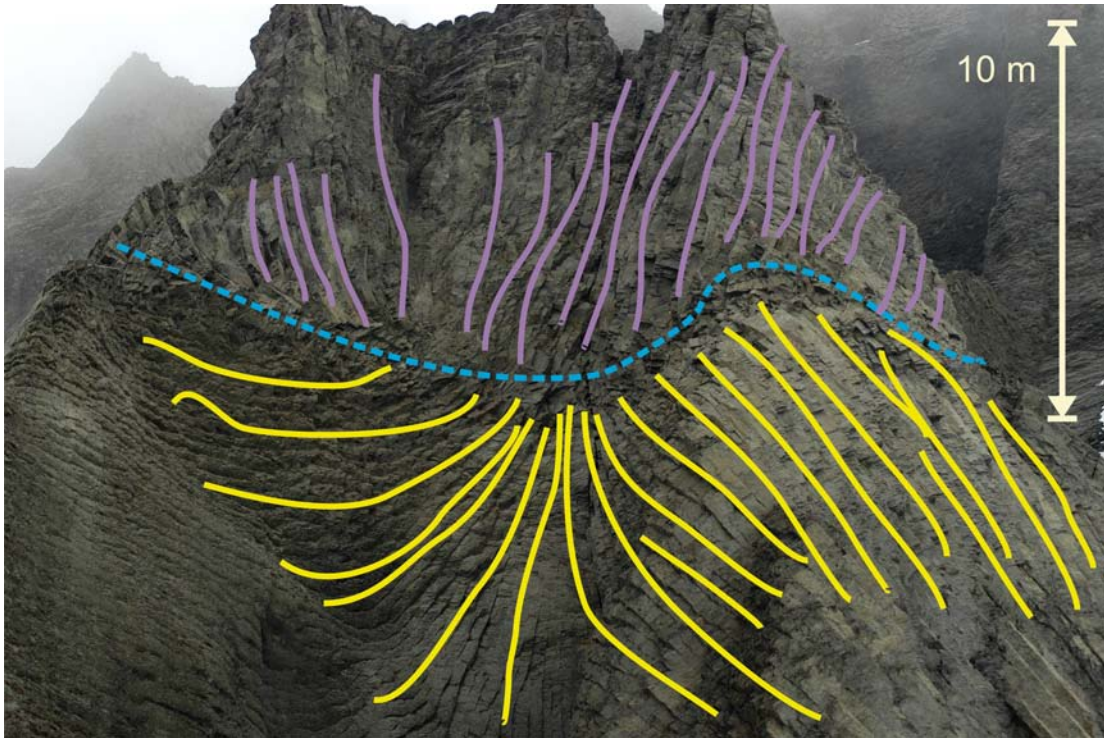


Figure 23: Photo of radial columns at Triangle Dome

Blue dashed line indicates the approximate contact between the lower colonnade and the upper entablature zones. Note that the yellow lines highlighting the long axis of the polygonal columns appears to radiate from a central source near the contact with the upper entablature. The upper portion in this photo has relatively well formed columns (long axis in purple).

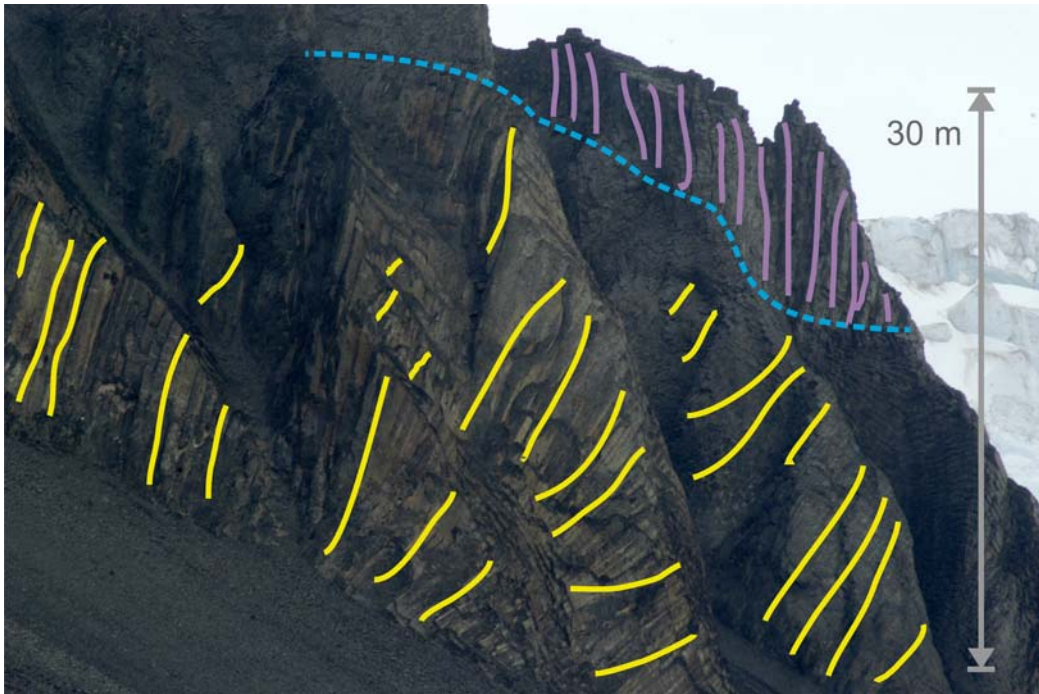


Figure 24: Vertical to sub-horizontal fanning columns

These column orientations indicate cooling against an ice surface perpendicular to the axis of the columns. View from the west of the lower portions of Triangle Dome. Blue dotted line = approximate contact between lower colonnade and upper entablature. Yellow lines = long axis of lower well-formed polygonal columns, radiating outward to a subvertical cooling surface. Purple = long axis of upper entablature columns.



Figure 25: The ends and 'lizard skin' appearance on the lower portions of Triangle Dome. Columns formed perpendicular to the cooling surface and propagating inward.



Figure 26: Radial columnar jointing at Triangle Dome

The columns in the lower half of the image are part of the lower colonnade zone, note they appear to be propagating from a point source near the center of the picture.

12.2 ORNOSTAY BLUFF

Ornostay Bluff is a small trachytic steep-sided bluff of lava flows along the southwestern side of the Mount Edziza caldera (Fig 27). The source of the flows is shrouded by the ice cap that currently fills the caldera. The bluff is 600 m wide, 1800 m long (as currently exposed), and rises 60 m above the surrounding plateau. The top surface of the bluff slopes gently a few degrees to the west, which is also assumed to be the direction of lava flow advance. The top of the bluff flow has been glaciated and is relatively featureless and flat with only small amount of visible debris (Fig 30). The sides of the bluff are very steep with extensive piles of talus at the base of their slopes. The northern side of the bluff abuts alpine glacial moraine and glacier ice. Two waterfalls incise the southwestern and mid-southern side of the bluff and provide good accessible sections through the lava flows (Fig 32). Here a well formed lower step of lavas approximately 40 m thick, that creates a 50 m wide bench upon which another 10-20 m of upper lavas rest.

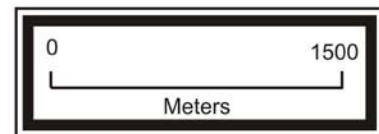
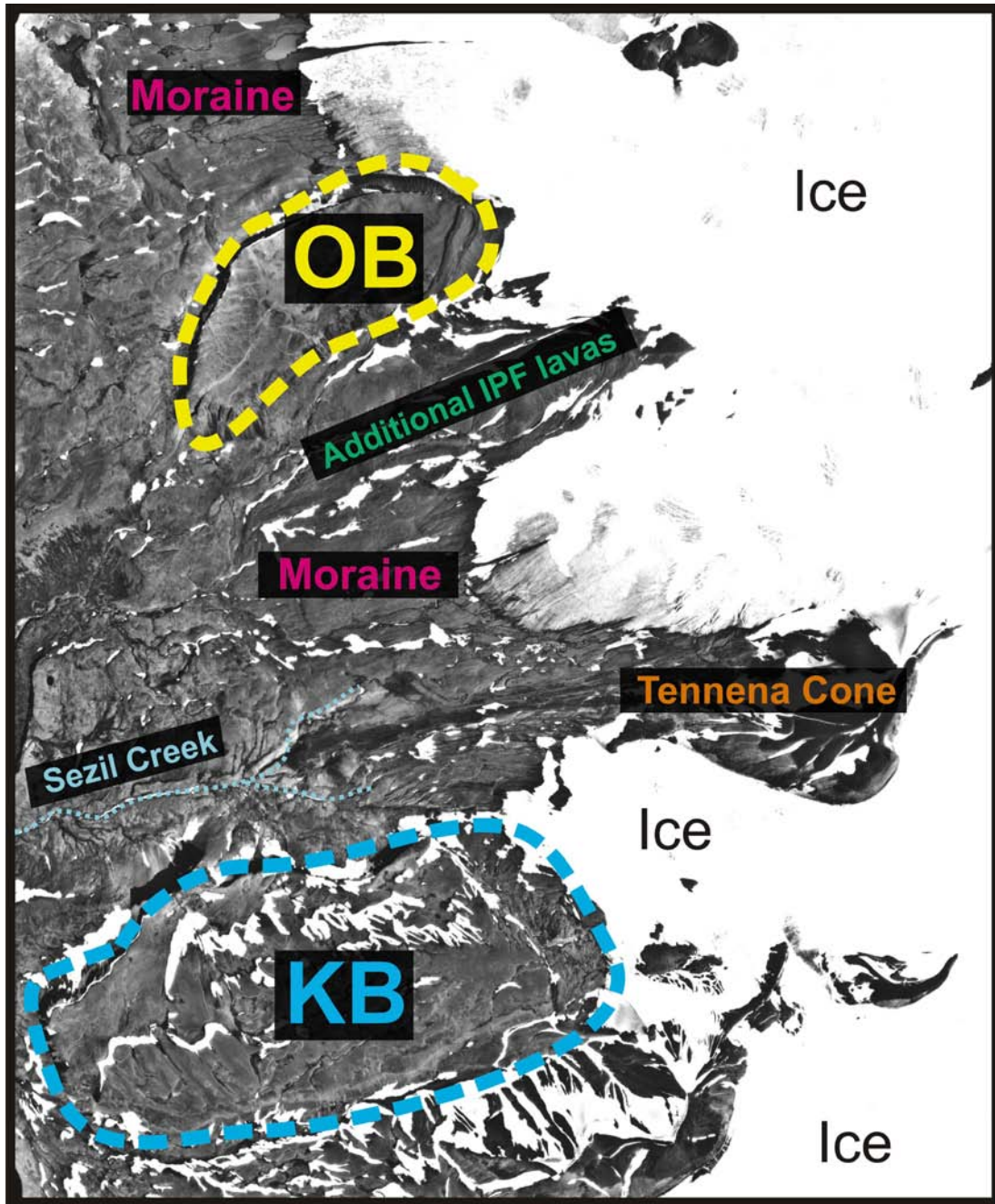


Figure 27: Aerial photo of Koosick Bluff (KB) and Ornostay Bluff (OB) and surrounding area. Note the extent of the moraine on either side of OB and KB as well as current ice location.

OB is approximately 0.2 km³ in volume and composed of 2-3 trachytic lava flows, with the basal flow being the thickest (Fig 29). The basal flow is 75 m in total thickness although portions of the flow are below the cliff forming lavas and only exposed on the hillside beneath the cliff due to erosion. This basal flow is comprised of three distinct structural units (Fig 39). Unit 1, 18 m thick and the lowest stratigraphically, is a basal clast-supported breccia. The clasts within the breccia appear to be fractured in situ. Dark flow banding within the clasts is more prominent within the lower portions of Unit 1 (Fig 40). It is unknown what this breccia lies upon as no basal contact was observed in the field (Fig 32). The contact between the Unit 1 unit and Unit 2 is gradational. Unit 2 is a 10 m thick unit of glass that has orange to yellow altered rinds several mm to 1 cm thick (Fig 33). Within the rind is black devitrified glass. Some crude jointing is visible here and is only a few cm in width with axial traces inclined towards the northeast. The next unit within the sequence is the thickest structural unit and has a gradational contact with the Unit 2 below. Unit 3 is 47 m thick and characterized by columnar joints 30-201 cm thick (Fig 38) accompanied by horizontal fracturing of creating sub-cm to 17 cm thick plates (Fig 34). The columns at OB are however not as well formed as those in the basal unit at TD (Fig 37). Fracture surfaces in this unit exhibit conchoidal fracture surfaces and expose tension gashes (Fig 35). The columns are not hexagonal in shape and vary from 6-sided polygonal to rectangular, (Fig 34) the latter being much more common. The tan-grey trachyte of this unit has some areas of flow banding.

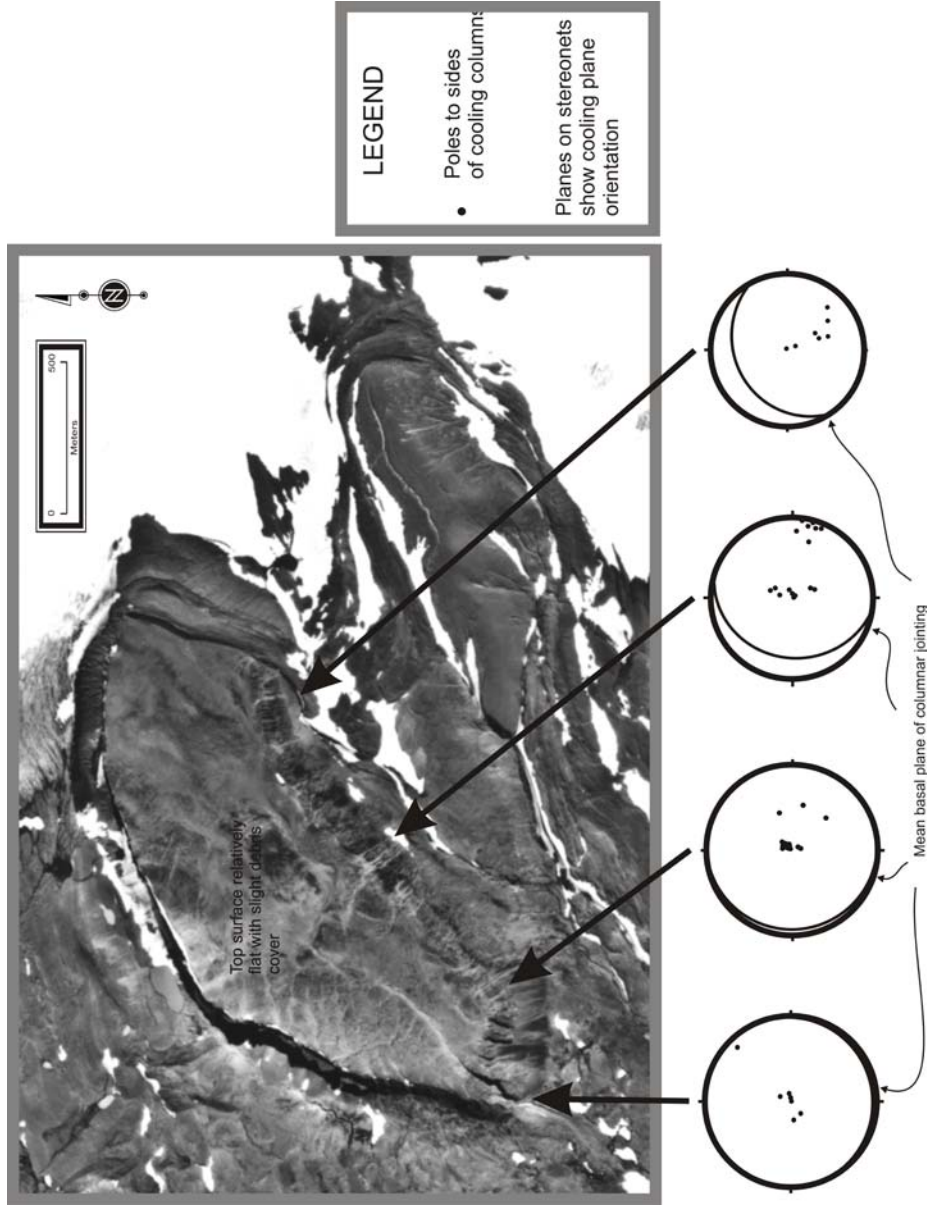


Figure 28: Ornostay Bluff column orientation diagram and aerial photo.

Orientations of primary columns were taken in the field and plotted onto stereonets. These stereonets now show the column orientations (dots) and the plane to those which represents the orientation of the cooling surface (plane). The resulting surface of cooling is horizontal or near-horizontal. This suggests this portion of the flow cooled normal to a basal cooling surface and not against a vertical surface or irregular surface.

Above the basal lava flow at OB lays another lava flow comprising a comparable set of structural units only proportionally much thinner than the basal flow, an additional third flow may also be present although it was difficult to determine and close inspection was not possible due to the steep cliff faces. The aspect ratio for OB is 0.069 (basal flow only) to 0.08 (entire 2-3 flows comprising OB) (Table 5). The aspect ratio for OB was calculated using the widest part of the flow and length of the flow, measured on aerial photos as well as Souther's (1992) geological map of MEVC and the total thickness of all the possible flows (2-3) at OB and the measured basal flow. All of the area measurements were made using maps and images, where true non-geometric shape and variation were not taken into account. Also, the source of OB is cloaked by ice and only the portion exposed was measured. This aspect ratio also only portrays the portion of the bluff that remains at the present time and does not give a good indication as to an original aspect ratio for the flow at the time of emplacement. Since then extensive, but immeasurable amounts of weathering have occurs (Fig 36).

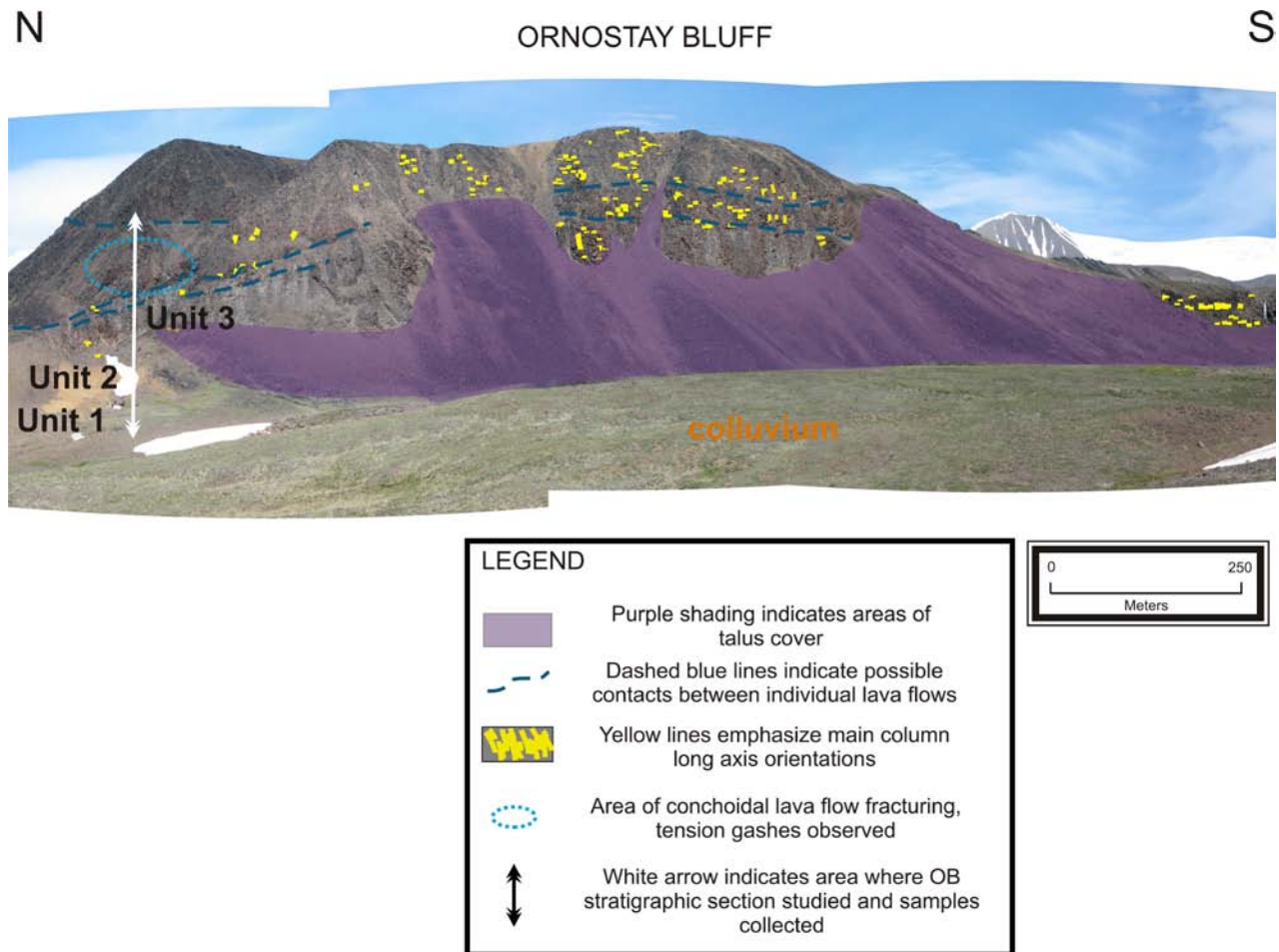


Figure 29: Ornostay Bluff photo mosaic overlay.

Units are referenced in the Ornostay Bluff stratigraphic column Fig 39.

Because cooling joints are recognized as forming perpendicular to cooling surfaces, by plotting the orientations of columns measured in the field at OB, the data generally indicate cooling surfaces near horizontal or slightly sloping (Fig 28).

The lavas at OB are microporphyrific alkali trachytes of the Ice Peak Formation. The microphenocrysts are alkali feldspar in lath or tabular shape, less than 1 cm across. The groundmass is composed of predominately feldspar laths at times crudely oriented in flow directions creating trachytic textures that are visible in thin section. Limited quantities of small pyroxenes, opaque oxides, and aenigmatite are also present within the rock. Souther (1992)

dated the Ice Peak formation from a sample of trachyte from OB at 1.5 ± 0.4 Ma using K-Ar methods.

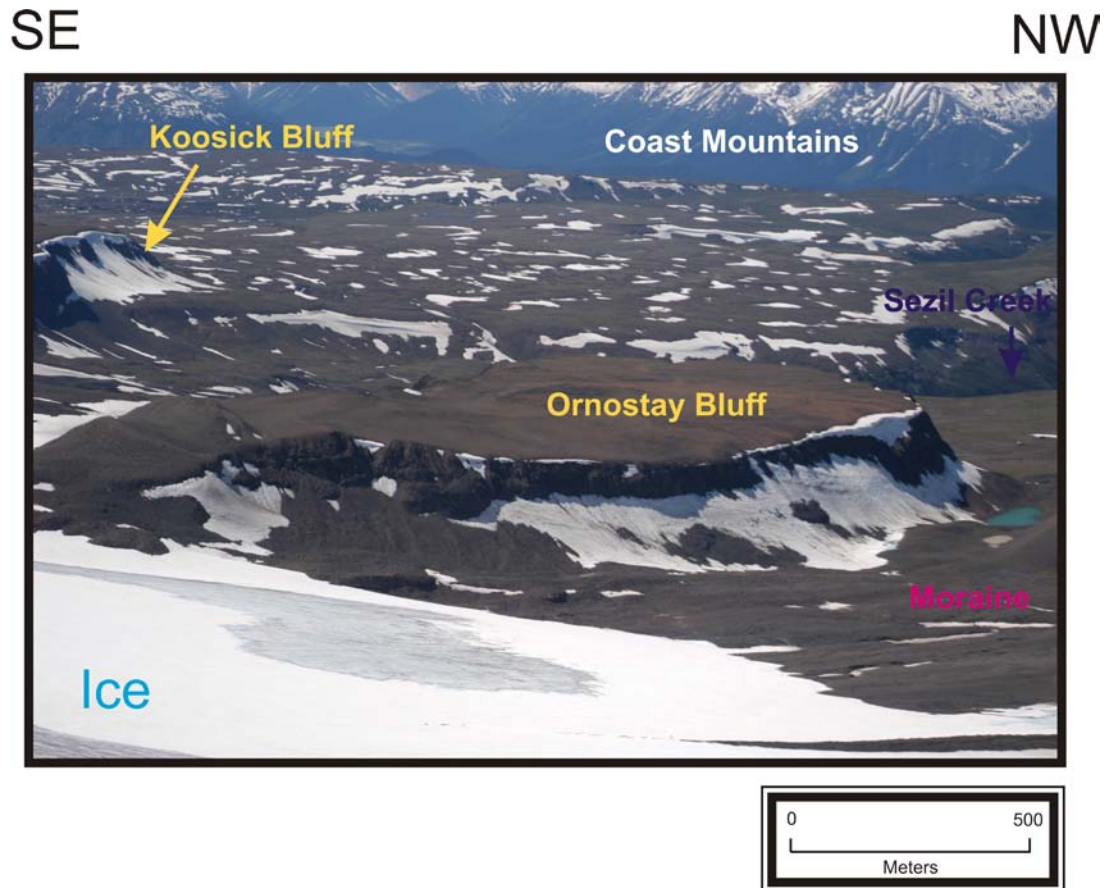


Figure 30: Photo of Ornostay Bluff from the north

This image illustrating Ornostay Bluff's steep-sided and flat-topped geomorphology

ORNOSTAY BLUFF

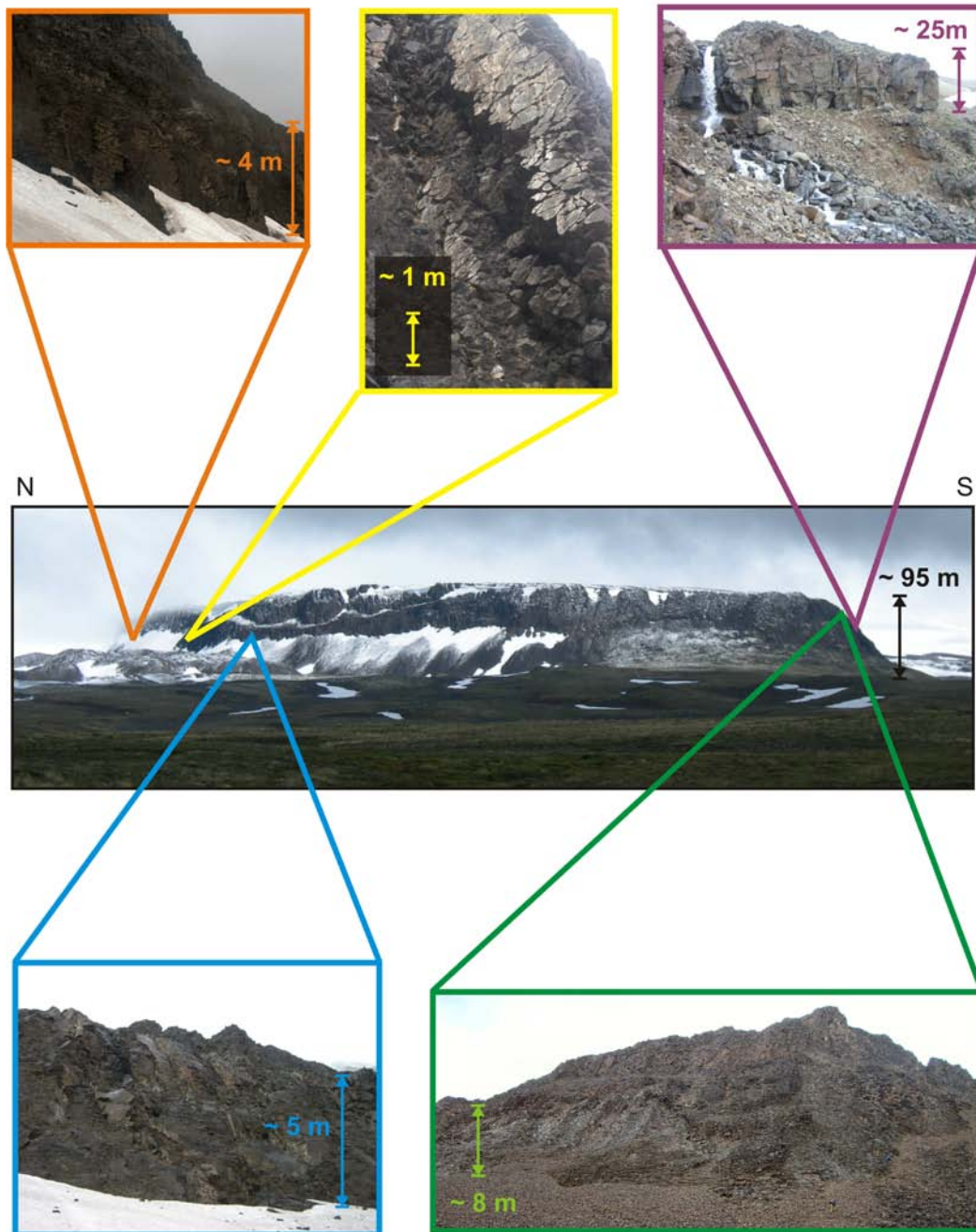


Figure 31: Ornostay Bluff mosaic and close-up images

(clockwise from top) Orange: the ends of the columns are visible more prominently on the north side of OB. Yellow: close up of the ends of columns. Pink: massive flow unit visible near the second waterfall on the southern side of OB. Green: Upper portion of OB with extensive platy jointing. Blue: Conchoidal and irregular fracture surfaces (see also Fig 35).

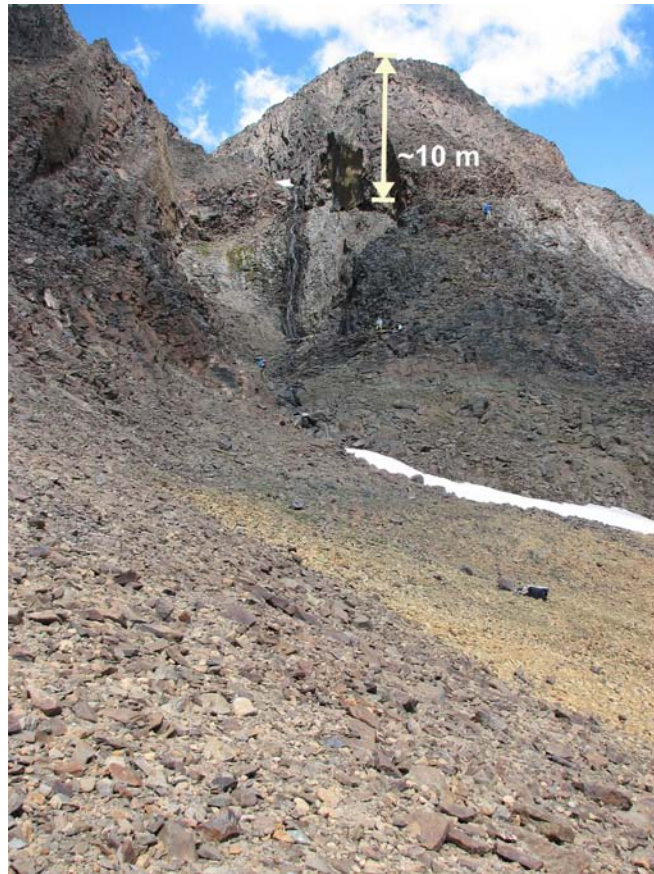


Figure 32: Photo of the southwest corner of OB and the first waterfall.

The cut of the waterfall allowed the study of the lowermost lava flow. Note that the yellowish area in the lower foreground is the Unit 2 of OB (Stratigraphic section of this area in Fig 39).

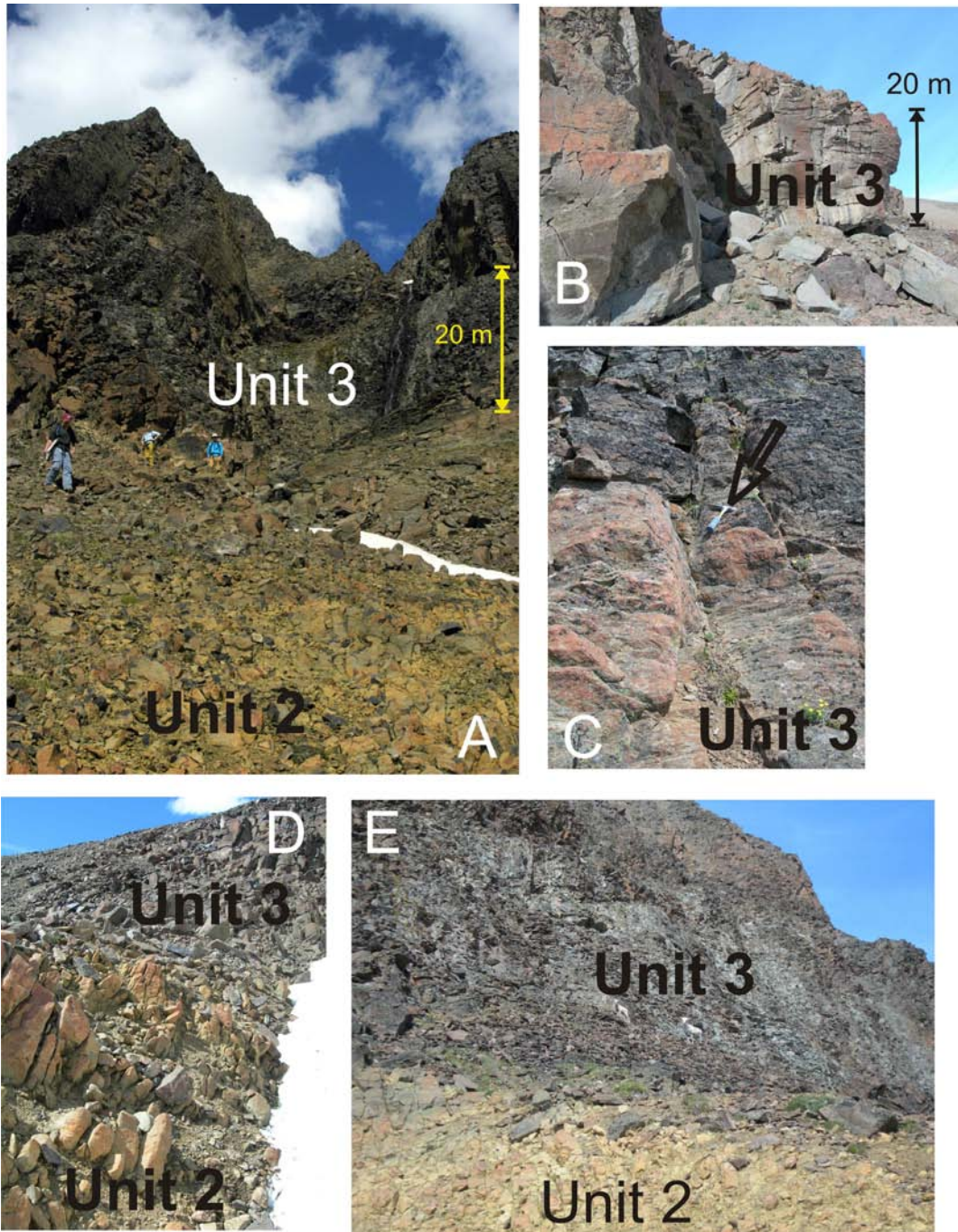


Figure 33: Ornostay Bluff

(A) Waterfall near the southwest corner of OB where the OB stratigraphic section was studied. (B) Upper massive flow Unit 3 to the east of the waterfall. (C) Crude columns near the base of Unit 3 (hammer for scale (arrow)) (D) Contact of Unit 2 (yellow) and Unit 3. (E) Gradational contact of Unit 2 (yellow) into Unit 3 (red and grey) (See OB stratigraphic column Fig 39)

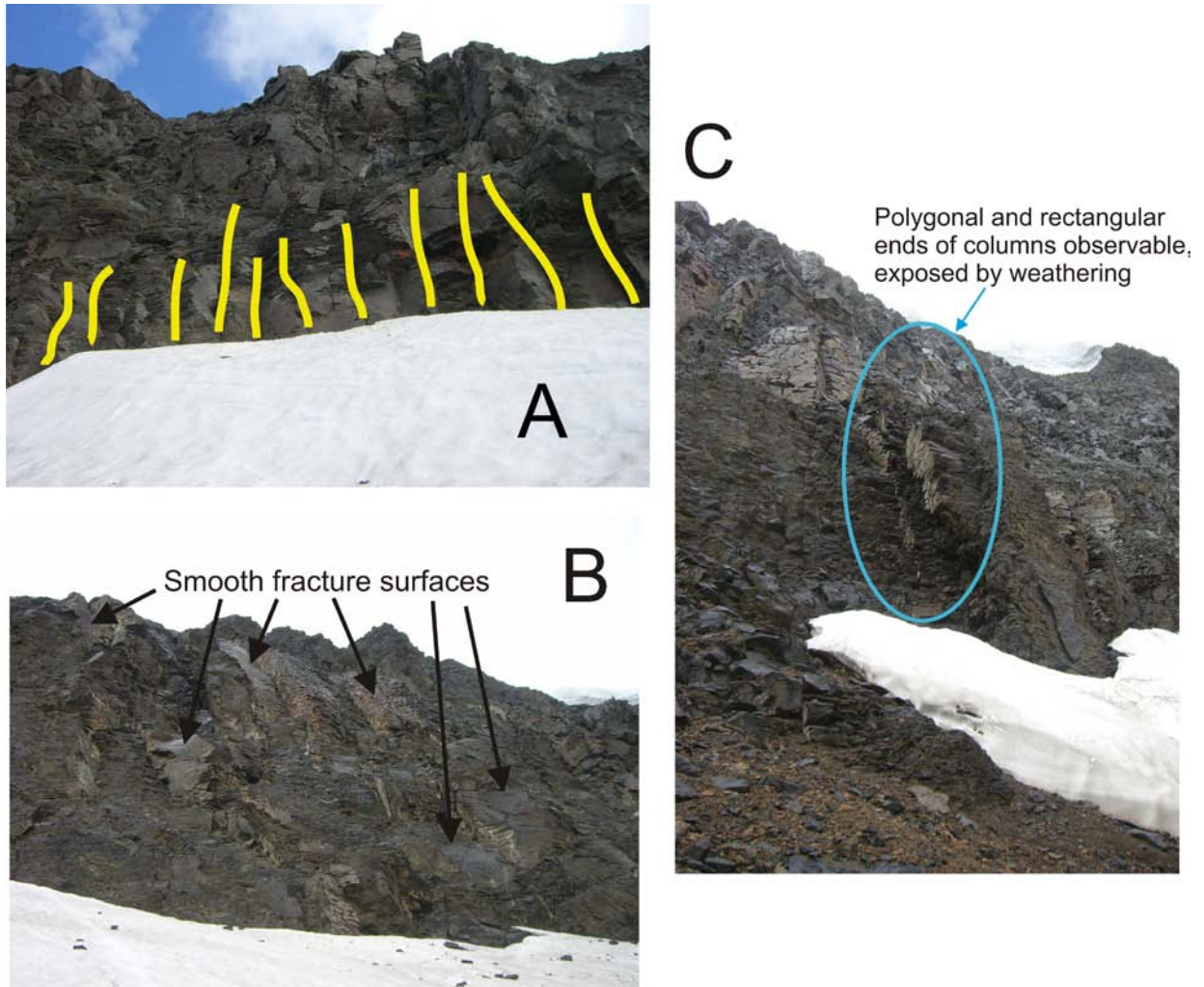


Figure 34: Ornostay Bluff columnar and platy jointing on the north side of the bluff.

(A) The jointing at this location is not as well formed as at other location in the flow. (B) Smooth fracture surfaces and abundant platy jointing on the north side of OB. (C) The columnar joints here are short and not well formed, often with polygonal or rectangular shapes. In places along this side of the bluff the ends of the columns are observable on the smooth fracture surfaces of the larger columns.

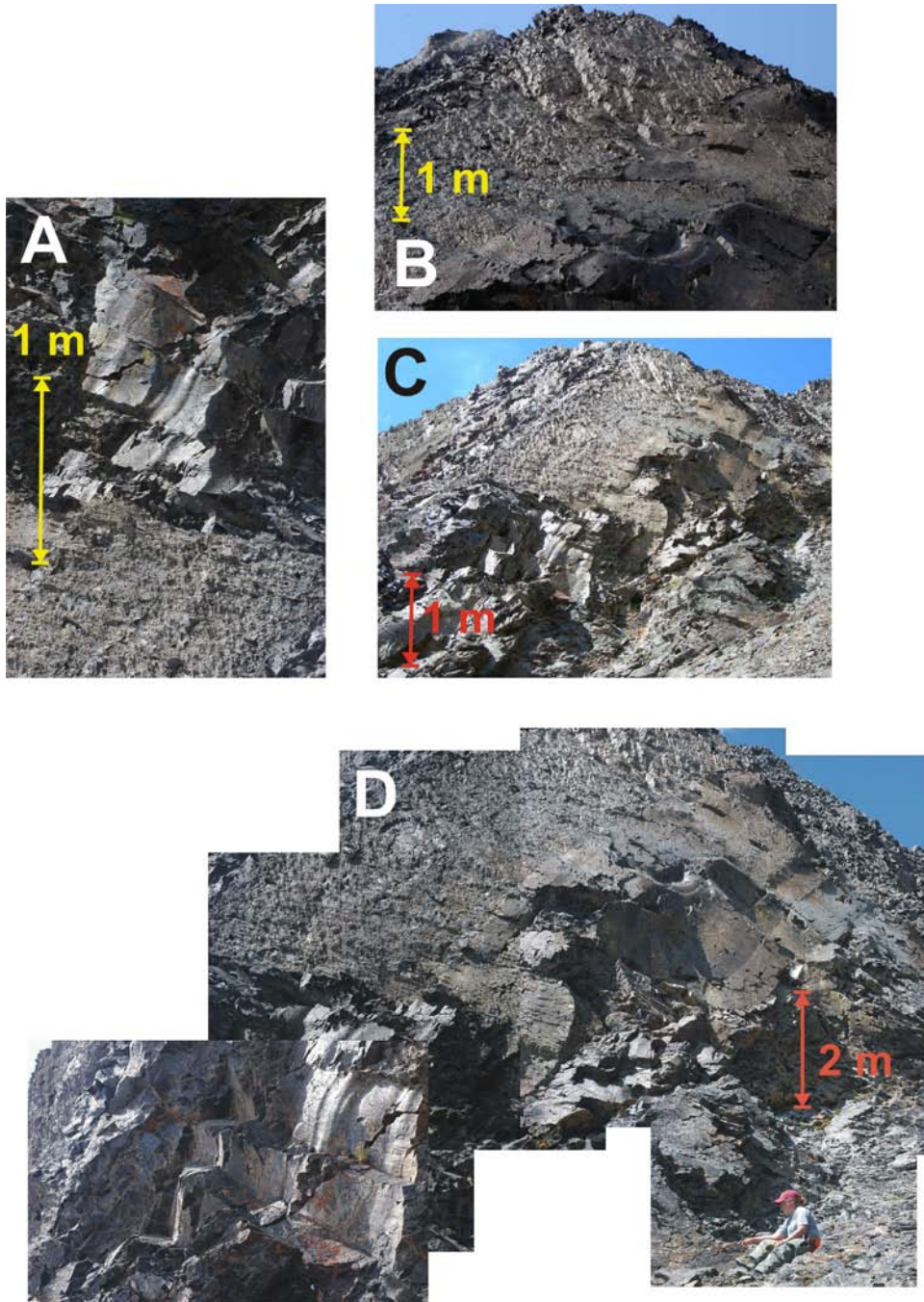


Figure 35: Ornostay Bluff Unit 3

Unit 3 (Fig 39) - areas of conchoidal fractured columns in central parts of lava flows. The smooth shiny surfaces in these photos show the irregular surfaces of fracture.

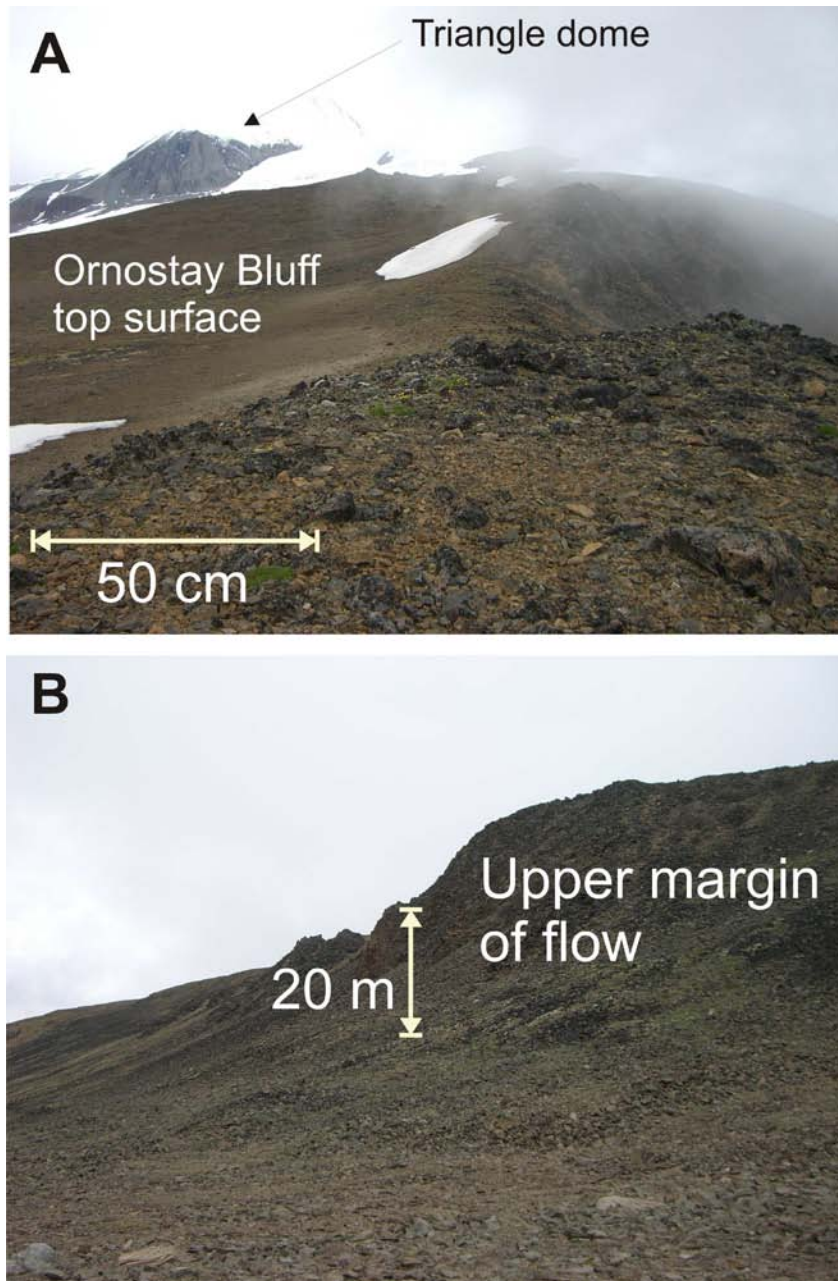


Figure 36: Photos of the top of Ornostay Bluff.

The surface is a level surface with small rubble covering (A). The upper portions of the flow with prevalent flaggy jointing and platy weathering (B). OB has clearly been glaciated and its margins and top surface are largely talus-covered making interpretation of ice-contact surfaces difficult. However, this is very typical of intermediate lavas in glacioclastic environments and it is important to research.

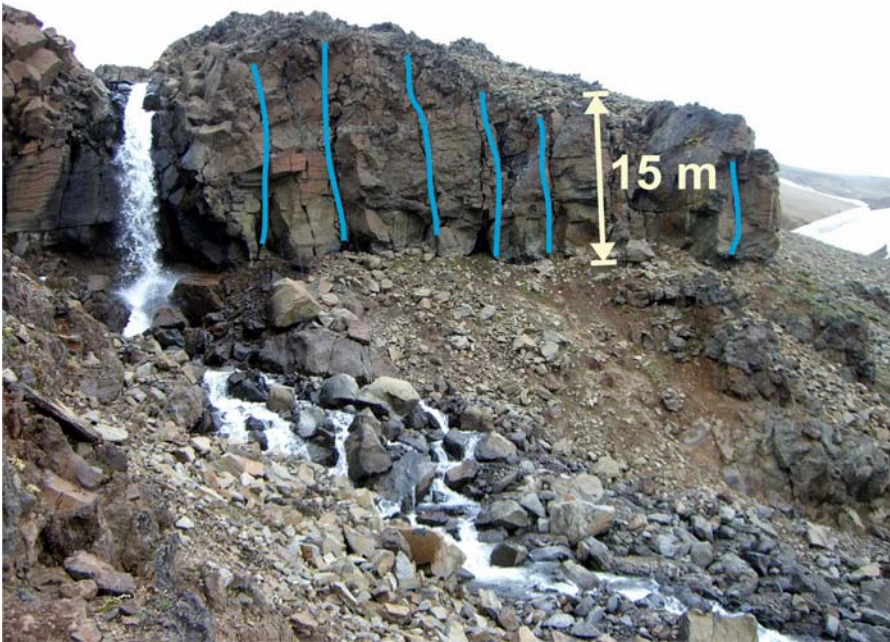


Figure 37: Ornostay Bluff Unit 3 further east along the bluff's southern face.

The vertical, crudely formed, wider columns (highlighted in blue) can be seen here with smooth and more curved fracture surfaces than the narrow overlying columns. View from the southwest. See Ornostay Bluff stratigraphic section in Fig 39.

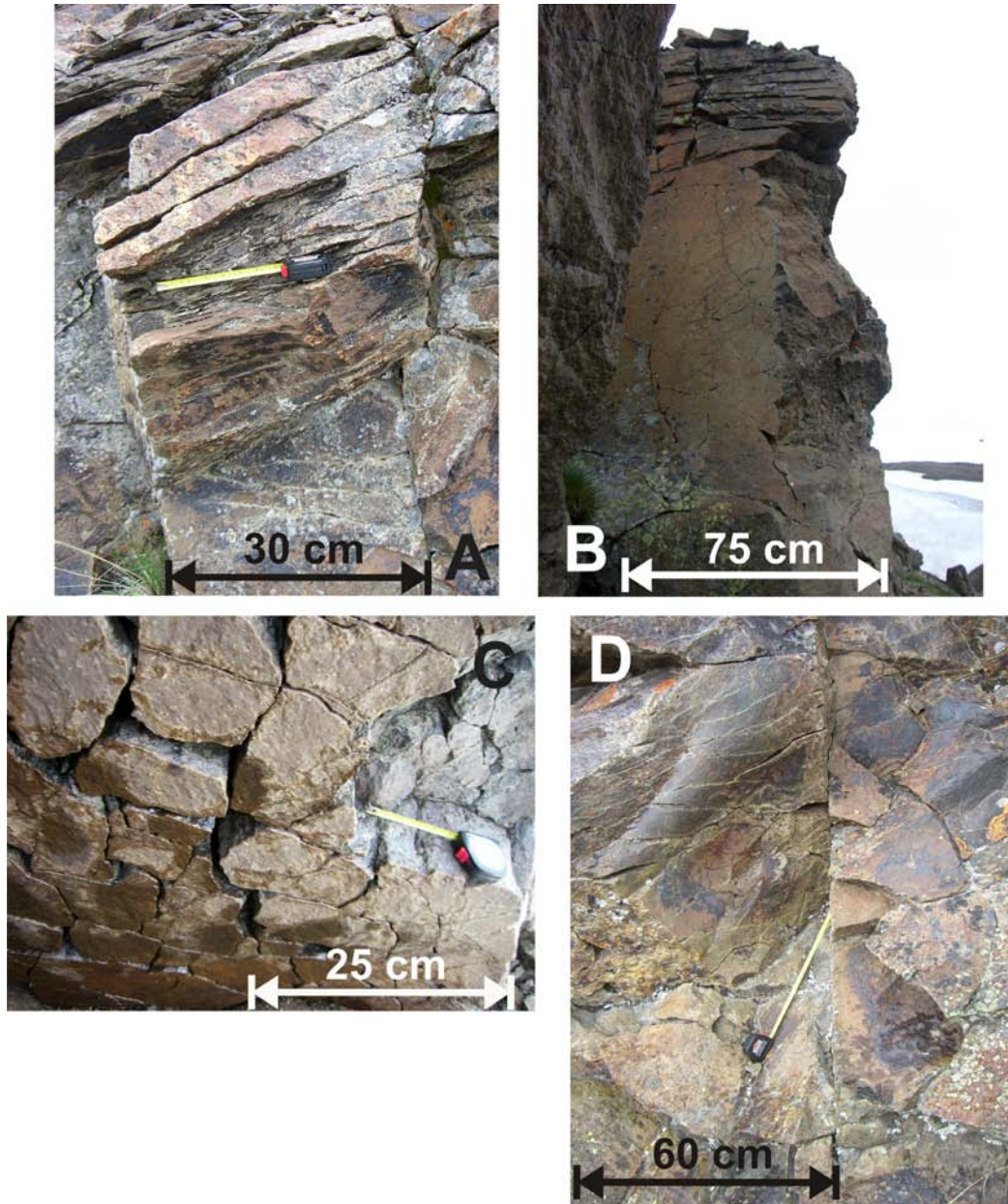


Figure 38: Ornostay Bluff cooling-contraction columns all within Unit 3.

(A) Main column (vertical) and thinner platy (sub-horizontal) jointing. (B) Smooth face along the lower column with platy jointing near the top. (C) The ends of columns showing dominantly crudely rectangular cross-sections. (D) Curved fracture surfaces of primary columns. See Fig 39 for Ornostay Bluff stratigraphic column.

ORNOSTAY BLUFF STRATIGRAPHY COLUMN

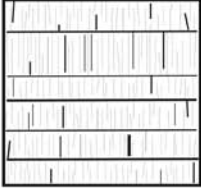
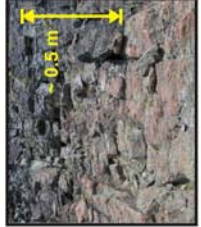
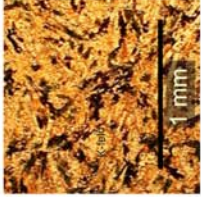




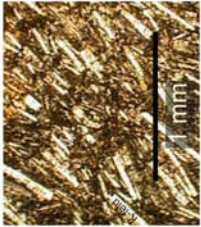


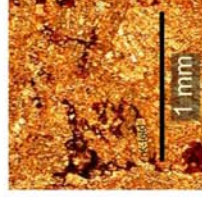
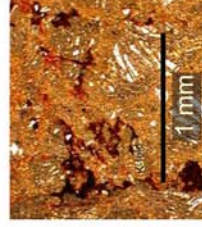
SYMBOL	MACRO PHOTO	MICRO PHOTO (PPL)	MICRO PHOTO (XPL)	DESCRIPTION
				<p>UNIT 3 - Flow unit Grey-brown trachyte, non vesicular, some alkali feldspar phenocrysts, column size 30-40 cm across becoming 1-201 m across, flaggy jointing perpendicular to primary column orientation spaced sub cm to a few cm apart, flow becomes smooth in areas with prominent curved surface joints, tension gaps also observed. Unit is</p>
.....				
				<p>UNIT 2 -Glassy flow unit Columnar jointed, non-vesicular vitric trachyte, columns here are a few cm wide with an accompanying joint set roughly perpendicular to main column joint orientation, an altered surface of orange and yellow weathering is prevalent, glass has weathered rinds up to a few mm to a cm thick with a dark green-black</p>
.....				
				<p>UNIT 1 - Flow breccia Basal unit of bluff, clast-supported, angular trachyte lithic/vitric breccia, some flow banding in clasts with banding continuous across the clast. Very well cemented with secondary minerals in some locations. Largest in-tact (but jointed) clast is approximately 1 m across. Unit is approximately 19 m thick.</p>

Figure 39: Ornostay Bluff stratigraphy column
 Ornostay Bluff basal flow stratigraphy is divided into 3 units. Each unit represents here with a unit symbol, a field photo of the unit, thin section images in both plain polarized (PPL) and cross polarized light (XPL), and a field description of each unit.

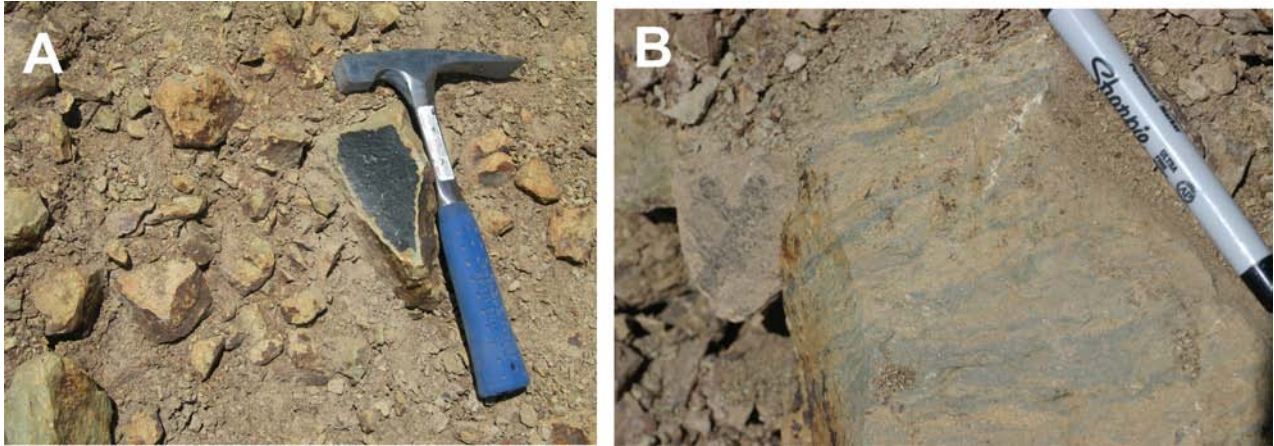


Figure 40: Ornostay Bluff field photos

(A) A fresh face on a loose piece of the glassy Unit 2 (Fig 39) showing the orange-yellow altered rind and devitrified glassy interior. (B) Clast from flow breccia Unit 1 (Fig 39) showing prominent flow banding.

12.3 KOOSICK BLUFF

Koosick Bluff (Fig 27) is a similar trachytic bluff to Ornostay Bluff, although there are some significant differences. The bluff appears to be comprised of a single lava flow unit that is at least 1000 m wide, 3000 m long (exposed portion), and about 100 m high with an aspect ratio of 0.03 (Fig 41, Table 5). As is the case with OB, the source area and eastern portion of the flow is obscured by the ice cap that fills Mount Edziza caldera and Tencho Glacier as well as the much younger Tennana Cone and its associated basaltic flows and pyroclastic units of late Pleistocene to early Holocene in age. The northern and western faces of KB are steep exposures with large talus slopes at their base (Fig 42). The southern side of KB lies alongside the basaltic flows and pyroclastic units of the late Pleistocene early Holocene Coco Crater. The base of this flow is not visible, but the top of KB is relatively smooth with little debris and maintains a westward slope of approximately 5%.

KB is approximately 0.5 km³ volume and composed of microporphyrific alkali trachyte of the Ice Peak Formation as described at OB. As previously mentioned, Souther (1992) dated Ice Peak lavas from a sample of trachyte from OB at 1.5 +/- 0.4 Ma using K-Ar methods. Field work at KB was limited to a quick reconnaissance stop and therefore additional observations were not made.

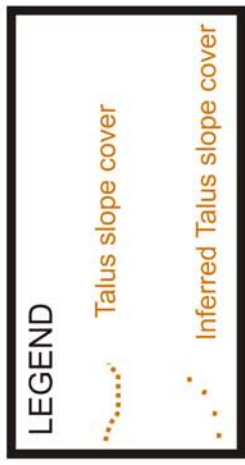
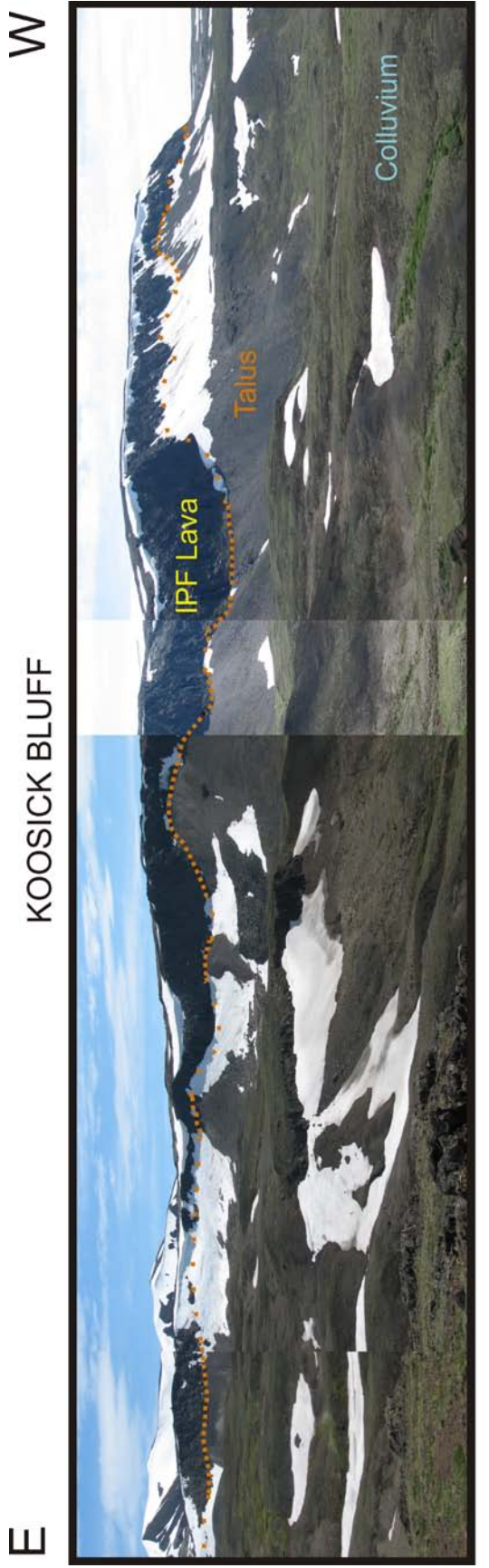


Figure 41: Koosick Bluff, view from the north
 Unlike OB it appears KB is one lava flow approximately
 90 m thick.

NNE

KOOSICK BLUFF

SSW

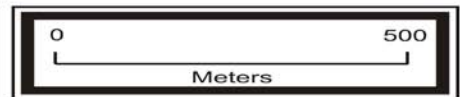
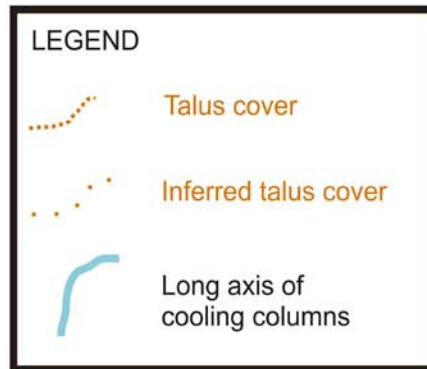
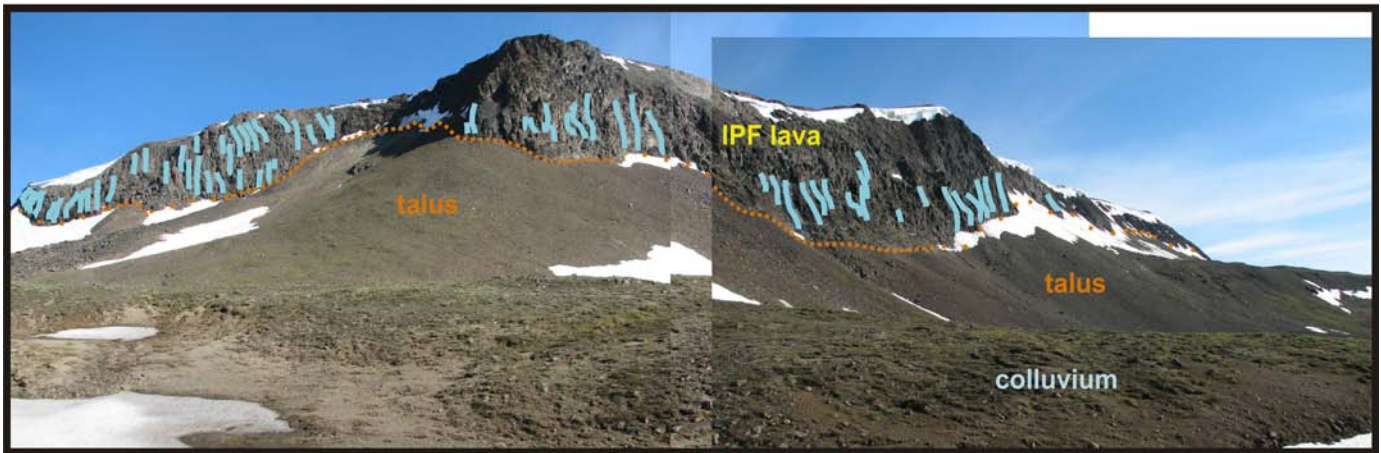


Figure 42: Koosick Bluff

In this figure some of the prominent larger scale cooling columns are highlighted with blue lines (long axis of the columns).

13.0 INTERPRETATION OF STUDIED TRACHYTE LAVAS AT MOUNT EDZIZA VOLCANIC COMPLEX

The pattern and dimensions of cooling-contraction joints in lavas at glaciovolcanic centers can often provide important evidence for former ice contact and minimum ice thickness. In particular, narrow columns that are perpendicular to subvertical flow margins are commonly interpreted as evidence for contact with steep ice (Lescinsky and Fink 2000; Lescinsky and Sisson, 1998). Examples of the range of fractures types observed in ice-contact lava flows are illustrated in Figure 43 (after Lescinsky and Fink, 2000). However, interpretation of joint patterns in such lavas can be very complex, as several factors need to be considered, including the topography of the contacted ice, basal bedrock topography, fluctuations in water levels during cooling, ingress of water and steam along earlier joints, lava effusion rates and rheology, lava intrusion (endogenous growth), ice unloading, recent freeze-thaw processes, etc.

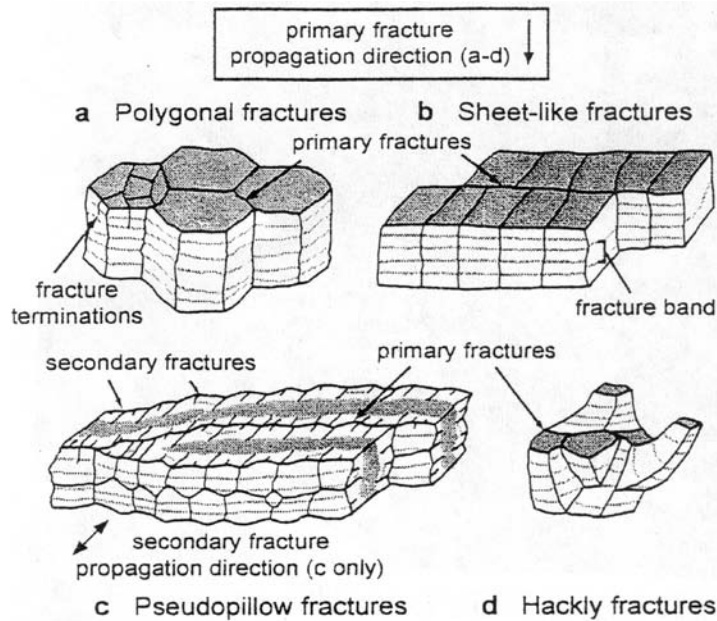


Figure 43: Sketches of fracture morphologies in ice-contact lava flows.

(a) Polygonal fractures. (b) Sheet-like fractures. (c) Pseudopillow fractures. (d) Hackly fractures.

White surfaces correspond to cooling fracture faces, with grey lines representing incremental fracture terminations. Heavy black lines represent cooling fractures. In (c) these are secondary fractures. Propagation for all primary fractures (a-d) is toward the bottom of the figure. Propagation direction for the secondary fractures in (c) are into and out of the figure. (after Lescinsky and Fink, 2000).

13.1 INTERPRETATION OF TRIANGLE DOME

TD and its complex fanning column and joint patterns are interpreted as being the result of a complex cooling regime within a partially water-flooded sub-ice cavity. The cooling surface was most likely in a continually variable state causing complex cooling surfaces against the lava as it was being emplaced. Curved columnar cooling joints are very common (Fig 44). The basal fanning “colonnade” suggests that the lava formed in a cavity in the ice during emplacement, the

movement of water and steam throughout the cavity flushed through portions of the dome during emplacement causing new cooling surfaces to form almost continuously (Fig 45). Possible controls for the shape of these subglacially emplaced domes includes the shape of the ice or ice cavity, rate of melting of the ice during emplacement, and amount and flow rate of water surrounding the emerging lava. Similarly, the controls of the elaborate fanning patterns (Fig 44) include the changing cooling surface and the temperature of the fluid/ice in immediate contact with the lava.

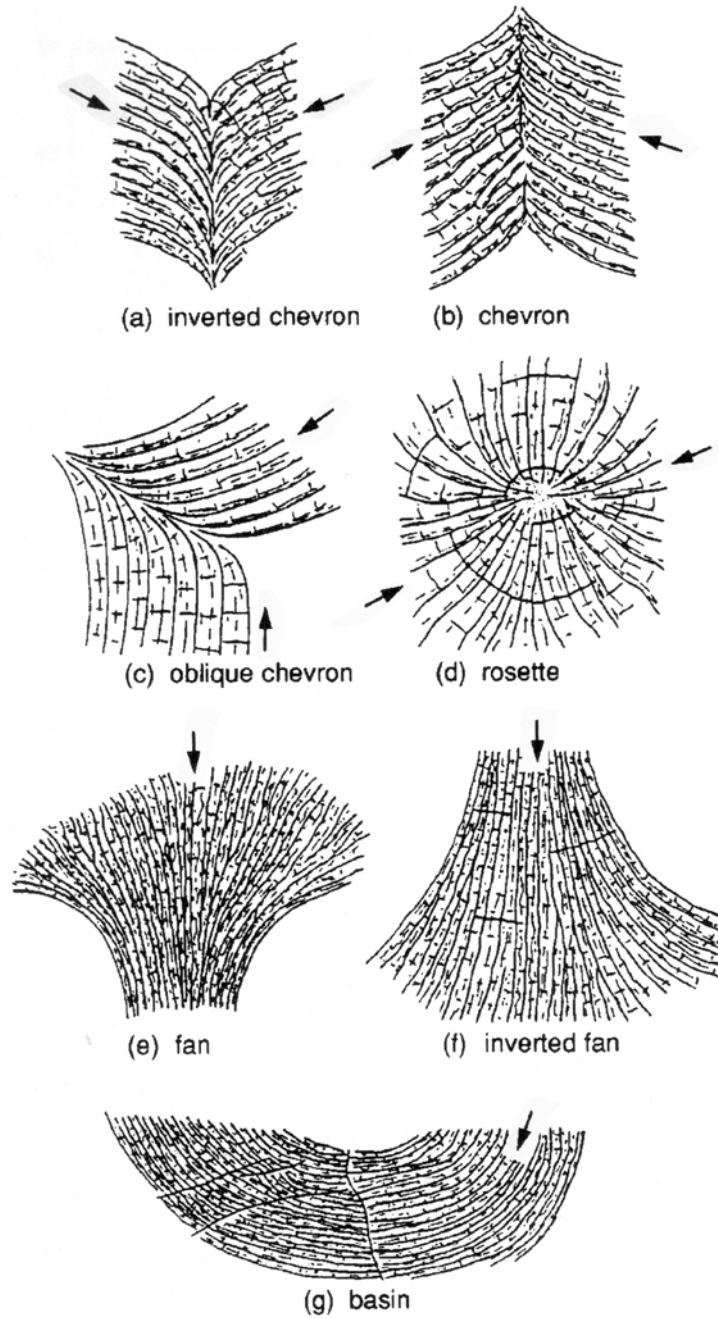


Figure 44: Curved columnar structures formed in basalt lava flows

Arrows marking the probable direction of growth of primary fracture. From Hull and Caddock, 1999. Many such fracture patterns of these curved columnar types were observed particularly at Triangle Dome.

The upper zone of TD, where regular columns are much less common, is interpreted as a type of “entablature” as commonly described from water-flooded basaltic lava flow as in the Columbia River basalts by Long and Wood (1986), (Fig 45). The entablature is an area where initial set of joints has been overprinted by cooling joints due to water infiltration. The origin of the prominent sheet-like planar jointing that dips into the core is unclear, but one possibility is that it may reflect ice unloading during or after emplacement. Some of these dipping surfaces may also reflect lava flow contacts, but were not accessible to directly observe. The local areas with well-developed coarser (relative to their immediate neighbors) columnar jointing and often S or C-like columns (Fig 22) in the upper zone may reflect endogenous growth by dike and sill intrusion after parts of the dome had already begun to cool, or some at least may also be lava flow contacts. The lower zone of TD, with its well developed hexagonal columnar joints, is interpreted as a thick “lower colonnade” with slower cooling and likely more regular cooling history likely due to less water ingress during cooling. The absence of an upper colonnade (Fig 46) may be due to removal by erosion, or it may never have developed because of water ponding, as opposed to direct lava-ice contact, in the upper part of the cavity.

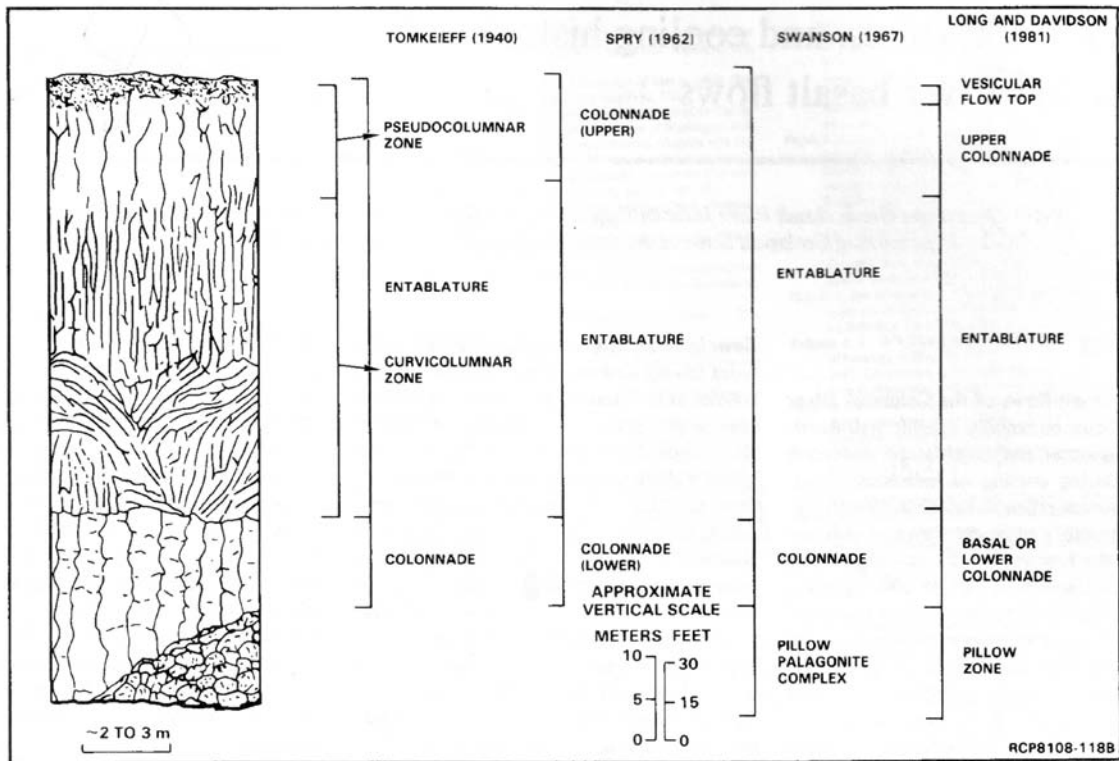


Figure 45: Typical intraflow structures present in Grande Ronde Basalt flows.

This figure correlates nomenclature across various studies of these structures. Fracture widths not to scale within the figure. From Long and Wood, 1986.

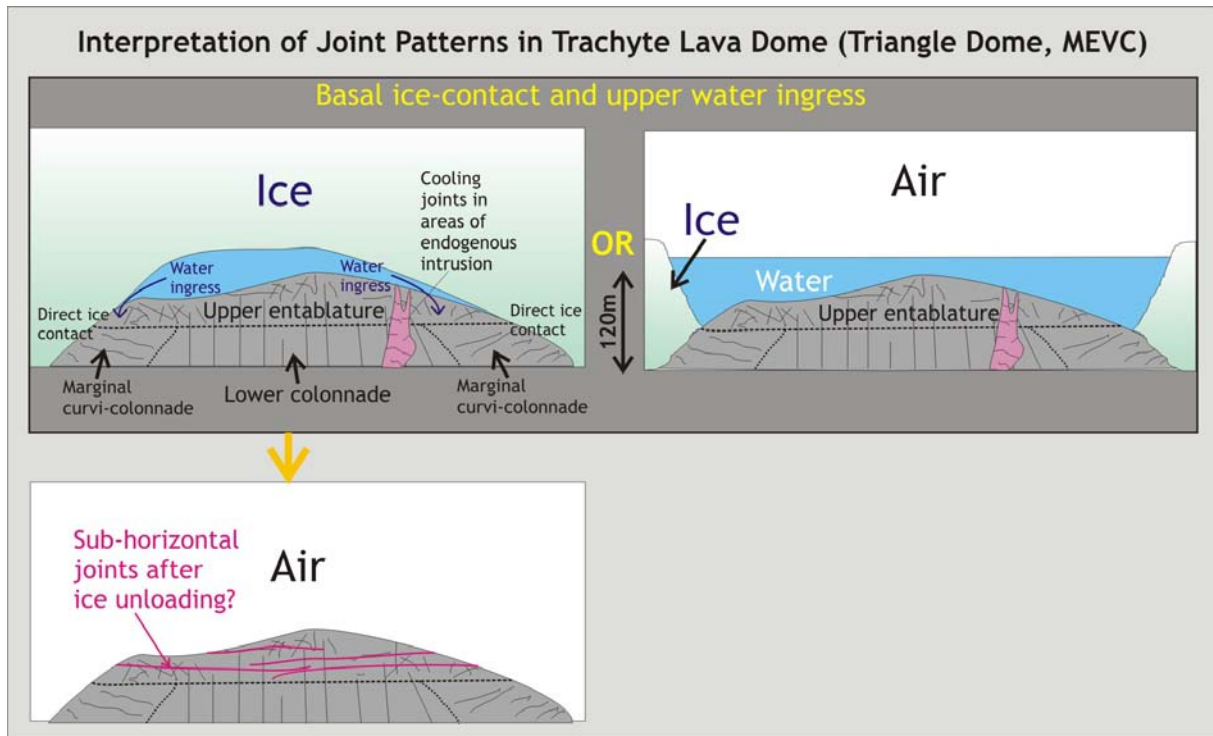


Figure 46: Possible emplacement scenario for Triangle Dome.

In first frame, a lower colonnade is formed by direct contact with ice and an upper entablature by water ingress. Note that sub-ice emplacement is not necessarily a requirement, but ice-contact along margins at the base is necessary (second frame). The estimated minimum thickness of ice-contact zone is about 60m. Prominent subhorizontal sheet-like jointing may be due to ice unloading (?)

13.2 INTERPRETATION OF ORNSTAY AND KOOSICK BLUFFS

OB and KB, although not anomalously thickened for a magma of that viscosity (Tables 3 and 4) nor exhibiting the complex cooling patterns of TD are still of interest in studying and recognizing ice-contact lavas. This is because similar glacially-eroded thick steep-sided lavas are common on many intermediate to felsic volcanoes and deciding if they have contacted ice is

frequently a challenging task. Some of the cooling joints observed and measured in the field exhibit the same cooling column geometry, joint patterns, visible textures, and other structures as those described in other subglacial environments (Table 2, Figs 43 and 47). Due to the uncertainty associated with the emplacement environment of OB and KB bluffs a variety of possible emplacement scenarios is illustrated in Figure 48.

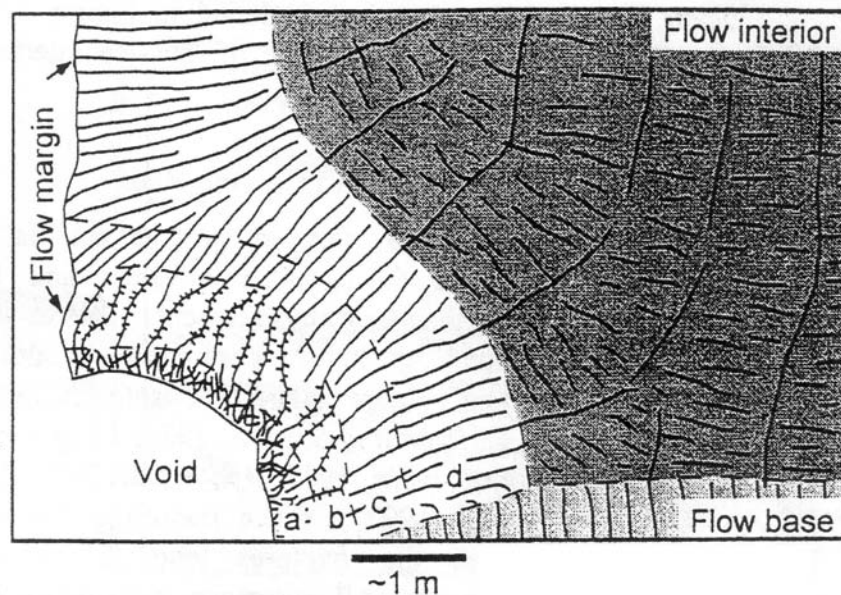


Figure 47: Sketch showing progression of fracture from a void along the flow base inward towards the flow interior.

(a) hackly fractures, (b) pseudopillow fractures, (c) sheet like fractures, (d) polygonal fractures. The transition between each type of fracture is gradational. Wider well developed polygonal fractures are found closer to the flow base and more irregular, broad polygonal fractures and platy jointing are in the flow interior. Cross reference with Fig 43 for sketches of characteristics of each type of fracture morphology (a-d; after Lescinsky and Fink, 2000). The larger columns at OB, TD, KB are similar in dimensions of the “flow interior” zone in this figure. This suggests that much of the key structural data for ice-contact has been removed by erosion (perhaps several meters of the margin have been removed).

Lava Flow Emplacement Scenarios

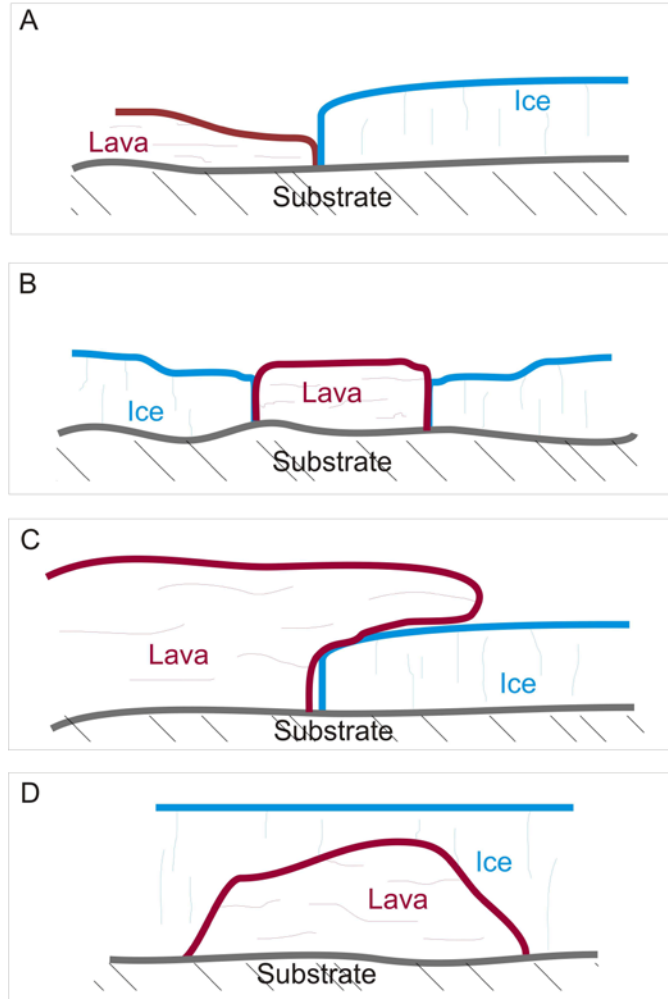


Figure 48: Simplified lava flow emplacement scenarios for Ornostay and Koosick Bluffs.

(A) Local ice-contact margin (B) Lava flow ice-bound on both sides (C) Lava flow overtops ice.

Probably unlikely? Evidence would not be preserved. (D) Sub-ice lava emplacement Scenario B or

D is considered the most likely for both OB and KB

14.0 DISCUSSION OF STUDIED TRACHYTE FLOW VELOCITY AND ICE MELTING RATES

To see if the studied trachyte bluffs (specifically KB) at MEVC would have contacted ice directly or just produced meltwater, a study of the rate of ice melting compared with estimated flow velocity was performed, as follows:

Taking Jeffreys equation (Jeffreys, 1925) to calculate the flow of a viscous body on an inclined plane (Tuffen et al., 2001), bulk melt density calculated from geochemical data from Edziza samples (Koosick Bluff), acceleration due to gravity, the thickness of Koosick Bluff (90 m), slope angles of 1-30 degrees, and a viscosity of 10^3 Pa s we calculated an average flow velocity for a KB trachyte lava flow to be $< 0.001 - 0.01$ m/s (Fig 49, Table 8). Note that Jeffreys equation (Jeffreys, 1925) relates viscosity (η), gravitational acceleration at Earth's surface (g), density (ρ), angular measurement of slope (α), flow velocity (v), and the thickness of the flow (d).

Table 8: Jeffreys Equation

Table of values used in velocity calculation

Table 8: Jeffreys Equation

Symbol	Property	Units	Values
v	velocity	m s ⁻¹	0-0.0099
ρ	magma density	kg m ⁻³	2506
g	acceleration due to gravity	m s ⁻²	9.8
h	thickness of viscous body	m	90
α	slope angle	°	0-30
μ	viscosity	Pa s	10 ⁷

$$v = \rho g h \sin \alpha / 3\mu$$

The Einstein-Roscoe Equation (Marsh, 1981) was used to approximate the effect of the crystal content of a melt on viscosity. The equation uses the viscosity of the liquid of the melt, a constant based on the volumetric ratio of solids at maximum packing (R), and the volume fraction of solids. The volume fraction of solids was determined via thin section of the rock sample.

Einstein-Roscoe Equation:

$$(\mu_{\text{liq} + \text{xtals}}) = (\mu_{\text{liq}}) * (1 - R * \text{volume fraction of solids})^{-2.5}$$

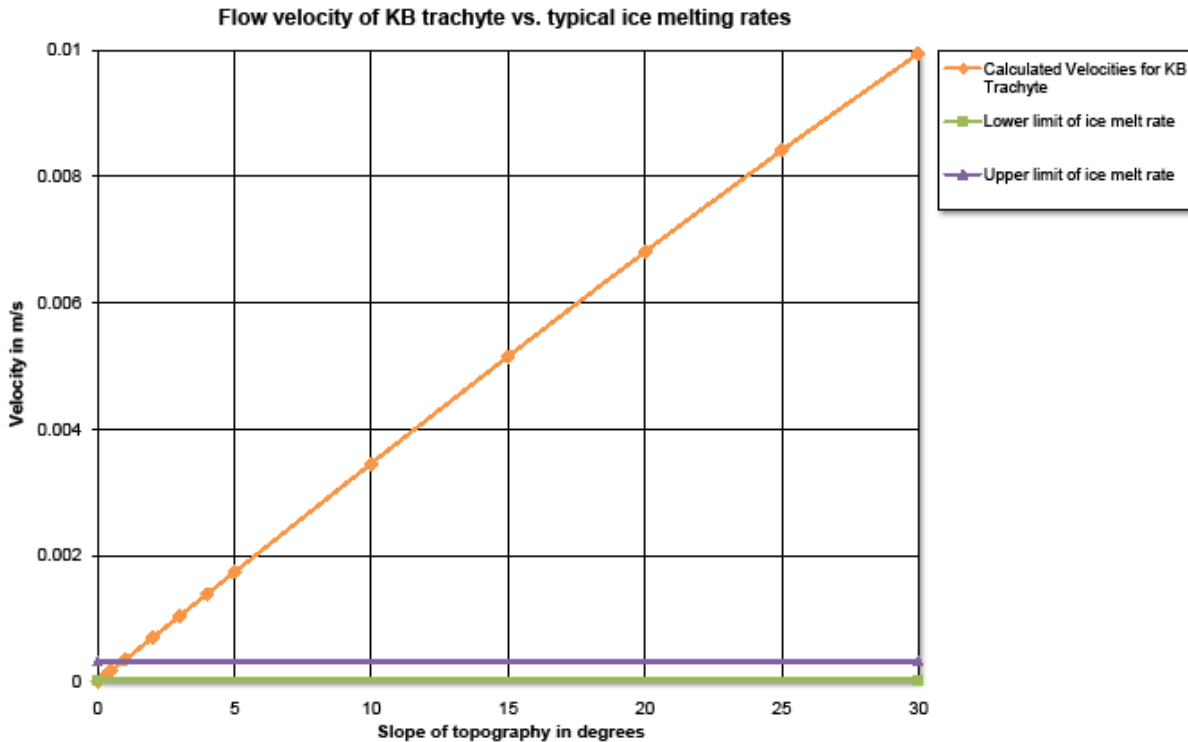


Figure 49: Estimated velocity of the Koosick Bluff lava flow compared with typical ice melting rates. This graph shows the relationship of flow movement to possible ice melt-back rates as lava flows encounter ice. This shows that there would likely be interaction of the lava and ice and not just melting. Hence ice-contact structures should have formed.

Höskuldsson and Sparks (1997) estimated ice would be melted at a rate of 10^{-6} m s^{-1} during the emplacement of rhyolite lavas. This lower end member of melting is based on the rate of heat transfer due to conductive cooling and includes the effects of a chilled rind on the flow. On the upper end of the scale, rates as high as 10^{-3} m s^{-1} were observed during the Gjálp

subglacial basaltic eruption. These higher rates have been interpreted as indicative of more rapid heat exchange through explosive magma-water interaction (Tuffen et al., 2001). Typical ice melting rates are realistically 2.5×10^{-5} to 3.2×10^{-4} m/s (Höskuldsson and Sparks, 1997), markedly slower than lava advance (Fig 49). It is evident that if the lava encountered ice it would pond against and further interact with the ice without completely melting it upon contact. This favors interaction by flowing into cavities within the ice or by other means rather than simply the melting back of the ice. If the ice was thick enough, this would also allow the ice to constrain the flow of lava or divert and change the flows natural path. Further support of this interaction would be found in evidence of the meltwater run off that must be created during these interactions.

The melting rate of ice is governed by the rate at which heat is being released from the lava flow. The rates of ice melt produced by the equation suggest only a few days to weeks are necessary to melt ice of 500-2000 m in thickness. This is, however, largely dependent upon numerous factors including how fractured the lava becomes through cooling as jointing allows further steam and water infiltration making flow cooling more efficient, temperature of the flow, condition of the contact surface and how chilled the exterior is at the point of contact, as well as relative quantity of lava compared with that of ice (Höskuldsson and Sparks, 1997).

15.0 DISCUSSION: RECOGNIZING ICE-CONTACT TRACHYTE LAVAS

The spectacular fanning and curved columns at the base of TD are an important indicator for ice contact, suggesting emplacement against a steep wall of ice, or at least within a cavity that able to pond water at that position on the MEVC. These features as previously mentioned were not seen at KB or OB but due to the possibility of erosion in the time since emplacement, it does not necessarily rule out sub-ice emplacement for both of these bluffs also.

Geomorphic evidence is an important indicator of the presence of former ice in glaciovolcanic settings. Lava flows comprised of lava of average viscosity for a given composition, but markedly over-steepened landforms when compared with similar lavas at other locations (Table 3, Table 6) may suggest the lava had pooled against and been further formed by a body of ice (Fig 46). Of the three similar domes Souther (1992) described of the Edziza Formation, Nanook Dome, Glacier Dome, and Triangle Dome (TD), TD most likely to have been molded by ice. The splaying columns in the basal colonnade zone of TD most likely suggest steep walls of ice surrounded the cooling lava of the newly formed dome. Additionally, for the amount of water needed to create the upper entablature zone at TD would likely need water ponded in a sub-ice lens or ice-bound lake (Fig 46). Nanook Dome is associated with an outer rind of frothy, agglutinated trachyte scoria and blocks which may not have formed if lava had been extruded into the base of a >200m (?) ice sheet where pressure may be sufficient enough to suppress vesicle formation and degassing to such an extent. Additionally, these

materials would have been waterlain, hydrothermally altered, and/or fragmental deposits if ice-dammed water and meltwater were encountered. Although there is little description of Glacier Dome from Souther (1992) it is said to exhibit the concentric flow layering typical of other subaerially erupted domes. The only photograph of Glacier Dome from Souther's work (1992) displays the regular, well formed basal colonnade as seen at TD, although none of the columns seem to splay outward near the base and maintain vertical to sub-vertical orientations.

Similar to geomorphic evidence, locational and situational evidence may also be present and lead to a specific environmental determination. For example, the perched ridge-top flows at Mount Rainier provide situational evidence for an emplacement scenario involving glacier filled valleys (Fig 13; Lescinsky and Sisson, 1998). The steep sided flows along with sub-horizontal cooling columns along the flow's margins further indicate cooling and confinement against a steep surface of ice occupying the U-shaped valleys on either sides of the flows. Retreat of ice left these flows high on the sides of ridges and along ridge crests. This is an important tool, especially for use in other high-latitude stratovolcanoes. No situational evidence exists for the OB, KB or TD. Any chilled margins or regions of clearly defined sub-horizontal jointing if they had existed upon emplacement have since been eroded away at OB and KB. Much of what we see at OB and KB is the larger diameter columns that relate to the slower-cooled interiors of such flows (Fig 12; Lescinsky and Sisson, 1998).

The lava flow margins at Mount Rainier have zones of glassy columns 8-20 cm in diameter sub-horizontally oriented and perpendicular to present day cliff faces (Lescinsky and Sisson, 1998). This zone of cooling joints extends into the flow 2-4 m terminating abruptly at a 2-4 m zone of subvertical columns or at the massive flow interior. There are only a few locations on the north side of OB where columns are similar in size and chaotically oriented

some sub-horizontal or inclined, although none are glassy or as prevalent as those seen at Mount Rainier. Basal breccias at Mount Rainier are a scant 5 cm or less indicating flow advancement analogous to basaltic lava tubes where sheath like cooled margins acted as a shell for the molten interior and therefore very little autobrecciation occurred.

The ‘column on column’ structures identified at Ruapehu (Spörli and Rowland, 2006) provide information for not only the modes of fracture and column formation but the relative timing of such fracture as well. Spörli and Rowland’s (2006) ice interaction model (Fig 50) for the formation of the column on column jointing attributes water ingress as the main cause responsible for the creation of the jointing. As the lava flow advances in their model, the water that is produced effects the front and lateral margins of the flow. As mentioned before, it is certain that the margins of both OB and KB have experienced extensive erosion and evidence for the water ingress may have been lost. A second scenario however would be an ice sheet with sufficient drainage beneath and perhaps a well established drainage system may be able to handle a sufficient amount of meltwater that would be produced from the lava-ice interaction. In this case, the water would not be available to create the column on column jointing. Furthermore, the meltwater involved in the lava-ice interaction would act as a cooling fluid for the lava removing heat from the margins of the flow creating a thicker cooled margin than would be on subaerially erupted flows. Column-on-column, pseudopillow pillow, and other steam-generated fracturing would only be expected when the environment beyond the lava is more impermeable than the lava, so that steam is pushed into the earlier formed contraction cracks and further propagates these cracks under pressure. If any of the surroundings (sub-ice, ice cracks, tunnels, existing drainage channels) allowed rapid enough water drainage, then pressure and containment may not occur and these structural elements would not form.

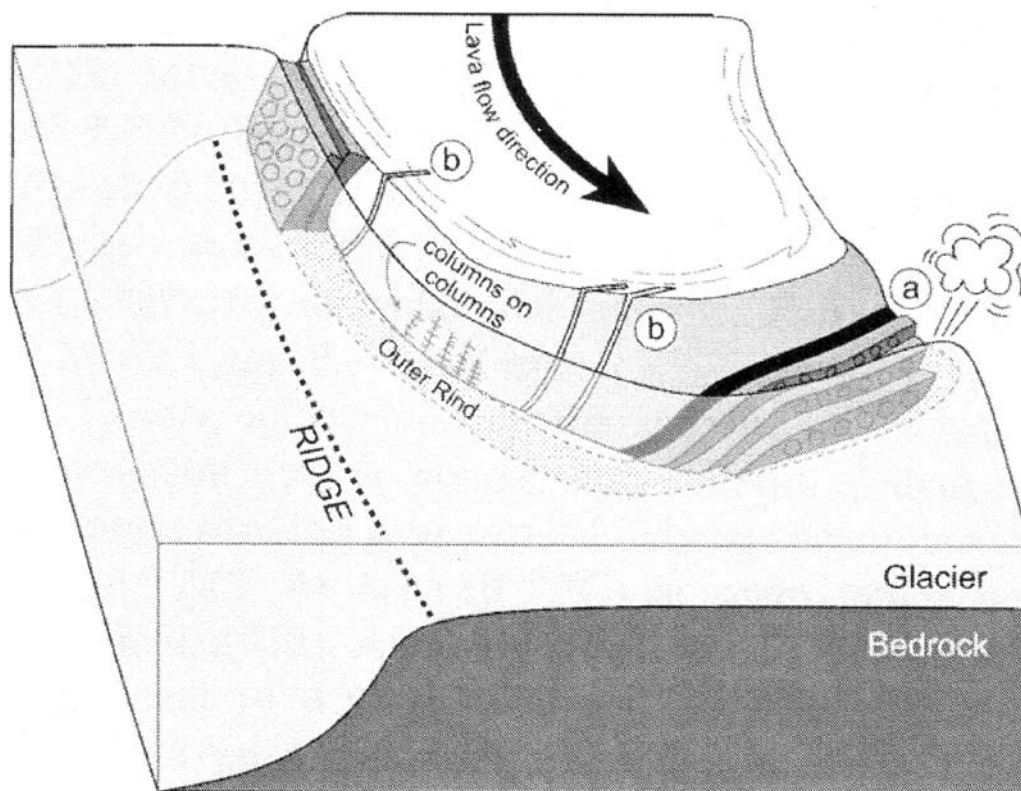


Figure 50: The model for formation of ‘column-on-column’ structures on the outer margins of lava flows. Lateral and frontal egress of water is the dominant force in the structure formation. (a) zone of platy jointing, (b) primary columns (after Spörli and Rowland, 2006)

Much like the large columns at Ruapehu (Spörli and Rowland, 2006) the columns at OB, KB and TD also lack the glassy rind that was observed at Mount Rainier (Lescinsky and Sisson, 1998). This suggests that the large primary columns at Ruapehu and those of OB, KB and TD fractured and began to form below the glass transition temperature whereas those at Mount Rainier must have fractured at temperatures above the solidus (Spörli and Rowland, 2006). The timing of lava-ice interaction in relation the cooling history of the flow may therefore play an

important role in the types of lava-ice interaction evidence produced. A lack of glassy rinds is not particularly indicative and not a good sole indicator for the lack of ice-contact.

The large, well formed, sub-vertical primary columns observed at Ruapehu tended more towards rectangular in shape, a characteristic also observed at OB and KB. These columns at both OB and KB as well as at Ruapehu cross cut the platy jointing that is prevalent at both locations as well. Although the platy jointing itself is not particularly indicative of emplacement environment it occurs at other locations where ice-contact emplacement has been identified such as Mount Rainier, Öraefajökull stratovolcano, and Hoodoo Mountain. (Lescinsky and Sisson, 1998; Stevenson et al, 2006; Lescinsky and Fink, 2000; Spörli and Rowland, 2006; Edwards et al., 2002) The formation of the platy jointing is not well explained. It may be due to thermal contractions although for this mechanism to be the sole cause of the platy jointing a temperature drop of at least 1400 C would be required, which is unreasonable in most situations (Spörli and Rowland, 2006). A mechanical force may be responsible for the formation of this platy jointing due to expansion across the jointing or due to the detachment of outer zones of the flow possibly due to deflation of the flow (Spörli and Rowland, 2006). These platy joint may also simply be due to frost wedging (Stevenson et al., 2006), or as suggested for TD, due to ice unloading.

It is important to note that facies associations with surrounding units can provide critical evidence for emplacement environment. Interbedding with unequivocal glacial tills would provide indisputable evidence for emplacement in a setting where ice-contact could have occurred.

Subaqueously erupted domes often form thick margins and carapaces (100's m thick) of hyaloclastite material as seen at Ponza Island (DeRita et al., 2001). These domes were erupted as pulses and jets of activity into a subaqueous environment which created these thick piles of

hyaloclastite material. The quantity of water present for interaction and fluidal cooling likely played a role in this rather efficient exhibit example of fragmentation as the result of magma-water interaction. No thick carapace of hyaloclastite was observed at TD, no hyaloclastite at all was found. The basal colonnade of TD with well-developed hexagonal columns suggests a relatively regular and consistent cooling regime for this section of the dome. The only evidence in this section for ice contact is the splaying outward of these columns at the margins of the dome, which is interpreted as indicating (perhaps) direct contact with ice. During the initial stages of TD eruption, lava flowed from a vent beneath ice into a cavity that had sufficient enough existing drainages to efficiently transport meltwater created from the lava-ice interaction away from the lava and eruption. However, these drainages eventually ceased efficiently moving water away from the dome resulting in water inundation of already forming columns, creating the entablature zone in the upper portions of the dome.

Complex and irregular cooling contraction jointing and abundant glass are indicators of rapid cooling of lava by water. The lack of hyaloclastite and other quenched materials at OB, KB, and TD is not necessarily problematic in relation to an ice contact environment when the extensive weathering and erosion that has taken place since these features were emplaced 1.5-0.9 Ma ago is taken into account. These are all features within an alpine environment with harsh weather extremes that speed freeze thaw fracturing and removal of clastic material from exposed surfaces.

16.0 FUTURE WORK

Note that we would have liked to analyze glass within these trachytes for H₂O, CO₂, S, Cl and F to constrain the confining pressure during emplacement. Using the solubilities of these gases and their measured values, minimum confining pressures can be calculated, although this turned out to be a problematic endeavor with the Edziza trachytes because of the lack of glass remaining in the samples and the overall lack of knowledge regarding the solubilities of these gasses within trachytes in general.

17.0 CONCLUSIONS

Mount Edziza Volcanic Complex (MEVC) lies within the Northern Cordilleran Volcanic Province (NCVP), in northwest British Columbia, Canada. The eruption products include basalt, trachyte, phonolite and rhyolite that have been emplaced in a variety of subaerial, sub-ice and subaqueous environments from about 8Ma to less than 2000 y.b.p.

The MEVC includes several trachytic (and compositionally very similar, phonolitic) lava bodies that had previously been interpreted as having either contacted ice or at least having been emplaced in a glacial environment. Three such bodies were studied for this project, namely Triangle Dome (TD), Koosick Bluff (KB) and Ornostay Bluff (OB). Triangle Dome, displays features which most clearly indicates emplacement in direct contact with ice, including a spectacular basal colonnade of radial fanning columns, suggestive of cooling against a steep wall of ice. An upper “entablature zone” indicates that the lava was flooded by meltwater during cooling, generating a pattern of jointing architecture similar to that previously described from water-flooded basaltic lava flows. It is not clear if TD was emplaced entirely beneath ice, or if it just contacted ice only contact ice around its basal margins within an ice-confined lake open to the air. The estimated minimum thickness of the ice-contact zone is about 60m, corresponding to a minimum thickness of overlying ice, if sub-ice emplacement is postulated. The origin of the widespread prominent subhorizontal sheet-like jointing at TD is difficult to ascertain, but one possibility is that it may be due to ice unloading.

Identifying ice-contact or sub-ice emplacement at the other two studied bluffs (Ornostay and Kooskick Bluffs) at the MEVC was much more difficult. However, it is important to note that such steep-sided glacially-eroded bluffs are common at many glaciovolcanic centers, so it is a worthwhile challenge. Impressive curvicolumns and jointing patterns present at TD are not present at Ornostay Bluff (OB) and Koosick Bluff (KB). A study of trachytic lava flow dimensions in the published literature revealed that the observed flow thickness for OB and KB (75 m and 90 m) did not necessarily suggest ponding against ice. Similarly, calculation of viscosities from published analyses of trachytes ranging from 4.33 to 11 log [η (Pas)] and their corresponding flow dimensions (including aspect ratios) demonstrated that OB (5.96 log [η (Pas)]) and KB (7.46 log [η (Pas)]) lava flows also do not necessarily require confinement for a lava of their viscosity. However, study of estimated flow velocity of KB trachyte compared to rates of ice melting did demonstrate that direct ice contact was likely, and that ice-contact structures were likely to have formed. However, the diameter of preserved columns at OB and KB suggest that several meters of the margins of both bluffs have likely been removed by erosions, and hence key structural data that may have preserve clearer evidence of ice contact has been lost.

In conclusion, identifying ice-contact structures in trachytic-phonolitic lavas is difficult, especially in glacially eroded examples, where marginal joint sets are likely to have been eroded off. Trachytes display a wide range of viscosities and hence flow thicknesses and aspect ratios, so caution is required in interpreting “overthick” flows as confinement by former ice. Study of comparisons of estimated lavas flow velocities and ice melting rates is a useful exercise to determine if direct ice contact may have occurred, though caution is required due to the large number of variables and assumptions such as uniformity of temperatures, completely liquid

melts, no atmospheric or conductive cooling, and assumed volatile and water contents of the melt in these models.

APPENDIX A

THIN SECTION DESCRIPTIONS AND PHOTOMICROGRAPHS

Thin section:	E6KL23
Rock name:	Phonolite
Location:	Triangle Dome
UTM / Elevation:	400455 E 6398846 N, 2257 m (± 5 m)
Primary mineralogy:	Alkaline Feldspar

Unit:	Triangle Dome lava
Grain size:	Microporphyritic
Date sampled:	7/17/2006
Observer(s):	KL, VP

Phenocrysts	Percent Present	Size (mm)			Approximate composition	Morphology	Comments
		min	max	average			
K Feldspar	1	0.65 x 1.1	1.3 x 5.95	0.77 x 2.88	Potassic anorthoclase	Euhedral or subhedral	Twinning, some zoning
Arfvedsonite	trace	0.175 x 0.2	0.25 x 0.8	0.225 x 0.39		Euhedral or subhedral	
Pyroxene	trace	0.1 x 0.125	0.25 x 0.4	0.62 x 0.285	Clinopyroxene	Euhedral or subhedral	Iron oxide rim/corona
Glass	25						Devitrified

Groundmass / matrix	Percent Present	Size (mm)			Approximate composition	Morphology	Comments
		min	max	average			
K Feldspar	55	0.02 x 0.07	0.23 x 0.08	0.074 x 0.106	Potassic anorthoclase	Microlites - ragged, interlocking laths	Trachytic texture
Arfvedsonite	7					Intergranular	
Pyroxene	5				Augite	Intergranular	
opaque oxides	7				Magnetite/ aenigmatite	Intergranular	

Secondary mineralogy

Iron oxide

Vesicles / cavities

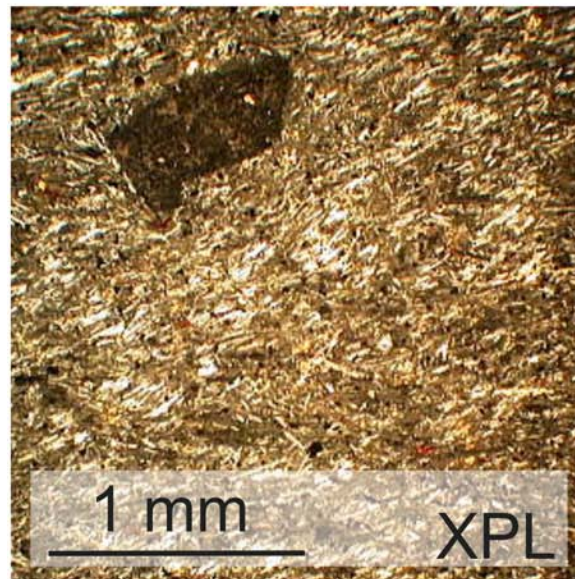
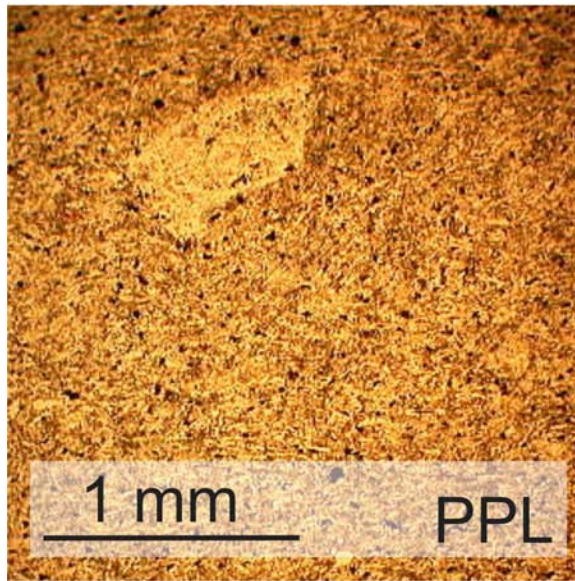
< 1%, none observed in thin section

Comments

Some glomerophorphyritic/cumuloporphyritic cluster inclusions
Sperulitic devitrified glass

E6KL23

Triangle Dome Lava



Thin section:	E6KL5
Rock name:	Trachyte
Location:	Ornostay Bluff
UTM / Elevation:	397580 E 6396229 N, 1844 m (±6 m)
Primary mineralogy:	Alkaline Feldspar

Unit:	Unit 1 - basal flow breccia clast
Grain size:	Microporphyritic
Date sampled:	7/5/2006
Observer(s):	KL, VP

Phenocrysts	Percent Present	Size (mm)			Approximate composition	Morphology	Comments
		min	max	average			
K Feldspar	1	0.35 x 0.4	1.45 x 1.65	0.68 x 1.07		Euhedral to subhedral	
Amphibole	trace	0.125 x 0.125	0.175 x 0.4	0.125 x 0.335		Subhedral	
Glass	60					Vitric to de-vitrified	

Groundmass / matrix	Percent Present	Size (mm)			Approximate composition	Morphology	Comments
		min	max	average			
K Feldspar	18	0.02 x 0.12	0.08 x 0.34	0.058 x 0.228		Microlites - ragged, interlocking laths	Trachytic texture
Amphibole	1					Microlites - ragged, interlocking laths	
opaque oxides	trace				Magnetite		Embayed, amphibole rim
Accessory minerals	20						

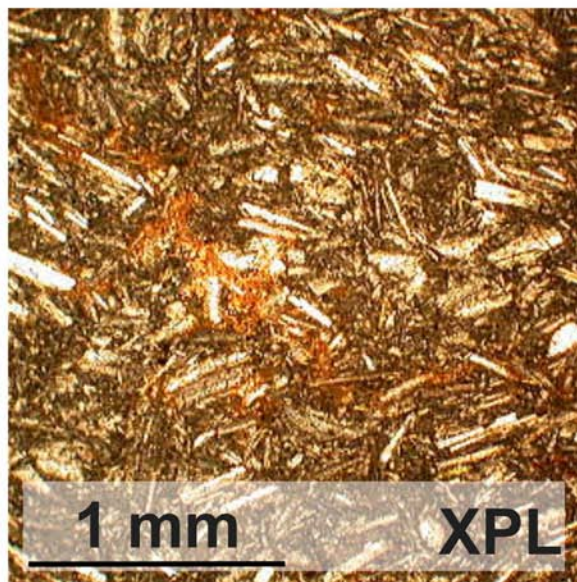
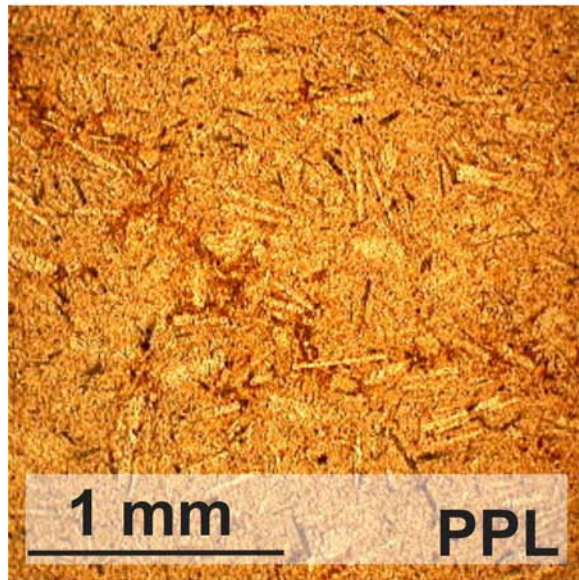
Secondary mineralogy
Pervasive clays

Vesicles / cavities
None observed

Comments
Pervasive alteration

E6KL5

OB - Unit 1



Thin section:	E6CE4
Rock name:	Trachyte
Location:	Ornostay Bluff
UTM / Elevation:	397594 E 6396248 N, 1855 m (± 6 m)
Primary mineralogy:	Alkaline Feldspar

Unit:	Unit 2 - glass
Grain size:	Mircoporphyritic
Date sampled:	7/5/2006
Observer(s):	KL, VP

Phenocrysts	Percent Present	Size (mm)			Approximate composition	Morphology	Comments
		min	max	average			
K Feldspar	1	0.15 x 1.15	0.6 x 3.85	0.53 x 1.19	Sanidine/Anorthoclase	Euhedral to subhedral	Poikilitic, twinning
Pyroxene	8				Clinopyroxene	Euhedral to subhedral	
Ferrohedenbergite	trace					Subhedral	
Magnetite	trace	0.1 x 0.2	0.9 x 0.95	0.38 x 0.42		Subhedral to anhedral	Corroded, embayed

Groundmass / matrix	Percent Present	Size (mm)			Approximate composition	Morphology	Comments
		min	max	average			
K Feldspar - medium	20	0.06 x 0.4	0.1 x 0.4	0.09 x 0.34	Sanidine/Anorthoclase	Microlites - ragged, interlocking laths	Trachytic texture - medium generation
K Feldspar - fine	60	0.01 x 0.06	0.03 x 0.14	0.02 x 0.09	Sanidine/Anorthoclase	Microlites - ragged, interlocking laths	Trachytic texture - smaller generation
Pyroxene	2					Intergranular	
Ferrohedenbergite	3					Intergranular	
Amphibole	5					Intergranular	

Secondary mineralogy

none observed

Vesicles / cavities

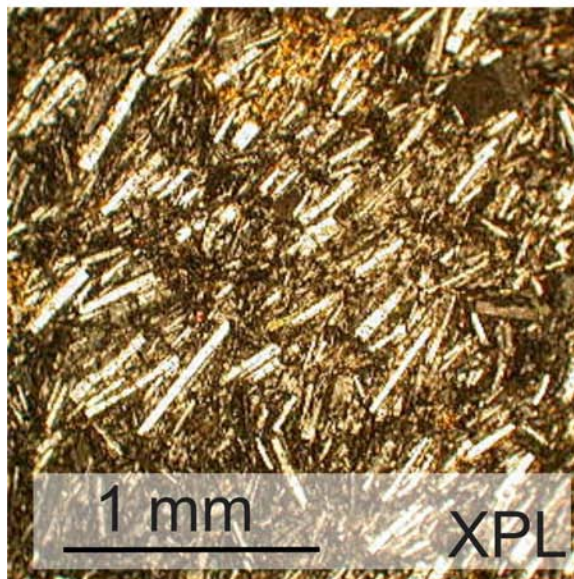
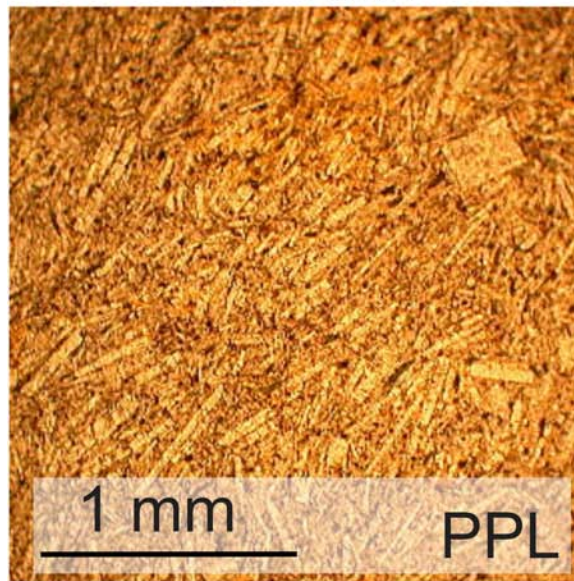
< 1%, none in thin section

Comments

Ornostay Bluff, Southwest corner, basal (?) trachyte flow glass unit
 Trachytic texture not as prevalent as in other samples
 Devitrified glass, spherulitic splays of feldspar laths
 Cracked K-feldspar phenocrysts with pyroxene/ferrohedenbergite filling

E6CE4

OB - Unit 2



Thin section:	E6KL9
Rock name:	Trachyte
Location:	Ornostay Bluff
UTM / Elevation:	397618 E 6396271 N, 1874 m (±6 m)
Primary mineralogy:	Alkaline Feldspar

Unit:	Unit 3 - main flow
Grain size:	Microporphyritic
Date sampled:	7/5/2006
Observer(s):	KL, VP

Phenocrysts	Percent Present	Size (mm)			Approximate composition	Morphology	Comments
		min	max	average			
K Feldspar	1	0.35 x 0.55	1.55 x 2.6	0.85 x 1.78	Sanidine/Anorthoclase	Euhedral to subhedral	Poikolitic, twinning
Pyroxene	trace	0.12 x 0.22	0.2 x 0.44	0.16 x 0.29	Sanidine/Anorthoclase	Euhedral to subhedral	
Opaque oxides	trace	0.7 x 0.9	0.95 x 1.8	0.83 x 1.35	Magnetite	Subhedral to anhedral	Uralitization

Groundmass / matrix	Percent Present	Size (mm)			Approximate composition	Morphology	Comments
		min	max	average			
K Feldspar - medium	20	0.08 x 0.36	0.1 x 0.56	0.08 x 0.5	Sanidine/Anorthoclase	Microlites - ragged, interlocking laths	Trachytic texture - medium generation
K Feldspar - fine	55	0.02 x 0.06	0.02 x 0.24	0.02 x 0.16	Sanidine/Anorthoclase	Microlites - ragged, interlocking laths	Trachytic texture - smaller generation
							Groundmass feldspar laths are interlocking and wrap around larger feldspar phenocrysts
Pyroxene	10				Clinopyroxene	Interstitial	
Opaque oxides	9				Magnetite	Anhedral, intergranular	Amphibole/Biotite alteration rim and filling voids
Amphibole	5					Anhedral, intergranular	
Accessory minerals	trace				Ferrohedenbergite, aenigmatite, arfvedsonite, acmitic pyroxene	Interstitial	

Secondary mineralogy

none observed

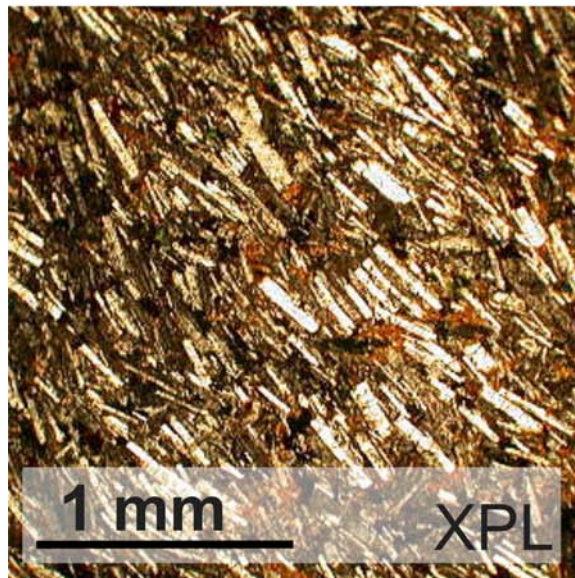
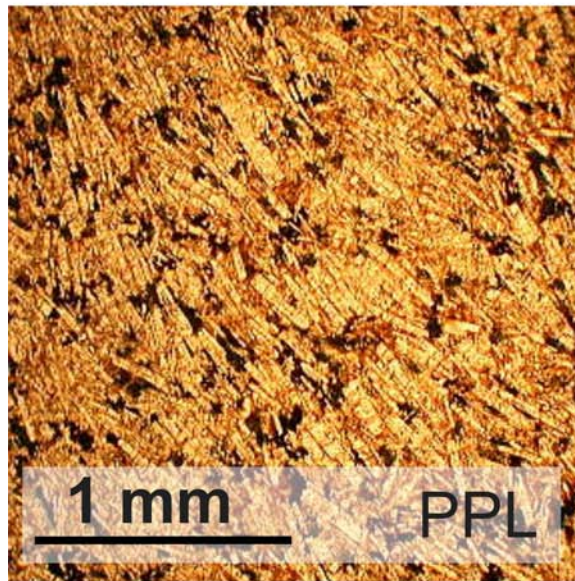
Vesicles / cavities

< 1%, none in thin section

Comments

Ornostay Bluff, Southwest corner, basal (?) trachyte flow
 Trachytic texture not as prevalent as in other samples
 Cracked K-feldspar phenocrysts with pyroxene filling

E6KL9
OB - Unit 3



Thin section:	E6KL22
Rock name:	Trachyte
Location:	Koosick Bluff
UTM / Elevation:	397078 E 6394016 N, 1710 m (± 7 m)
Primary mineralogy:	Alkaline Feldspar

Unit:	Koosick Bluff main flow
Grain size:	Microporphyritic
Date sampled:	38908
Observer(s):	KL, VP

Phenocrysts	Percent Present	Size (mm)			Approximate composition	Morphology	Comments
		min	max	average			
K Feldspar	10	0.4 x 0.85	0.85 x 3.65	0.73 x 1.85	sanidine/anorthoclase	Euhedral to subhedral	Cumulate, glomerophyritic, fine twinning

Groundmass / matrix	Percent Present	Size (mm)			Approximate composition	Morphology	Comments
		min	max	average			
K Feldspar - medium	10	0.05 x 0.9	0.1 x 1.0	0.09 x 0.78	sanidine/anorthoclase	Microlites - ragged, interlocking laths	Trachytic texture - medium generation
K Feldspar - fine	64	0.01 x 0.06	0.02 x 0.2	0.016 x 0.136	sanidine/anorthoclase	Microlites - ragged, interlocking laths	Trachytic texture - smaller generation
							Groundmass feldspar laths are interlocking and wrap around larger felspar phenocrysts
Pyroxene - medium	1	0.05	0.25	0.12	clinopyroxene	Intergranular	Medium generation
Pyroxene - fine	9	0.02	0.08	0.037	clinopyroxene	Intergranular	Small generation
Opaque oxides	3					Intergranular	
Accessory minerals	3				ferrohedenbergite, aenigmatite, arfvedsonite, acmitic pyroxene	Intergranular	

Secondary mineralogy

Iron oxide staining, weathering along crack and within phenocrysts proximal to the crack

Vesicles / cavities

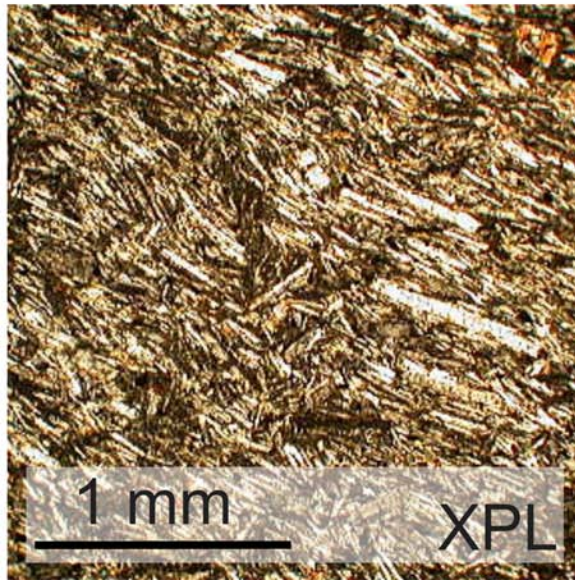
< 1%, none in thin section

Comments

Koosick Bluff, north side, trachyte flow
Some glomerophyritic cumulate cluster inclusions appear broken and microlites 'flow' through

E6KL22

Koosick Bluff Lava



APPENDIX B

VISCOSITY SPREADSHEETS

Paper / Source	Sample ID	Chemistry	Temperature (C) (unless otherwise noted)	Hyrdous?	Viscosities log[n (Pas)]	Viscosity source
Edziza field sample 2006	Koosick Bluff Lava	Trachyte	700	no - 0%	10.75	Calculated by this author using Giordano et al (2008) Model
Edziza field sample 2006	Koosick Bluff Lava	Trachyte	700	2%	6.20	Calculated by this author using Giordano et al (2008) Model
Edziza field sample 2006	Koosick Bluff Lava	Trachyte	850	no - 0%	7.64	Calculated by this author using Giordano et al (2008) Model
Edziza field sample 2006	Koosick Bluff Lava	Trachyte	850	2%	4.5	Calculated by this author using Giordano et al (2008) Model
Edziza field sample 2006	Koosick Bluff Lava	Trachyte	1000	no - 0%	5.59	Calculated by this author using Giordano et al (2008) Model
Edziza field sample 2006	Koosick Bluff Lava	Trachyte	1000	2%	3.26	Calculated by this author using Giordano et al (2008) Model
Edziza field sample 2006	Triangle Dome Lava	Phonolite	700	no - 0%	10.64	Calculated by this author using Giordano et al (2008) Model
Edziza field sample 2006	Triangle Dome Lava	Phonolite	700	2%	6.09	Calculated by this author using Giordano et al (2008) Model
Edziza field sample 2006	Triangle Dome Lava	Phonolite	850	no - 0%	7.6	Calculated by this author using Giordano et al (2008) Model
Edziza field sample 2006	Triangle Dome Lava	Phonolite	850	2%	4.42	Calculated by this author using Giordano et al (2008) Model
Edziza field sample 2006	Triangle Dome Lava	Phonolite	1000	no - 0%	5.57	Calculated by this author using Giordano et al (2008) Model
Edziza field sample 2006	Triangle Dome Lava	Phonolite	1000	2%	3.2	Calculated by this author using Giordano et al (2008) Model
Edziza Field sample 2006	Ornostay Bluff Lava	Trachyte	700	no - 0%	10.53	Calculated by this author using Giordano et al (2008) Model
Edziza field sample 2006	Ornostay Bluff Lava	Trachyte	700	2%	5.76	Calculated by this author using Giordano et al (2008) Model

Edziza field sample 2006	Ornostay Bluff Lava	Trachyte	850	no - 0%	5.96	Calculated by this author using Giordano et al (2008) Model
Edziza field sample 2006	Ornostay Bluff Lava	Trachyte	850	2%	3.44	Calculated by this author using Giordano et al (2008) Model
Edziza field sample 2006	Ornostay Bluff Lava	Trachyte	1000	no - 0%	3.51	Calculated by this author using Giordano et al (2008) Model
Edziza field sample 2006	Ornostay Bluff Lava	Trachyte	1000	2%	1.96	Calculated by this author using Giordano et al (2008) Model
"Water and the viscosity of andesite melts" (Richetet al, 1996)	ME1311e	Andesite	996.2 - 1123.8	no - 0%	13.76 - 9.92	From the paper
"Water and the viscosity of andesite melts" (Richetet al, 1996)	ME1311e	Andesite	793.7 - 866.4	2%	12.87 - 10.49	From the paper
"The viscosity of hydrous phonolites and trachytes" (Whittington et al, 2001)	"Phonolite samples"	Phonolite	889.2 - 1046.4 (K) (616.05 - 773.25 C)	no - 0%	13.12 - 8.66	From the paper
"The viscosity of hydrous phonolites and trachytes" (Whittington et al, 2001)	"Phonolite samples"	Phonolite	676.4 - 747.9 (K)	2.15%	12.34 - 10.05	From the paper
"The viscosity of hydrous phonolites and trachytes" (Whittington et al, 2001)	"trachyte samples"	Trachyte	951.1 - 1113.7 (K)	no - 0%	12.77 - 8.37	From the paper
"The viscosity of hydrous phonolites and trachytes" (Whittington et al, 2001)	"trachyte samples"	Trachyte	725.4 - 802.2 (K)	2.19%	12.31 - 10.01	From the paper
"The evolution of an active silicic lava flow field: an ETM+ perspective" (Harris et al, 2004)	"Mount Hood Andesite, Oregon, USA"	andesite	900-100 C	yes, of unknown extent	5-7	(Murase and McBirney, 1973) - lab based
"The evolution of an active silicic lava flow field: an ETM+ perspective" (Harris et al, 2004)	"Chao Dacite Flow, N. Chile"	dacite	unknown	yes, of unknown extent	9	(Fink, 1980) - surface folds
"The evolution of an active silicic lava flow field: an ETM+ perspective" (Harris et al, 2004)	"Colima Andesite Flow"	Andesite	unknown	yes, of unknown extent	9-10	(Navarro-Ochoa, et al., 2002) - Equation

"The evolution of an active silicic lava flow field: an ETM+ perspective" (Harris et al, 2004)	"Santiaguito Dacite Flow, Guatemala"	dacite	unknown	yes, of unknown extent	9-10	equation / measurement of flow front migration
"The evolution of an active silicic lava flow field: an ETM+ perspective" (Harris et al, 2004)	"Karisimbi trachyte, Rwanda"	trachyte	unknown	yes, of unknown extent	10-11	(McKay, et al, 1998) - surface folds
"Thermodynamic and rheological properties of rhyolite and andesite melts" (Neuville et al, 1993)	"andesite melts"	andesite	939.3 - 1036.8 (K) (666.15 - 763.65 C)	unknown	13.66 - 10.67	creep apparatus
"Thermodynamic and rheological properties of rhyolite and andesite melts" (Neuville et al, 1993)	"andesite melts"	andesite	1670.0 - 1867.0 (K) (1396.85 - 1593.85 C)	unknown	3.19 - 2.33	creep apparatus
"Subglacial and ice-contact volcanism at the Oraefajokull stratovolcano, Iceland" (Stevenson et al, 2006)	JS203	trachy-dacite	850	no - 0%	5.43	Calculated by this author using Giordano et al (2008) Model and chemistry from literature
"Subglacial and ice-contact volcanism at the Oraefajokull stratovolcano, Iceland" (Stevenson et al, 2006)	JS203	trachy-dacite	850	2%	3.93	Calculated by this author using Giordano et al (2008) Model and chemistry from literature
"Subglacial and ice-contact volcanism at the Oraefajokull stratovolcano, Iceland" (Stevenson et al, 2006)	JS226	trachy-dacite	850	no - 0%	5.60	Calculated by this author using Giordano et al (2008) Model and chemistry from literature
"Subglacial and ice-contact volcanism at the Oraefajokull stratovolcano, Iceland" (Stevenson et al, 2006)	JS226	trachy-dacite	850	2%	4.12	Calculated by this author using Giordano et al (2008) Model and chemistry from literature
"Subglacial and ice-contact volcanism at the Oraefajokull stratovolcano, Iceland" (Stevenson et al, 2006)	JS257	trachy-dacite	850	no - 0%	5.10	Calculated by this author using Giordano et al (2008) Model and chemistry from literature
"Subglacial and ice-contact volcanism at the Oraefajokull stratovolcano, Iceland" (Stevenson et al, 2006)	JS257	trachy-dacite	850	2%	3.62	Calculated by this author using Giordano et al (2008) Model and chemistry from literature

"The Pitcarin hotspot in the South Pacific: distribution and composition of submarine volcanic sequences" (Hekinian et al, 2002)	1-01	trachyte	850	no - 0%	4.33	Calculated by this author using Giordano et al (2008) Model and chemistry from literature
"The Pitcarin hotspot in the South Pacific: distribution and composition of submarine volcanic sequences" (Hekinian et al, 2002)	1-01	trachyte	850	2%	2.86	Calculated by this author using Giordano et al (2008) Model and chemistry from literature
"The Pitcarin hotspot in the South Pacific: distribution and composition of submarine volcanic sequences" (Hekinian et al, 2002)	13-01	trachyte	850	no - 0%	4.79	Calculated by this author using Giordano et al (2008) Model and chemistry from literature
"The Pitcarin hotspot in the South Pacific: distribution and composition of submarine volcanic sequences" (Hekinian et al, 2002)	13-01	trachyte	850	2%	3.31	Calculated by this author using Giordano et al (2008) Model and chemistry from literature
"The Pitcarin hotspot in the South Pacific: distribution and composition of submarine volcanic sequences" (Hekinian et al, 2002)	13-02	trachyte	850	no - 0%	4.31	Calculated by this author using Giordano et al (2008) Model and chemistry from literature
"The Pitcarin hotspot in the South Pacific: distribution and composition of submarine volcanic sequences" (Hekinian et al, 2002)	13-02	trachyte	850	2%	2.66	Calculated by this author using Giordano et al (2008) Model and chemistry from literature
"The Pitcarin hotspot in the South Pacific: distribution and composition of submarine volcanic sequences" (Hekinian et al, 2002)	13-08	trachyte	850	no - 0%	4.54	Calculated by this author using Giordano et al (2008) Model and chemistry from literature
"The Pitcarin hotspot in the South Pacific: distribution and composition of submarine volcanic sequences" (Hekinian et al, 2002)	13-08	trachyte	850	2%	2.84	Calculated by this author using Giordano et al (2008) Model and chemistry from literature

"The Pitcarin hotspot in the South Pacific: distribution and composition of submarine volcanic sequences" (Hekinian et al, 2002)	13-10	trachyte	850	no - 0%	4.64	Calculated by this author using Giordano et al (2008) Model and chemistry from literature
"The Pitcarin hotspot in the South Pacific: distribution and composition of submarine volcanic sequences" (Hekinian et al, 2002)	13-10	trachyte	850	2%	2.90	Calculated by this author using Giordano et al (2008) Model and chemistry from literature
"The Pitcarin hotspot in the South Pacific: distribution and composition of submarine volcanic sequences" (Hekinian et al, 2002)	13-11	trachyte	850	no - 0%	4.49	Calculated by this author using Giordano et al (2008) Model and chemistry from literature
"The Pitcarin hotspot in the South Pacific: distribution and composition of submarine volcanic sequences" (Hekinian et al, 2002)	13-11	trachyte	850	2%	2.82	Calculated by this author using Giordano et al (2008) Model and chemistry from literature
"The Pitcarin hotspot in the South Pacific: distribution and composition of submarine volcanic sequences" (Hekinian et al, 2002)	13-13	trachyte	850	no - 0%	4.48	Calculated by this author using Giordano et al (2008) Model and chemistry from literature
"The Pitcarin hotspot in the South Pacific: distribution and composition of submarine volcanic sequences" (Hekinian et al, 2002)	13-13	trachyte	850	2%	2.84	Calculated by this author using Giordano et al (2008) Model and chemistry from literature
"The Pitcarin hotspot in the South Pacific: distribution and composition of submarine volcanic sequences" (Hekinian et al, 2002)	13-16	trachyte	850	no - 0%	4.5	Calculated by this author using Giordano et al (2008) Model and chemistry from literature
"The Pitcarin hotspot in the South Pacific: distribution and composition of submarine volcanic sequences" (Hekinian et al, 2002)	13-16	trachyte	850	2%	2.82	Calculated by this author using Giordano et al (2008) Model and chemistry from literature

"The Cerro Mencionares volcanic center, Baja California Sur: Source and tectonic control on postsubduction magmatism within the Gulf Rift" (Bigioggero et al,1995)	MV-1	Alkali Rhyolite (dacite)	850	no - 0%	4.55	Calculated by this author using Giordano et al (2008) Model and chemistry from literature
"The Cerro Mencionares volcanic center, Baja California Sur: Source and tectonic control on postsubduction magmatism within the Gulf Rift" (Bigioggero et al,1995)	MV-1	Alkali Rhyolite (dacite)	850	2%	3.38	Calculated by this author using Giordano et al (2008) Model and chemistry from literature
"The Cerro Mencionares volcanic center, Baja California Sur: Source and tectonic control on postsubduction magmatism within the Gulf Rift" (Bigioggero et al,1995)	MV-2	Alkali Rhyolite (dacite)	850	no - 0%	4.33	Calculated by this author using Giordano et al (2008) Model and chemistry from literature
"The Cerro Mencionares volcanic center, Baja California Sur: Source and tectonic control on postsubduction magmatism within the Gulf Rift" (Bigioggero et al,1995)	TJ	Alkali Rhyolite (dacite)	850	no - 0%	4.29	Calculated by this author using Giordano et al (2008) Model and chemistry from literature
"The Cerro Mencionares volcanic center, Baja California Sur: Source and tectonic control on postsubduction magmatism within the Gulf Rift" (Bigioggero et al,1995)	TJ	Alkali Rhyolite (dacite)	850	2%	3.17	Calculated by this author using Giordano et al (2008) Model and chemistry from literature
"The Cerro Mencionares volcanic center, Baja California Sur: Source and tectonic control on postsubduction magmatism within the Gulf Rift" (Bigioggero et al,1995)	YM	Dacite	850	no - 0%	4.63	Calculated by this author using Giordano et al (2008) Model and chemistry from literature

"The Cerro Mencionares volcanic center, Baja California Sur: Source and tectonic control on postsubduction magmatism within the Gulf Rift" (Bigioggero et al,1995)	YM	Dacite	850	2%	3.14	Calculated by this author using Giordano et al (2008) Model and chemistry from literature
"The Cerro Mencionares volcanic center, Baja California Sur: Source and tectonic control on postsubduction magmatism within the Gulf Rift" (Bigioggero et al,1995)	SB	Alkali Rhyolite (dacite)	850	no - 0%	4.86	Calculated by this author using Giordano et al (2008) Model and chemistry from literature
"The Cerro Mencionares volcanic center, Baja California Sur: Source and tectonic control on postsubduction magmatism within the Gulf Rift" (Bigioggero et al,1995)	SB	Alkali Rhyolite (dacite)	850	2%	3.7	Calculated by this author using Giordano et al (2008) Model and chemistry from literature
"The Cerro Mencionares volcanic center, Baja California Sur: Source and tectonic control on postsubduction magmatism within the Gulf Rift" (Bigioggero et al,1995)	SJN	Alkali Rhyolite (dacite)	850	no - 0%	4.67	Calculated by this author using Giordano et al (2008) Model and chemistry from literature
"The Cerro Mencionares volcanic center, Baja California Sur: Source and tectonic control on postsubduction magmatism within the Gulf Rift" (Bigioggero et al,1995)	SJN	Alkali Rhyolite (dacite)	850	2%	3.51	Calculated by this author using Giordano et al (2008) Model and chemistry from literature
"The Cerro Mencionares volcanic center, Baja California Sur: Source and tectonic control on postsubduction magmatism within the Gulf Rift" (Bigioggero et al,1995)	XL	trachyte/andesite	850	no - 0%	4.07	Calculated by this author using Giordano et al (2008) Model and chemistry from literature

"The Cerro Mancenares volcanic center, Baja California Sur: Source and tectonic control on postsubduction magmatism within the Gulf Rift" (Bigioggero et al, 1995)	XL	trachyte/andesite	850	2%	3.11	Calculated by this author using Giordano et al (2008) Model and chemistry from literature
"Petrology of two continental alkaline intraplate series at Emi Koussi volcano, Tibesti, Chad" (Gouraud and Vincent, 2003)	K46	phonolite	850	0%	4.49	Calculated by this author using Giordano et al (2008) Model and chemistry from literature
"Petrology of two continental alkaline intraplate series at Emi Koussi volcano, Tibesti, Chad" (Gouraud and Vincent, 2003)	K46	Phonolite	850	2%	2.70	Calculated by this author using Giordano et al (2008) Model and chemistry from literature
"Petrology of two continental alkaline intraplate series at Emi Koussi volcano, Tibesti, Chad" (Gouraud and Vincent, 2003)	K32	trachyte	850	0%	5.10	Calculated by this author using Giordano et al (2008) Model and chemistry from literature
"Petrology of two continental alkaline intraplate series at Emi Koussi volcano, Tibesti, Chad" (Gouraud and Vincent, 2003)	K32	trachyte	850	2%	3.60	Calculated by this author using Giordano et al (2008) Model and chemistry from literature
"Northern Trans-Pecos magmatic province: Introduction and comparison with the Kenya rift" (Barker, 1977)	T-29	Phonolite	850	0%	4.50	Calculated by this author using Giordano et al (2008) Model and chemistry from literature
"Northern Trans-Pecos magmatic province: Introduction and comparison with the Kenya rift" (Barker, 1977)	T-29	Phonolite	850	2%	2.96	Calculated by this author using Giordano et al (2008) Model and chemistry from literature
"Northern Trans-Pecos magmatic province: Introduction and comparison with the Kenya rift" (Barker, 1977)	T-23	Trachyte	850	0%	5.09	Calculated by this author using Giordano et al (2008) Model and chemistry from literature
"Northern Trans-Pecos magmatic province: Introduction and comparison with the Kenya rift" (Barker, 1977)	T-23	Trachyte	850	2%	3.62	Calculated by this author using Giordano et al (2008) Model and chemistry from literature

"The geology of Damavand volcano, Alborz Mountains, northern Iran" (Davidson et al, 2004)	DMV12	trachyandesite	850	0%	4.33	Calculated by this author using Giordano et al (2008) Model and chemistry from literature
"The geology of Damavand volcano, Alborz Mountains, northern Iran" (Davidson et al, 2004)	DMV12	trachyandesite	850	2%	2.71	Calculated by this author using Giordano et al (2008) Model and chemistry from literature
"Open-system processes in the genesis of silica-oversaturated alkaline rocks of the Rallier-du-Baty Peninsula, Kerguelen Archipelago (Indian Ocean)" (Gagnevin et al, 2003)	521	trachyte	850	0%	4.98	Calculated by this author using Giordano et al (2008) Model and chemistry from literature
"Open-system processes in the genesis of silica-oversaturated alkaline rocks of the Rallier-du-Baty Peninsula, Kerguelen Archipelago (Indian Ocean)" (Gagnevin et al, 2003)	521	trachyte	850	2%	3.20	Calculated by this author using Giordano et al (2008) Model and chemistry from literature
"Evolution and Genesis of Magmas from Vico Volcano, Central Italy: Multiple Differentiation Pathways and Variable Parental Magmas" (Perini et al, 2004)	VCO 177B	trachyte	850	0%	5.20	Calculated by this author using Giordano et al (2008) Model and chemistry from literature
"Evolution and Genesis of Magmas from Vico Volcano, Central Italy: Multiple Differentiation Pathways and Variable Parental Magmas" (Perini et al, 2004)	VCO 177B	trachyte	850	2%	3.56	Calculated by this author using Giordano et al (2008) Model and chemistry from literature
"Rates and Timescales of Fractional Crystallization from ¹³⁸ U- ¹³⁰ Th- ²²⁶ Ra Disequilibria in Trachyte Lavas from Longonot Volcano, Kenya" (Rogers et al, 2004)	26Lt2	trachyte	850	0%	4.40	Calculated by this author using Giordano et al (2008) Model and chemistry from literature

"Rates and Timescales of Fractional Crystallization from 138U-130Th-226Ra Disequilibria in Trachyte Lavas from Longonot Volcano, Kenya" (Rogers et al, 2004)	26Lt2	trachyte	850	2%	2.66	Calculated by this author using Giordano et al (2008) Model and chemistry from literature
"Geochemistry of the Cape Verde Islands and Fernando de Noronha" (Gunn and Watkins, 1976)		trachyte/phonolite	850	0%	4.86	Calculated by this author using Giordano et al (2008) Model and chemistry from literature
"Geochemistry of the Cape Verde Islands and Fernando de Noronha" (Gunn and Watkins, 1976)		trachyte/phonolite	850	2%	3.54	Calculated by this author using Giordano et al (2008) Model and chemistry from literature
"Subglacial, phonolitic volcanism at Hoodoo Mountain volcano, northern Canadian Cordillera" (Edwards et al, 2002)	94-76	trachyte	850	0%	4.96	Calculated by this author using Giordano et al (2008) Model and chemistry from literature
"Subglacial, phonolitic volcanism at Hoodoo Mountain volcano, northern Canadian Cordillera" (Edwards et al, 2002)	94-76	trachyte	850	2%	3.28	Calculated by this author using Giordano et al (2008) Model and chemistry from literature
"Subglacial, phonolitic volcanism at Hoodoo Mountain volcano, northern Canadian Cordillera" (Edwards et al, 2002)	93-29	phonolite	850	0%	4.09	Calculated by this author using Giordano et al (2008) Model and chemistry from literature
"Subglacial, phonolitic volcanism at Hoodoo Mountain volcano, northern Canadian Cordillera" (Edwards et al, 2002)	93-29	phonolite	850	2%	2.47	Calculated by this author using Giordano et al (2008) Model and chemistry from literature
"Geochemistry of high-potassium rocks from the mid-Tertiary Guffey volcanic center, Thirtynine Mile volcanic field, central Colorado" (Wobus et al, 1990)		trachyte	850	0%	5.78	Calculated by this author using Giordano et al (2008) Model and chemistry from literature
"Geochemistry of high-potassium rocks from the mid-Tertiary Guffey volcanic center, Thirtynine Mile volcanic field, central Colorado" (Wobus et al, 1990)		trachyte	850	2%	4.85	Calculated by this author using Giordano et al (2008) Model and chemistry from literature

APPENDIX C

MOUNT EDZIZA VOLCANIC COMPLEX STRATIGRAPHIC COLUMN

MOUT EDZIZA VOLCANIC COMPLEX

BRITISH COLUMBIA, CANADA

HOLOCENE

SURFICIAL DEPOSITS

Fluvial Deposits

Glacial Deposits

Talus and Landslide Deposits

----- · Mostly Conformable, Locally Disconformable · -----

BIG RAVEN FORMATION

Desolation Lava Field

Williams Cone, Eve Cone: plagioclase-phyric hawaiiite; pyroclastic cone, lava flows, air-fall tephra

Moraine Cone: plagioclase-olivine-phyric alkali olivine basalt and hawaiiite; pyroclastic cone, lava flows

Sidas Cone (2nd Stage), Twin Cone: Plagioclase-olivine-phyric alkali olivine basalt and hawaiiite; pyroclastic cone, lava flows

Sidas Cone (1st Stage): plagioclase-olivine-phyric alkali olivine basalt and hawaiiite; pyroclastic cone, lava flows

Triplex Cone: plagioclase-olivine-phyric alkali olivine basalt; bombs, agglutinated spatter, blocky lava flows

Sleet Cone, Storm Cone: plagioclase-olivine-phyric alkali olivine basalt, minor picrite; pyroclastic cone, lava flows, tuff-breccia

Klastline Valley Centers

SHEEP TRACK MEMBER

Unconsolidated comenditic trachyte pumice

Snowshoe lava field

"The Saucer", Slf-9: plagioclase-olivine-pyroxene-phyric hawaiiite; subaerial pyroclastic cone, lava flows

Cocoa Crater, Slf-11: plagioclase-olivine-pyroxene-phyric hawaiiite; subaerial pyroclastic cone, lava flows

Coffee Crater, Slf-4, Slf-5, Slf-6, Slf-8: plagioclase-olivine-pyroxene-phyric alkali olivine basalt, minor hawaiiite; subaerial pyroclastic cones and subaqueous tuff-rings, lava flows

Tennena Cone, Slf-2, Slf-3: plagioclase-pyroxene-olivine-phyric alkali olivine basalt; tuff breccia, pillow breccia, pillow lava

Mess Lake Lava Field (ML)

The Ash Pit: plagioclase-pyroxene-olivine-phyric hawaiiite; pyroclastic cones, lava flows, air fall tephra

ML-1: plagioclase-pyroxene-olivine-phyric alkali olivine basalt; bombs and agglutinate, lava flow

ML-2: plagioclase-pyroxene-olivine-phyric alkali olivine basalt; bombs and agglutinate

Arctic Lake Plateau

Nahta Cone: plagioclase-olivine-phyric hawaiiite; pyroclastic cone, air fall tephra, lava flow

Other post glacial centers: plagioclase-olivine-phyric hawaiiite; pyroclastic cone, lava flow

PLEISTOCENE

Ashwell Cone: plagioclase-olivine-pyroxene-phyric alkali olivine basalt and hawaiite; nested pyroclastic cones, lava flows

East Slope Centers

Cinder Cliff: plagioclase-olivine-phyric basalt; pillow lava, tuff-breccia and intercalated gravel, thin slaggy lava flows

Icefall Cone, Ridge Cone: plagioclase-olivine-phyric alkali olivine basalt; bombs and agglutinate, lava flows

Walkout Creek and Mess Creek Centers

Alkali olivine basalt; bombs, agglutinated spatter, lava flows

----- Disconformity -----

KLASTLINE FORMATION

North Slope of Mount Edziza: olivine-pyroxene-plagioclase-phyric alkali olivine basalt; pyroclastic breccia, agglutinate, tuff breccia, lava flows, minor pillow lava with some lenses of fluvial gravel and glacial deposits

KAKIDDI FORMATION

Tennaya-Sorcery Creek area

Aphyric trachyte, minor tristanite; coarse, loosely agglutinated pumice, intravalley lava flows

Central Plateau

Punch Cone: trachyte, comenditic trachyte, minor tristanite; agglutinated spatter and breccia, neck and lava flow

ARCTIC LAKE FORMATION

Arctic Plateau

Olivine-plagioclase-microphyric alkali olivine basalt; bombs, agglutinate, minor tuff-breccia and pillow breccia, subaerial lava flows, minor pillow lava, including lenses of fluvial gravel and glacial deposits

----- Mostly Conformable, Locally Disconformable -----

EDZIZA FORMATION

Mount Edziza and satellitic domes

Aphyric and slightly potassium feldspar-phyric trachyte and comenditic trachyte; pyroclastic breccia, lahar and ash flow deposits, lava flows and endogenous domes

Aphyric trachyte; lava lakes ponded in summit crater

Hydrothermally altered vent breccia in central conduit

Subvolcanic intrusions

Aphyric and vitreous trachyte; dykes, cupolas

-- Conformable Contact --

PILLOW RIDGE FORMATION

Pillow Ridge, Tsekone Ridge

Plagioclase-pyroxene-olivine-phyric alkali olivine basalt and hawaiite; tuff-breccia, pillow breccia, pillow lava, minor and subaerial lava flows

Feeder Dykes

-- ? Conformable Contact ----- Disconformity -----

ICE PEAK FORMATION

Upper Assemblage

Ice Peak and flanking shield

Aphyric to highly porphyritic alkali olivine basalt, trachybasalt, tristanite, mugearite, benmoreite and trachyte; lava flows, domes and pyroclastic breccia, locally intercalated with fluvial and glacial deposits

Satellitic centers

The Neck, Ornostay and Koosick centers: tristanite, trachyte, comenditic trachyte; pyroclastic breccia and agglutinate, lava flows and necks

Subordinate centers

Cache Hill and Camp Hill shields: plagioclase-pyroxene-olivine-phyric alkali olivine basalt and hawaiite, intercalated fluvial gravel; bombs and agglutinate, subaerial lava flows, tuff-breccia and pillow lava

Lower Assemblage

Ice Peak and flanking shield

Plagioclase-pyroxene-phyric alkali olivine basalt and hawaiite, minor tristanite, trachybasalt and mugerite; ice-contact deposits, sideromelane tuff-breccia, pillow lava and pillow breccia, subaerial lava flows and pyroclastic breccia

Subvolcanic Intrusions (Correlation unknown): trachyte, diabase

----- Disconformity (glaciation and fluvial erosion) -----

PYRAMID FORMATION

Aphyric to microporphyritic comendite, comenditic trachyte and pantellerite, minor obsidian; lacustrine tuff and pyroclastic breccia, lahar deposits, till and glacial-fluvial gravel, lava flows and domes

Pyramid dome: coarsely porphyritic sanidine trachyte; exogenous dome

Basalt flows and breccia, basal pyroclastic surge deposit of trachytic pumice and lithic clasts, intercalated fluvial gravel

PLIOCENE

--- Disconformity ---

SPECTRUM FORMATION

KITSU MEMBER

Plagioclase-olivine-microphyric alkali olivine basalt, intercalated fluvial gravel and paleosols

Main Lava Dome

Aphyric, vitreous and locally microporphyritic comendite, pantellerite, and pantelleritic trachyte; domes, lava flows, minor breccia and ash flow deposits, hydrothermally altered vent breccia

Subvolcanic intrusions: medium grained soda granite

--- Disconformity ---

NIDO FORMATION

TENCHEN MEMBER (north of Raspberry Pass)

Gamma Peak Piles

Upper unit: subaerial lava flows of aphyric to highly plagioclase-olivine-pyroxene-phyric alkali olivine basalt, subaqueous, ice-contact facies, sidermelane tuff-breccia, pillow lava, gabbro intrusion

Lower unit: aphyric alkali olivine basalt, minor coarsely plagioclase-phyric hawaiiite, subaerial lava flows, flow breccia and agglutinate

Alpha peak, Beta peak and satellitic piles

Aphyric to microporphyritic alkali olivine basalt, minor coarsely plagioclase-phyric hawaiiite; breccia and agglutinate, subaerial lava flows and flow breccia, ice-contact facies, tuff-breccia, pillow lava, pillow breccia and intercalated gravel

--- Mostly conformable, local disconformity ---

KOUNUGU MEMBER (south of Raspberry Pass)

Swarm peak, Exile peak, Vanished peak and Lost peak piles

Aphyric to microporphyritic alkali olivine basalt, minor plagioclase-phyric hawaiiite and olivine-phyric picrite; subaerial flows, flow breccia and agglutinate, subaqueous facies, tuff-breccia, pillow lava

MIOCENE

Disconformity

ARMADILLO FORMATION

Felsic facies

Potassium feldspar-phyric, aphyric to vitreous comendite and alkali-rich trachyte; pumice, ash flows, sand and tuff, lava flows and domes

Proximal deposits

Armadillo caldera, Cartoona Ridge, IGC Dome: hydrothermally altered vent and intra-caldera breccia

Subvolcanic intrusions

Armadillo caldera: soda granite, gabbro (may be younger)

Basaltic facies

Aphyric alkali olivine basalt, minor sparsely porphyritic hawaiite; subaerial lava flows, flow breccia and agglutinate (locally interstratifies with distal rocks of the "Salic facies")

Conformable contact

LITTLE ISKUT FORMATION

Upper, subaerial facies

Trachybasalt, lava flows and flow breccia

Lower, subaqueous facies

"Crackle breccia", hydrothermally altered and quenched highly fractured trachybasalt

Subvolcanic structures

EOCENE

Conduit zone; fumerolically altered explosion breccia, dyke complex

Disconformity

Conformable contact

RASPBERRY FORMATION

Aphyric alkali olivine basalt, minor plagioclase-phyric hawaiite and mugearite; subaerial lava flows, flow breccia and agglutinate; locally includes pillow lava, tuff-breccia and intercalated gravel deposits

Unconformity

SLOKO GROUP

Volcanic rocks

Rhyolite, dacite and andesite pyroclastic breccia, epiclastic breccia, debris flow and landslide deposits; minor lava flows

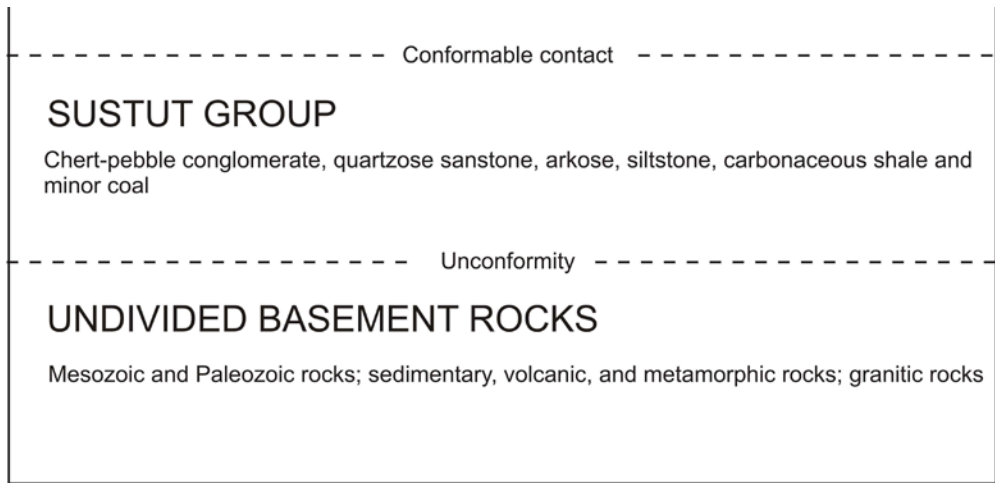
Porphyritic biotite andesite; lava domes, flows and (?) sills

Intrusive rocks

Elwyn Creek Pluton: biotite-hornblende leucogranite

PALEOZOIC AND MESOZOIC

CRETACEOUS AND PALEOCENE



LEGEND

MOUT EDZIZA AND NORTHERN PLATEAU	ICE PEAK, ARMADILLO PEAK, AND CENTRAL PLATEAU	SPECTRUM RANGE AND PLATEAU SOUTH OF RASPBERRY PASS
----------------------------------	---	--

REFERENCE

- Alho, P., Russell, A., Carrivick, J., Käyhkö, J., 2004. Reconstruction of the largest Holocene jökulhlaup within Jökulsá á Fjöllum, NE Iceland. *Quaternary Science Reviews*, v 24, i 22, p 2319-2334.
- Aydin, A., DeGraff, J., 1998. Evolution of Polygonal Fracture Patterns in Lava Flows. *Science*, v 239, n 4839, p 471-476.
- Barker, D., 1977. Northern Trans-Pecos magmatic province: Introduction and comparison with the Kenya rift. *Geological Society of America Bulletin*, v 88, p 1421-1427.
- Bigioggero, B., Chiesa, S., Zanchi, A., Montrasio, A., Vezzoli, L., September 1995. The Cerro Mancenares volcanic center, Baja California Sur: Source and tectonic control on postsubduction magmatism within the Gulf Rift. *Geological Society of America Bulletin*, v 107, n 9, p 1108-1122.
- Castillo, P., Batiza, r., Vanko, D., Malavassi, E., Barquero, J., Fernandez, E., September 1988. Anomalously young volcanoes on old hot-spot traces: I. Geology and petrology of Cocos Island. *Geological Society of America Bulletin*, v 100, p 1400-1414.
- Davidson, J., Hassanzadeh, J., Berzins, R., Stockli, D., Bashukooh, B., Turrin, B., Pandamouz, A., 2004. The geology of Damavand volcano, Alborz Mountains, northern Iran. *GSA Bulletin*, v 116, n 1-2, p 16-29.
- DeRita, D., Giordano, G., Cecili, A., 2001. A model for submarine rhyolite dome growth: Ponza Island (central Italy). *Journal of Volcanology and Geothermal Research*, v 107, p 221-239.
- Di Matteo, V., Carroll, M., Behrens, H., Vetere, F., Brooker, R., 2004. Water solubility in trachyte melts. *Chemical Geology*, v 213, p 187-196.
- Edwards, B., and Russell, J., 2002. Glacial influences on morphology and eruptive products of Hoodoo Mountain volcano, Canada. *Volcano-Ice interaction on Earth and Mars*. Geological Society, London, Special Publications, v 202, p 179-194.
- Edwards, B. and Russell, J., August 2000. Distribution, nature and origin of Neogene-Quaternary magmatism in the northern Cordilleran volcanic province, Canada. *GSA Bulletin*, v 112, n 8, p 1280-1295.

- Edwards, B., Russell, J., Anderson, R., January 2002. Subglacial, phonolitic volcanism at hoodoo mountain volcano, northern Canadian cordillera. *Bulletin of Volcanology*, v 64, p 254-272.
- Fink, J., Bridges, N., 1995. Effects of eruption history and cooling rate on lava dome growth. *Bulletin of Volcanology*, v 57, p 229-239.
- Gagnevin, D., Ethien, R., Bonin, B., Moine, B., Feraud, G., Gerbe, M., Cottin, J., Michon, G., Tourpin, S., Mamias, G., Perrache, C., Giret, A., 2003. Open-system processes in the genesis of silica-oversaturated alkaline rocks of the Rallier-du-Baty Peninsula, Kerguelen Archipelago (Indian Ocean). *Journal of Volcanology and Geothermal Research*, v 123, p 267-300.
- Garvin, J., Sakimoto, S., Frawley, J., Schnetzler, C., Wright, H., 2000. Topographic Evidence for Geologically Recent Near-Polar Volcanism on Mars. *Icarus*, v 145, i 2, p 648-652.
- Giordano D., Russell J., & Dingwell D., 2008. Viscosity of Magmatic Liquids: A Model. *Earth & Planetary Science Letters*, doi:10.1016/j.epsl.2008.03.038.
- Goto, Y. and McPhie, J., 1998. Endogenous growth of a Miocene submarine dacite cryptodome, Rebun Island, Hokkaido, Japan. *Journal of Volcanology and Geothermal Research*, v 84, p 273-286.
- Gouraud, A. and Vincent, P., 2003. Petrology of two continental alkaline intraplate series at Emi Koussi volcano, Tibesti, Chad. *Journal of Volcanology and Geothermal Research*, v 129, p 261-290.
- Gunn, B., and Watkins, N., 1976. Geochemistry of the Cape Verde Islands and Fernando de Noronha. *Geological Society of America Bulletin*, v 87, p 1089-1100.
- Harris, A., Flynn L., Matias, O., Rose, W., Cornejo, J., 2004. The evolution of an active silicic lava flow field: and ETM+ perspective. *Journal of Volcanology and Geothermal Research*, v 135, I 1-2, p 147-168.
- Head, J. and Wilson, L., 2007. Heat transfer in volcano-ice interactions on Mars: synthesis of environments and implications for processes and landforms. *Annals of Glaciology*, v 45.
- Hekinian, R., Cheminee, J., Dubois, J., Stoffers, P., Scott, S., Guivel, C., Garbe-Schonberg, D., Devey, C., Bourdon, B., Lackschewitz, K., McMurtry, G., Le Drezen, E., 2002. The Pitcarin hotspot in the South Pacific: distribution and composition of submarine volcanic sequences. *Journal of volcanology and geothermal research*, v 121, p 219-245.
- Hoskuldsson, A. and Sparks, R., 1997. Thermodynamics and fluid dynamics of effusive subglacial eruptions. *Bulletin of Volcanology*, v 59, p 219-230.

- Hull, D. and Caddock, D., 1999. Simulation of prismatic cracking of cooling basalt lava flows by the drying of sol-gels. *Journal of Materials Science*, v 34, p 5707-5720.
- Jeffreys, H. (1925) The flow of water in an inclined channel of rectangular section. *Philosophical Magazine*, 49, 793-807.
- Kelman, M., Russell, J., Hickson, C., 2002. Glaciovolcanism at Ember Ridge, Mount Cayley volcanic field, southwestern British Columbia. Geological survey of Canada, current research, 2002-A15, 7p.
- LeMasurier, 2002. *Volcano-Ice Interaction on Earth and Mars*. Geological Society, London, Special Publications, v 202, p 115-148.
- Lescinsky, D. and Fink, J., October 10, 2000. Lava and ice interaction at stratovolcanoes: Use of characteristic features to determine past glacial extents and future volcanic hazards. *Journal of Geophysical Research*, v 105, n B10, p 23,711-23,726.
- Lescinsky, D and Sisson, T. Ridge-forming, ice-bounded lava flows at Mount Rainier, Washington. *Geology*, v 26, n 4, p 351-354, April 1998.
- Long, P. and Wood, B., 1986. Structures, textures, and cooling histories of Columbia River basalt flows. *Geological Society of America Bulletin*, v 97, p 1144-1155.
- MacKay, M., Rowland, S., Mougini-Mark, P., and Garbeil, H., 1998. Thick lava flows of Kirisimbi Volcano, Rwanda: insights from SIR-C interferometric topography. *Bulletin of Volcanology*, v 60, p 239-251.
- Madsen, J., Throkelson, D., Friedman, r., Marshall, D., February 2006. Cenozoic to Recent plate configurations in the Pacific Basin: Ridge subduction and slab window magmatism in western North America. *Geosphere*, v 2, n 1, p 11-34.
- Marsh, B., 1981. On the crystallinity, probability of occurrence, and rheology of lava and magma, *Contrib. Min. Petrol.*, 78, 85-98.
- McGarvie, D., Stevenson, J., Burgess, R., Tuffen, H., Tindlw, A., 2007. Volcano-ice interactions at Prestahnúkur, Iceland: rhyolite eruption during the last interglacial-glacial transition. *Annals of Glaciology*, v 45.
- Milkovich, S., Head, J., Marchant, D., 2006. Debris-covered piedmont glaciers along the northwest flank of the Olympus Mons scarp: Evidence for low-latitude ice accumulation during the Late Amazonian of Mars. *Icarus*, v 181, I 2, p 388-407.
- Morris, A. and Mougini-Mark, P., 2006. Thermally distinct craters near Hrad Vallis, Elysium Planitia, Mars. *Icarus*, v 180, I 2, p 335-347.

- Mouginis-Mark, P., 1989. Recent water release in the Tharsis region of Mars. *Icarus*, v 84, I 2, p 362-373.
- Neuvville, D., Courtail, P., Dingwell, D., Richet, P., 1993. Thermodynamic and rheological properties of rhyolite and andesite melts. *Contributions to Mineralogy and Petrology*, v 113, n 4, p 572-581.
- Perini, G., Francalanci, L., Davidson, J., Conticelli, S., 2004. Evolution and Genesis of Magmas from Vico Volcano, Central Italy: Multiple Differentiation Pathways and Variable Parental Magmas. *Journal of Petrology*, v 45, n 1, p 139-182.
- Richet, P., Lejeune, A., Holtz, F., Roux, J., 1996. Water and the viscosity of andesite melts. *Chemical Geology*, v 128, I 1-4, p 185-197.
- Rogers, N., Evans, P., Blake, S., Scott, S., Hawkesworth, C., 2004. Rates and Timescales of Fractional Crystallization from ^{238}U – ^{230}Th - ^{226}Ra Disequilibria in Trachyte Lavas from Longnot Volcano, Kenya. *Journal of Petrology*, v 45, n 9, p 1747-1776.
- Scharrer, K., Spieler, O., Mayer, C., and Münzer, U., 2007. Imprints of sub-glacial volcanic activity on a glacier surface - SAR study of Katla volcano, Iceland. *Bulletin of Volcanology*, v 70, n 4, p 495-506.
- Schopka, H., Gundmundsson, M., Tuffen, H., 2005. The formation of Helgafell, southwest Iceland, a monogenetic subglacial hyaloclastite ridge: Sedimentology, hydrology and volcano-ice interaction. *Journal of Volcanology and Geothermal Research*, v 152, I 3-4, p 359-377.
- Scutter, C., Cas, R., Moore, C., November 1998. Facies architecture and origin of a submarine rhyolitic lava flow-dome complex, Ponza, Italy. *Journal of Geophysical Research*, v 103, n B11, p 27,551-27,566.
- Smellie J., 2002. The 1969 subglacial eruption on Deception Island (Antarctica): events and processes during an eruption beneath a thin glacier and implications for volcanic hazards. *In Smellie, J.L. and M.G. Chapman, eds. Volcano-ice interaction on Earth and Mars.*
- Smellie J. and Chapman, M., 2002. Volcano-ice interaction on Earth and Mars. Geological Society (London) special publication. 202. London, Geological Society.
- Smith, J., 1996. Ductile-brittle transition structures in the basal shear zone of a rhyolite lava flow, eastern Australia. *Journal of Volcanology and Geothermal Research*, v 72, p 217-223.
- Smith, J., Miyake, Y., and Oikawa, T., 2001. Interpretation of porosity in dacite lava domes as ductile-brittle failure textures. *Journal of Volcanology and Geothermal Research*, v 112, p 25-35.

- Smith, J., 2002. Structural analysis of flow-related textures in lavas. *Earth Science Reviews*, v 57, p 279-297.
- Sohn, Y., 1995. Geology of Tok Island, Korea: eruptive and depositional processes of a shoaling to emergent island volcano. *Bulletin of Volcanology*, v 56, p 660-674.
- Souther, J., 1992. The Late Cenozoic Mount Edziza Volcanic Complex, British Columbia. Geological Survey of Canada Memoir 420. 320 p.
- Souther, J., 1968. Cordilleran volcanic study, 1967, British Columbia; in Report of Activities Part A, Geological Survey of Canada, Paper 68-1A, p 42-43.
- Souther, J., 1972a. Telegraph Creek map-area, British Columbia; Geological Survey of Canada, Paper 71-44, 38 p.
- Souther, J., 1972b. Mesozoic and Tertiary volcanism of the western Canadian Cordillera; in *The Ancient Oceanic Lithosphere*, Irving, E. (ed), Department of Energy, Mines and Resources, Earth Physics Branch Publication, n 42, p 55-58.
- Souther, J., 1975. Geothermal potential of Western Canada; Second United Nations Symposium on Development and Use of Geothermal Resources, Proceedings, v 1, p 259-269.
- Souther, J., 1977. Volcanism and tectonic environments in the Canadian Cordillera – a second look; in *Volcanic Regimes in Canada*, Barager, W., et al (eds), Geological Association of Canada, Special Paper, v 16, p 3-24.
- Souther, J., 1981a. Volcanic hazards in the Stikine region of northwestern British Columbia; Geological Survey of Canada, Open File 770, 2 p.
- Souther, J., 1981b. Quaternary volcanism in the Stikine region of northwestern British Columbia and potential hazards from future eruptions; Geological Association of Canada, Annual Meeting, 1981, Abstracts, A-52.
- Souther, J. and Hickson C., 1984. Crystal fractionation of the basalt comendite series of the Mount Edziza Volcanic Complex, British Columbia: major and trace elements; *Journal of Volcanology and Geothermal Research*, v 21, p 79-106.
- Souther, J. and Symons, D., 1974. Stratigraphy and palaeomagnetism of Mount Edziza Volcanic Complex, northwestern British Columbia; Geological Survey of Canada, paper 73-32, 48 p.
- Souther, J., Armstrong, R., Harakal, 1984. Chronology of the peralkaline, late Cenozoic Mount Edziza Volcanic Complex, northern British Columbia; *Geological Society of America, Bulletin*, v 95, p 337-349.

- Sporli, K., and Rowland, J., 2006. "Column on column" structures as indicators of lava/ice interaction, Ruapehu andesite volcano, New Zealand. *Journal of volcanology and geothermal research*, v 157, p 294-310.
- Squyres, S., Wilhelms, D., Moosman, A., 1987. Large-scale volcano-ground ice interactions on Mars. *Icarus*, v 70, I 3, p 385-408.
- Stasiuk, M., Jaupart, C., 1997. Lava flow shapes and dimensions as reflections of magma system conditions. *Journal of Volcanology and Geothermal Research*, v 78, p 31-50.
- Stevenson, J., McGarvie, D., Smellie, J., Gilbert, J., 2006. Subglacial and ice-contact volcanism at the Oraefajökull stratovolcano, Iceland. *Bulletin of volcanology*, v 68, p 737-752.
- Tómasson, H., 1996. The jökulhlaup from Katla in 1918. *Annals of Glaciology*, v 22, p 249-254.
- Tuffen, H., Gilbert, J., McGarvie, D., 2001. Products of an effusive subglacial rhyolite eruption: Bláhnúkur, Torfajökull, Iceland. *Bulletin of Volcanology*, v 63, p 179-190.
- Tuffen, H., Pinkerton, H., McGarvie, D., and Gilbert, J., 2002. Melting of the glacier base during a small-volume subglacial rhyolite eruption: evidence from Bláhnúkur, Iceland. *Sedimentary Geology*, v 149, p 183-198.
- Ventura, G., De Rosa, R., Colletta, E., and Mazzuoli, R., 1995. Deformation and patterns in a high-viscosity lava flow inferred from the crystal preferred orientation and imbrications structures: an example from Salina (Aeolian Islands, southern Tyrrhenian Sea, Italy). *Bulletin of Volcanology*, v 57, n 7, p 555-562.
- Weaver, S., 1977. The Quaternary Caldera Volcano Emuruangogolak, Kenya Rift, and the Petrology of a Bimodal Ferrobasalt – Pantelleritic Trachyte Association. *Bulletin of Volcanology*, v 40-4, p 209-230.
- Webb, P. and Weaver, S., 1976. Trachyte Shield Volcanoes: a New Volcanic Form from South Turkana, Kenya. *Bulletin of Volcanology*, v 39, p 294-312.
- Whittington, A., Richet, p., Linard, Y., and Holtz, F., 2001. The viscosity of hydrous phonolites and trachytes. *Chemical Geology*, v 174, p 209-223.
- Wilson, L. and Head, J., 2007. Heat transfer in volcano-ice interactions. *Annals of Glaciology*, v 45.
- Wobus, R., Mochel, D., Mertzman, S., Eide, E., Rothwarf, M., Loeffler, B., Johnson, D., Keating, G., Sultze, K., Benjamin, A., Venzke, E., Filson, T., 1990. Geochemistry of high-potassium rocks from the mid-Tertiary Guffey volcanic center, Thirtynine Mile volcano field, central Colorado. *Geology*, v 18, p 642-645.